Photo-initiated ring-opening polymerization of N-carboxyanhydrides and its potential application in photolithography

By

Timo Stukenkemper (M.Sc.)

Supervisor: Professor Andreas Heise

Co-supervisor: Dr. Dermot Brougham (UCD)

May 2017

A thesis submitted to Dublin City University
in partial fulfillment of the requirements
for the degree of
Doctor of Philosophy (PhD)

Declaration

I hereby certify that this material, which I now submit for assessment on the programme of study leading to the award of a degree of Doctor of Philosophy is entirely my own work, that I have exercised reasonable care to ensure that the work is original, and does not to the best of my knowledge breach any law of copyright, and has not been taken from the work of others save and to the extent that such work has been cited and acknowledged within the text of my work.

Signed: ID No.: **13213115**

18-4-2017

Date:

Acknowledgement

I do remember the day in Nijmegen in 2012, when I attended the annual meeting of the PANOPTES consortium. During the lunch break, for the first time, I got in touch with the DSM Principle scientist, Dr. Aylvin Dias, who later was the crucial contact to give me the chance to be involved in the Marie Curie founded Neogel project.

First of all, I have to thank my supervisor Prof. Andreas Heise. Andreas, I have said this many times, but you helped me so much to form my practical results into a perfect scientific English, and to present these results in form of publications. You were the engine of my motivation in every bad and frustrating moment during my PhD. I have never met a supervisor, who was always positive, always friendly, always smiling, and always willing to discuss about the Bundesliga. Thank you so much for the great supervision!

In relation to that I have to thank my co-supervisors Dermot and Ayvlin. During our telephone conferences both of you asked critical questions, thereby giving me the right input and new ideas to achieve my goal. Aylvin, whenever I dropped into your office with a question. If you couldn't help me by yourself, at least you knew always a person who knows a person, who... With this, I also have to thank my Neogel colleagues Saltuk, Bing, and Kevin. We all went through a lot of frustration, but we always helped each other to return onto the right track. I hope you will make your way in science or industry

Thanks to the PRG group; although I could not share a long time with you guys, I always felt like to be a part of your group. Special thanks also go to the old members, Fabrice, Anton, Tushar, Mark, Rob, Zeliha, and of course Jaco. Zeliha, I really enjoyed our coffee breaks, and our competitive squash matches. Jaco, you ARE also a good friend who is responsible for my great time in Dublin with a lot of braais and rugby matches with the other South African people.

These people, including, Lara, Darren & Teagan, Matthew & Nikita, Richard & Tanya, Matthew and Max; thank you all for the great time in Dublin. The braais will be unforgettable, the same as the Saturday afternoons in the Woolshed, Church and Mc Gowan's, thanks for these moments!

Thanks Helga, Giane and Thomas for having me in Santry. Living with you in one apartment was a great experience, especially the Brazilian dinners on Sunday evening. Drinking cachaca and playing truco; it will be always in my mind.
In the second half of my PhD period, I was faced to a complete new scientific world, DSM. A company, with intense scientific knowledge, the best thing, that could happen to me.
Thanks to the people from Ahead TS. You guys could help me so much with my photo system. Thanks Johan, Guido, Marco, Carlo, and, of course my DSM Mum Iris. Iris, I cannot describe how much you helped me, thanks!
Special thanks goes to the member of the InnoSyn group. You guys are amazing you are one big family. Special thanks goes to my lab mates Michelle, Paul, Peter, and Jan. I felt confortable in your lab; you gave me all the freedom and trust I needed to work efficient for my thesis. None of my questions were unanswered you always found a solution. Thanks to Timo and his EnzyPep group. You gave me the opportunity to synthesize my peptides via SPPS. Thanks PQ for your ideas and input, and of course for mental support in really tough times, thanks Daniel for having so much fun during our football discussions. I hope, our dream will become true and the HSV won't win the relegation matches in one of the coming seasons.
That brings me to my Öcher homies, Felix, Jan, and Marcel. Without you, coffee breaks, lab work, cycling, car-pooling, or just watching football matches in Aachen, would not have been such a good time. Felix you are an organic super brain, Jan you are the second half of our ironman, Marcel you are my Zaccha-buddy.
Last but not least I have to thank the most important people in my life:
My best friends, Jonas, Virgilia, Dag, Hendrik & Ingar. Thanks for being with me during my PhD. I don't want to miss any of you, thanks that you are there!
Mama, Papa und Niklas. Ihr seid die Stütze in meinem Leben. Diese Doktorarbeit ist auch ein großer Verdienst von euch. Ich konnte mit all meinem Kummer und Sorgen immer zu euch kommen, ich konnte, kann und werde auch immer auf euch zählen können. Ich bin froh, dass ich euch hab, ich bin stolz, euch als Familie zu haben.

Table of Contents

List of Publications

T. Stukenkemper, J.F.G.A. Jansen, C. Lavilla, A.A. Dias, D.F. Brougham, and A. Heise, Polypeptides by light: photo-polymerization of N-carboxyanhydrides (NCA). *Polymer Chemistry* **2017**, 8, 828 – 832

Conference Presentations

T. Stukenkemper, J.F.G.A. Jansen, C. Lavilla, A.A. Dias, D.F. Brougham, and A. Heise, A novel way to synthetic polypeptide, ACS National Meeting, Philadelphia, USA, August 2016

List of Abbreviations

Ac	acetyl
AMM	Active Monomer Meachnism
APTES	(3-Aminopropyl)triethoxysilane
ATR	Attenuated Total Reflection
BLA	*β*-benzyl-L-aspartic acid
BLG	*γ*-benzyl-L-glutamic acid
BLO	Boc-L-ornithine
Boc	*tert*-Butyloxycarbonyl
$CDCl_3$	deuterated chloroform
CHA	cyclohexylamine
CMC	Critical Micelle Concentration
CPP	Cell-Penetrating-Peptide
DCM	Dichloromethane
DCTB	Trans-2-[3-(4-tert-butylphenyl)-2-methyl-2-propenylidene]malononitrile
DIC	*N*,*N*'-Diisopropylcarbodiimide
DIPEA	*N*,*N*-Diisopropylethylamine
DLS	Dynamic Light Scattering
DMF	Dimethylformamide
DMSO	Dimethyl sulfoxide
DNA	Deoxyribonucleic acid
EDAB	Ethyl 4- (dimethylamino)benzoate
EPR	Enhanced Permeability Retention
EtOAc	Ethyl Acetate
Fmoc	9-fluorenylmethoxycarbonyl
FT-IR	Fourier transform infrared spectroscopy
GPC	Gel Permeation Chromatography
HBTU	2-(1H-benzotriazol-1-yl)-1,1,3,3-tetramethyluronium hexafluorophosphate
HCl	Hydrogen chloride
HDI	Hexamethylene diisocyanates
HFIP	1,1,1,3,3,3-Hexafluoro-2-propanol
HMDS	Hexamethyldisilazane

HPLC	High Performance Liquid Chromatography
ITX	2-Isopropylthioxanthone
KTFA	Potassium trifluoroacetate
MALDI-Tof-MS	Matrix-Assisted Laser Desorption/Ionization Time-of-Flight Mass Spectrometry
$MgSO_4$	Magnesium sulfate
MSE	Mean Square Error
MTBE	Methyl tert-butyl ether
M_w	weighted average molecular weight
NAM	Normal Amine Mechanism
NCA	N-carboxyanhydride
NMP	N-Methyl-2-pyrrolidone
NMR	Nuclear Magnetic Resonance spectroscopy
Pbf	2,2,4,6,7-Pentamethyldihydrobenzofuran-5-sulfonyl
PBLA	Poly(*β*-benzyl-L- aspartate)
PBLG	Poly(*γ*-benzyl-L-glutamate)
PBLG-*b*-PBLR	Poly(*γ*-benzyl-L-glutamate)-*b*-poly(diboc-L-arginine)
PBLG-*b*-PLO	Poly(*γ*-benzyl-L-glutamate)-*b*-poly(L-ornithine)
PBLG-*b*-PLR	Poly(*γ*-benzyl-L-glutamate)-*b*-poly(L-arginine)
PBLO	Poly(boc-L-ornithine)
PDI	Polydispersity Index
PDMS	Poly(dimehtylsiloxane)
PEG	Polyethylene glycol
PLG	Poly(L-glutamate)
PLG-*b*-PZLL	Poly(*γ*-benzyl-L-glutamate)-*b*-poly(Z-L-lysine)
PMMA	Poly(methyl methacrylate)
poly(HIPE)	Porous polymers, synthesized from high internal phase emulsion
PTFE	Poly(tetrafluoroethylene)
PTLA	Poly(tert-butyl-L-aspartate)
PTLG	Poly(tert-butyl-L-glutamate)
PTLL	Poly(Tfa-L-lysine)
RNA	Ribonucleic acid
ROP	Ring-Opening Polymerization
RT-FTIR	Real-Time Fourier transform infrared spectroscopy
SEC	Size Exclusion Chromatography
Si-NP	Silica Nanoparticle

SPPS	Solid Phase Peptide Synthesis
TBA	Tert-*O*-butyl L-Aspartic acid
TBG	Tert-*O*-butyl L-Glutamic acid
TEA	Triethylamine
TED	Tetraethylthiuram disulfide
TEGDMA	Triethylene glycol dimethacrylate
TFA	Trifluoroacetic acid
TGA	Thermogravimetric Analysis
THF	Tetrahydrofuran
TIS	Trisopropylsilane
TLC	Thin-Layer Chromatography
TLL	Tfa-L-lysine
TMS	Trimethylsilane
ToF-SIMS	Time-of-Flight Secondary Ion Mass Spectrometry
UV	Ultraviolet light
UV-Vis	Ultraviolet–visible spectroscopy
UVC	Ultraviolet C light
XPS	X-ray Photoelectron Spectroscopy

Abstract

Timo Stukenkemper

Photoinitiation of N-carboxyanhydrides

This thesis describes a novel synthesis of polypeptides via N-carboxyanhydride (NCA) ring-opening polymerization (ROP). For the first time, NCA ROP photo-initiation by using a photoamine generator was demonstrated. The active initiator cyclohexylamine was produced *in situ* by the UV-induced breakdown of the photoamine generator. Two NCA monomers, benzyl-L-glutamate (BLG) and TFA-L-lysine (TLL) were chosen to demonstrate the process. Optimizing the photo system by exchanging of the chromophoric group of the photoamine generator and the associated exchange of the light source towards a blacklight lamp showed similar polypeptide products as in conventional polymerization. Moreover, synthesis of a silane-based photoamine generator, bearing the same chromophoric protection group allowed photo-initiated grafting of polypeptide from solid surfaces such as silica nanoparticles and silicon wafers. Polypeptide grafted silica nanoparticles showed a significant increase of their hydrodynamic diameter, detected by Dynamic Light Scattering (DLS), and a significant weight loss, detected by Thermogravimetric Analysis (TGA). Silicon wafer surfaces grafted by polypeptides showed a significantly higher hydrophobicity. Ellipsometry results, together with elemental analysis with X-ray Photoelectron Spectroscopy (XPS) and Time-of-Flight Secondary Ion Mass Spectroscopy (Tof-SIMS) confirmed non-homogeneous polypeptide layers with a thickness of 3 nm. In addition, a novel drug delivery system was investigated by first synthesizing an amphiphilic block copolypeptide poly(benzyl-L-glutamate-*b*-L-arginine) (PBLG-*b*-PLR). This approach uses the PLR block as hydrophilic part, but also as Cell-Penetrating-Peptide for a potential selective drug delivery to diseased tissue. Two synthesis routes were investigated: (1) block copolymerization of BLG and the non-natural amino acid L-ornithine, which is modified after polymerization to the desired PLR block. The second synthesis route includes the ligation of the ROP-derived PBLG block with the Solid Phase Peptide Synthesis (SPPS)-derived PLR block. Both polymer materials were used for self-assembly studies.

1. Literature review

1.1 Peptides

Peptides are crucial macromolecules in living organisms. Their function is universal and spread over every compartment inside a living cell. For example, peptides are responsible for the division of a living organism into cells, since they are the main component in every cell wall[1]. Peptides give the cell its structural and stealth property; peptide-based elastin and collagen build up connective tissue such as bones and cartilage and therefore are the most abundant peptides in mammals[2]. Peptides are responsible for supply of the living cells, recognizing and absorbing nutrition molecules. Peptides protect the body from bacteria and viruses since antibodies such as immunoglobulin, a special class of peptides, recognizes and neutralizes exogenous substances[3]. Peptides give cells their function, since every catalytic process is contrived by enzymatic peptides.

Peptides are a natural product processed by the transcription of the cellular DNA into RNA, followed by the transcription of the RNA by ribosomes into the protein product. With the help of enzymes, proteins can be degraded into their initial building blocks and therefore are absorbable. Amino acids are the building blocks of every peptide, organized and bonded covalently in a macromolecular chain. The 20 naturally occurring amino acids are put in a specific order and their sequence code (primary structure) gives each peptide its specific function. Peptides and proteins are classed by their size and number of amino acids. Commonly, amino acid chains with 50 or fewer amino acids are classed as peptides, whereas materials with a higher number of amino acids are referred to as proteins. Natural proteins adopt conformations that enable formation of certain secondary structures and result in particular bio-functionality. Typical motifs of proteins are α-helices, β-sheets and random coils. These motifs are stabilized by non-covalent interactions such as hydrogen bonds, van der Waals forces and π-π stacking.

Due to their universal function, high efficiency, and properties of proteins and peptides there is a high interest to obtain these biomaterials by synthetic approaches. Synthetic polypeptides currently find their applications in food industry, cosmetic and medicine[4],[5]. Using automated solid phase peptide synthesis (SPPS) short oligopeptides can easily be synthesized by this well-established method (Merrifield synthesis)[6]. Each monomer is added step-by-step to the amino acid chain, including deprotection and coupling steps. Silica beads act as a platform for the polymer chain that grows on the

resin surface. However, this method is generally limited to oligopeptides with a maximum length of ca. 50 residues. Furthermore, deprotection and final cleavage procedures limit the variety of achievable peptide products[7].

Bio-engineering methods offer an alternative for polypeptide synthesis[8]. Here, recombinant DNA techniques are used to introduce a peptide gene into a plasmid, following by the injection of the resulting plasmid into a microbial host cell. These microorganisms then synthesize the desired peptide product by natural peptide synthesis. The biggest advantage of this method is the monodisperse synthesis of those macromolecules, however many purification steps are included in the harvest procedure and large scale production of polypeptides is rarely achievable. If the priority of the desired product lies on the synthesis of poly(amino acid) materials with a secondary structure, rather than on the sequence of amino acids, another chemical synthesis approach can be used: Ring-opening polymerization (ROP) of N-carboxyanhydrides (NCA).

1.2 N-carboxyanhydrides

By NCA ROP polypeptides with a high molecular weight can be synthesized efficiently with the ability to form secondary structures, however, lacking of amino acid sequence control. NCA synthesis was carried out initially by Hermann Leuchs[9]. Later, T. Curtius[10]-, and F. Wessely[12]- synthesized the first polypeptides by ring-opening polymerization using primary amines, water, or alcohols as initiators[15],[16]. The accessibility of NCAs is quite broad since, in principle, every amino acid can be converted into its NCA by phosgenation or alternative methods[17],[18]. In some cases the amino acid side chain must be protected due to the incompatibility with the NCA ring. A variety of arrangements of amino acids is possible, ranging from the polymerization of two different monomers into random copolymers or by ordered administration of the monomers separately into block copolymers. The latter follows the characteristics of the living polymerization of NCA ROP[19]-. Choosing specific properties of the monomers, e.g. their polarity and hydrophobicity, amphiphilic block copolypeptides can be synthesized and assembled into non-covalent systems, which find applications in therapeutics[21].

1.2.1 Synthesis of N-carboxyanhydrides

Two different synthetic routes for NCA formation are available, the Leuchs method[11] in which N-alkyloxycarbonylamino acid and a halogenating agent are used, and the Fuchs-Farthing[22] method in which phosgene is facilitating the ring formation. While other

preparation procedures are reported using benzyl chloroformate[9] or carbonyl chlorides[23], the direct phosgenation to the amino acid is most commonly used as it is a rapid reaction and prevents racemization of the product[24].

Triphosgene **1.1**, but also diphosgene, and di-*tert*-butyltricarbonate are preferred for the synthesis of NCAs. Since triphosgene is a crystalline solid it is easy to handle and avoids the use of toxic phosgene gas[25]. No further catalysts are required and removal of side-products is accomplished by recrystallization of the product **1.3** since residual triphosgene, 2-isocyanatoacyl chlorides, and HCl-amino acid salts are soluble in typical solvents such as tetrahydrofuran (THF) and hexane. The resulting synthetic route is based on the Fuchs-Farthing-method (Figure 1.1)[26].

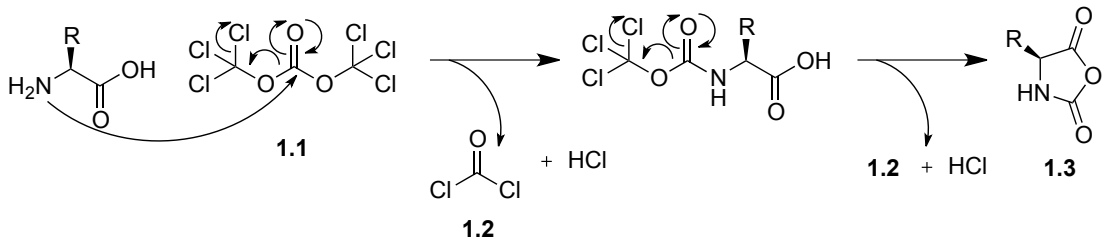

Figure 1.1: Mechanism of NCA formation according to the Fuchs-Farthing method

Applied conditions for NCA synthesis are in anhydrous THF with 1/3 mol eq. of triphosgene at 50°C. Triphosgene reacts under influence of the nucleophilic amine that attacks at the carbonyl carbon. The leaving trichloromethoxy (Cl_3CO-) forms hydrochloric acid and phosgene **1.2**, which reacts immediately with another amino acid to one equivalent of NCA. The second step is an intramolecular nucleophilic attack of the carboxylic alcohol at the carbonyl carbon. The second trichloromethoxy leaving group dissociates again into the named products. After complete conversion a clear solution is formed.

As shown in the reaction (Figure 1.1) two equivalent of HCl per NCA monomer is formed during the reaction. This by-product could either protonate unreacted amino acids or could also influence the protection of functional groups in the side chains. To prevent this, HCl must be removed from the resulting product by several recrystallization steps or by the addition of a HCl scavenger, for example α-pinene[18]. An alternative method is the use of di-tert-butyltricarbonate that forms an isocyanate acid intermediate and ends up in 2 eq. of CO_2 and tert-butyl alcohol[27].

1.2.2 Polymerization of N-carboxyanhydrides: the NAM and AMM mechanism

The polymerization of N-carboxyanhydrides and the resulting conversion of the monomers into a polypeptide can be achieved through two different mechanisms, the

"active monomer mechanism" (AMM) and "normal amine mechanism" (NAM). The mechanisms differ in their initiation and propagation, where the first mechanism is characterized by a deprotonation of the monomer by a base, while the latter is based on a direct nucleophilic attack by an initiator.

Normal Amine Mechanism (NAM):

This polymerization of NCAs is initiated mainly by primary, and secondary amines. The nucleophilic character of the amine causes the attack onto the NCA monomer (Figure 1.2). The intermediate carbamic acid is unstable, resulting in a decarboxylation and the formation of a new free amine group. Due to the stronger nucleophilic character of the initiating amine in comparison to the weaker nucleophilicity of the newly created amine, faster initiation than propagation rates are observed ($k_1 > k_3$). This phenomenon leads to lower polydispersity indices as was proven by Peggion and coworkers[28], as well as by Goodman and coworkers[29]. Researchers also investigated other initiators either based on transition metal complexes [30] or TMS-protected amines[31]. Among the usage of the secondary amine, hexamethyldisilazane (HMDS), a range of different primary TMS-protected amines was screened. These initiators showed not only the expected molecular weight control but also reduced the reaction times significantly.

In every propagation step decarboxylation at the chain end forms one eq. of CO_2 gas. The controlled polymerization can be negatively influenced by increase of gas pressure, thereby changing the carbamic acid-CO_2 equilibrium, but also the choice of solvent and the presence of water have influences. During propagation ROP of γ-benzyl-L-glutamate NCA (BLG-NCA) linear first order kinetics were observed, followed by an increased rate in further polymerization stages[32].

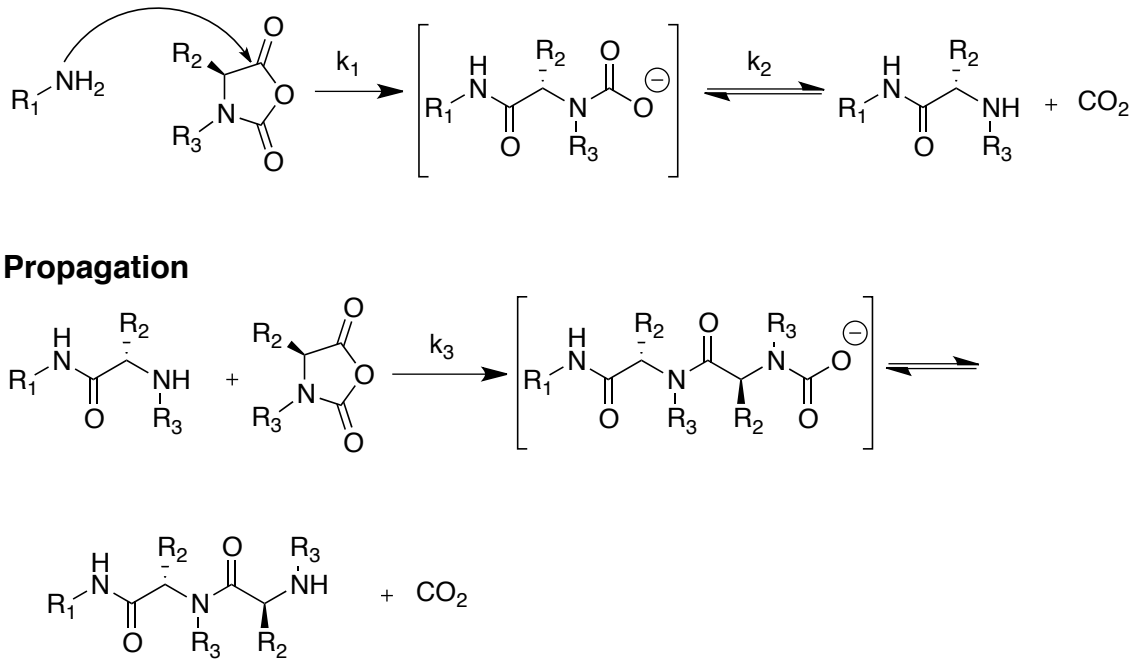

Figure 1.2: Normal amine mechanism (NAM) in presence of a nucleophile (amine).

Active Monomer Mechanism (AMM):

The Active Monomer Mechanism was first purposed by Ballard and coworkers[33] for the ROP initiation of N-unsubstituted NCAs by a base. Different from the NAM polymerization, there is a pre-initiation step, followed by initiation and the propagation.

In the pre-initiation step the initiator compound does not act as a polymerization-initiating compound but rather as a base. The basic compound abstracts the amine proton in the five-membered ring of the NCA, resulting in the corresponding anion. This anion then acts as the nucleophilic polymerization-initiating compound (Figure 1.3). The proton abstraction is the reason why the AMM can only occur for N-unsubstituted NCAs.

In the initiation the created NCA anion attacks the NCA monomer at the carbon-5 atom, resulting in the opening of the ring and decarboxylation that forms a new NCA monomer anion. During the propagation, in each repeating step the growing chain is attacked by an NCA monomer anion, causing the ring opening at the "head" group followed by a decarboxylation. The basic amine subtracts the proton from the next monomer leading to a new anion species that is ready to react for the next chain-growing step.

Since the deprotonated NCA can rearrange to α-isocyanatocarboxylates, followed by the attack of the polymeric amine, α-ureidocarboxylic acid can be formed as a product that results in a termination of the growing polymer chain[34]. Another termination is

suggested by an intramolecular coupling, in which the terminated amine can attack the cyclic end of the polymer chain[35],[36]. It is obvious that this termination mechanism is valid for low molecular weight polymers, since longer chains lower the probability of a ring closure and the formation of a cyclic polypeptide.

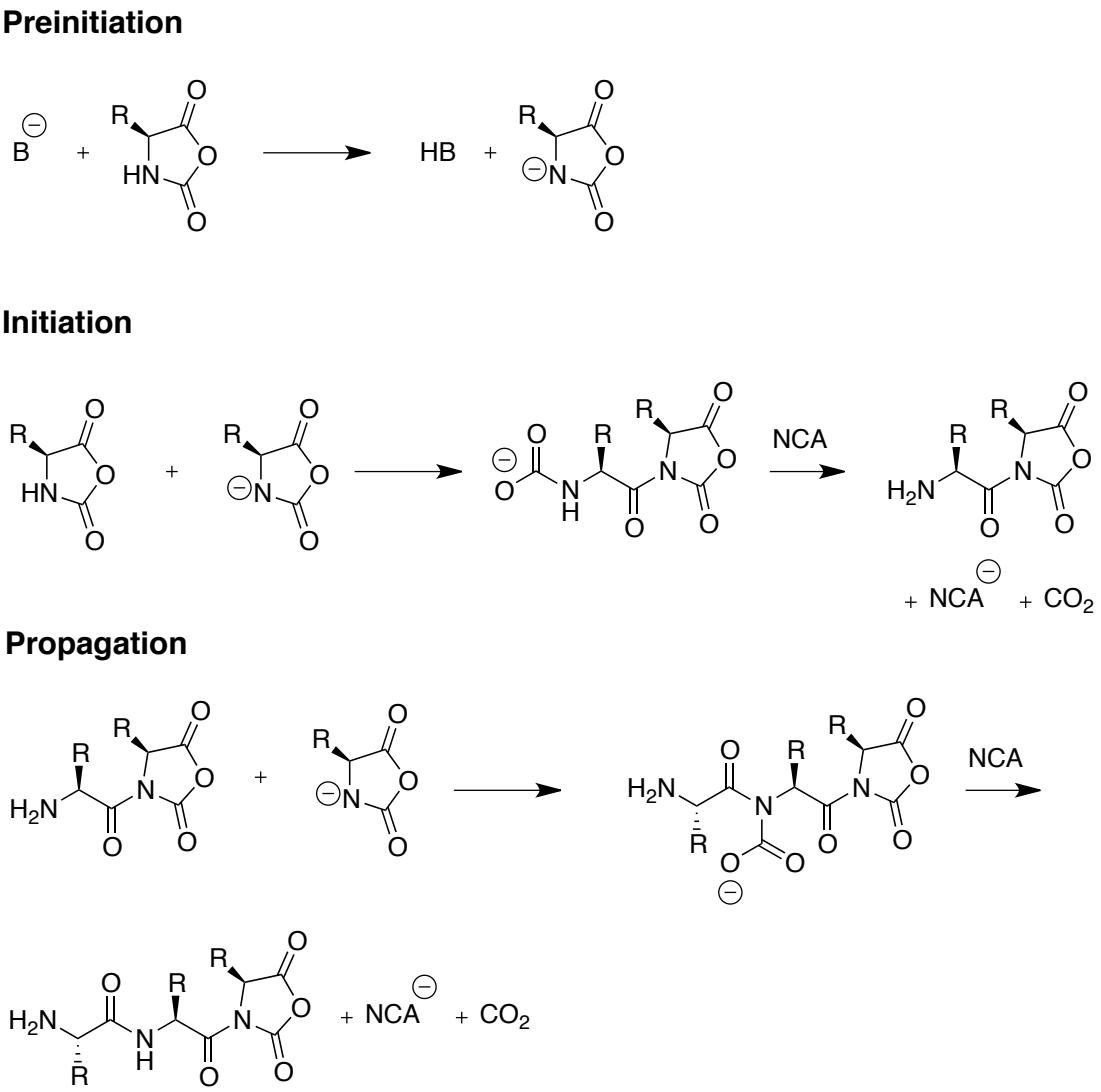

Figure 1.3: Active monomer mechanism (AMM) in presence of a base

In general, the AMM shows a faster propagation that results in an overall faster polymerization. However, the polydispersity index increase and water and other impurities can further expand the value. Also steric hindrance of base molecules can lower the preinitiation step.

1.2.3 Living N-carboxyanhydride ring-opening polymerization

A living polymerization is defined by the absence of termination reactions. In many examples, a fast initiation rate in comparison to the propagation rate results in near-equal polymer chain lengths and a narrow molecular weight distribution. The most prominent example is the Ni-catalyzed NCA polymerization first reported by Deming[37]. Recently, new approaches increasing the control of NCA ROP were investigated. As already mentioned above, trimethylsilyl carbamate acts as a soft protection group of the amine chain end, able to leave the amine efficiently and guiding the monomer for insertion[30]. Platinum complex-based initiators guide the NCA monomers to the chain end, undergoing further propagation, while protecting the *N*-terminus from possible side reactions[38]. Another approach involves the reduction of the reaction temperature, thereby lowering the possibility of side reactions on the *N*-terminus such as intramolecular cyclization with amino acid side-group or formyl addition, since those are temperature-dependent[39]. The living polymerization character is essential for the creation of different polymer architecture based on chain extension, e.g. block copolypeptides. After full conversion of the NCA monomer a second monomer can be added reacting with the *N*-terminus of the homo polypeptide, undergoing further conversion.

1.2.4 Block copolypeptide and other possible polymer architectures

The existence of 20 different amino acids, varying in the functionality and characteristics in their side chain, together with a wide range of side-chain protecting groups and non-natural amino acids enables a large structural variability of polypeptides (Figure 1.4). Moreover, using multifunctional initiators star-shape, graft and branched polypeptides can be synthesized[39],[40]. Recently also polypeptide networks were reported. This can be achieved by using difunctional monomers such as dicystine, which consists out of two L-cysteine molecules, covalently bonded by a sulfur-sulfur bond[41]. A second approach is the "post-polymerizational" deprotection of site chains, followed by crosslinking with another difunctional molecule[42]. One example is the deprotection of poly(benzyl-glutamate), followed by the addition of 1,6-dimanohexane, or 1,12-diaminododecane and ligation reagents[43]. As mentioned before, living NCA ROP also allows composition variability in linear polymer chains. For example, block copolypeptides, consisting of two blocks with different physical properties, can form lipid-like mimics and often show secondary structures[44],[45]. If further blocks are added to the growing polymer chain, even pentablock copolypeptides

can be synthesized allowing the macromolecule to fold into additional shapes and additional functionalities can be added[46].

Another approach is the introduction of a non-amino acid derived polymeric material as macroinitiator, obtaining hybrid block copolymers. Reported materials include polypeptide-saccharides[47], PEG-polypeptide[48], polyester-polypeptide[49], and polyacrylate-polypeptide hybrids[50],[51]. Most of these materials are proposed for biomedical applications such as drug, gene, or protein delivery systems.

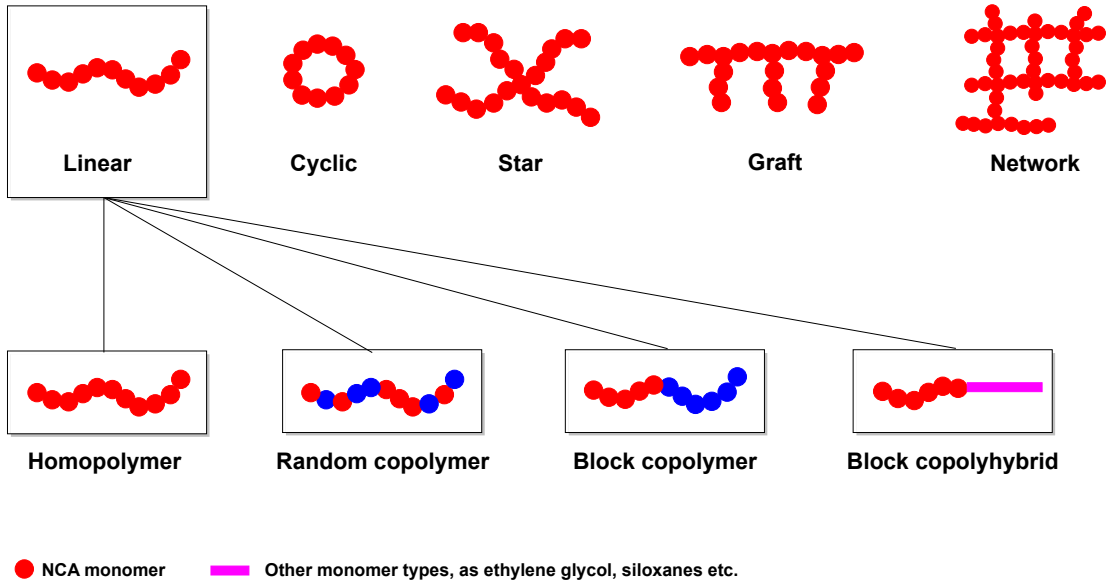

Figure 1.4: Possible topology and compositions of NCA ROP synthesized polypeptides

1.3 NCA ROP prepared polypeptides: applications

Due to the broad number of possible combinations of amino acid NCA monomers as well as the diversity in architecture, functionality and physical properties, NCA ROP derived polypeptides have been proposed and investigated for many application, including pharmaceutical delivery, recognition or functional surfaces among many others. In the following a few (non-exclusive) examples are briefly highlighted.

1.3.1 Self-assembled block copolymers for biomedical applications

Synthesis of block copolypeptides with opposite block polarity results in the creation of amphiphilic polypeptides. Amphiphilic block copolymers can self-assemble into nanoparticles such as micelles and vesicle, which contain a hydrophobic region suitable to carry a hydrophobic drug molecule. This is of particular relevance since hydrophobic drugs are hard to deliver due to their insolubility in an aqueous medium. An example for such approach was using polymethacrylate macroinitiators, synthesized by atom transfer radical polymerization, for ROP of L-histidine NCA. Doxorubicin was successful

encapsulated in the self-assembled particles at different pH conditions. Building on the release of doxorubicin these nanoparticles have a potential for drug delivery to cancer cells[52].

Recently a drug delivery system was described, using the amphiphilic block copolypeptide fully derived from synthetic polypeptides, i.e. poly(L-glutamate)-*b*-poly(Z-L-lysine) (PLG-*b*-PZLL), in which the polyglutamate block forms the hydrophilic part. The obtained self-assembled particles showed spherical and worm-like structures. While spherical particle had a hydrodynamic diameter of 30 nm, worm-like structures showed a much larger diameter. These particles were able to encapsulate a hydrophobic dye (Nile red), as a model compound for drug delivery systems (Figure 1.5)[53].

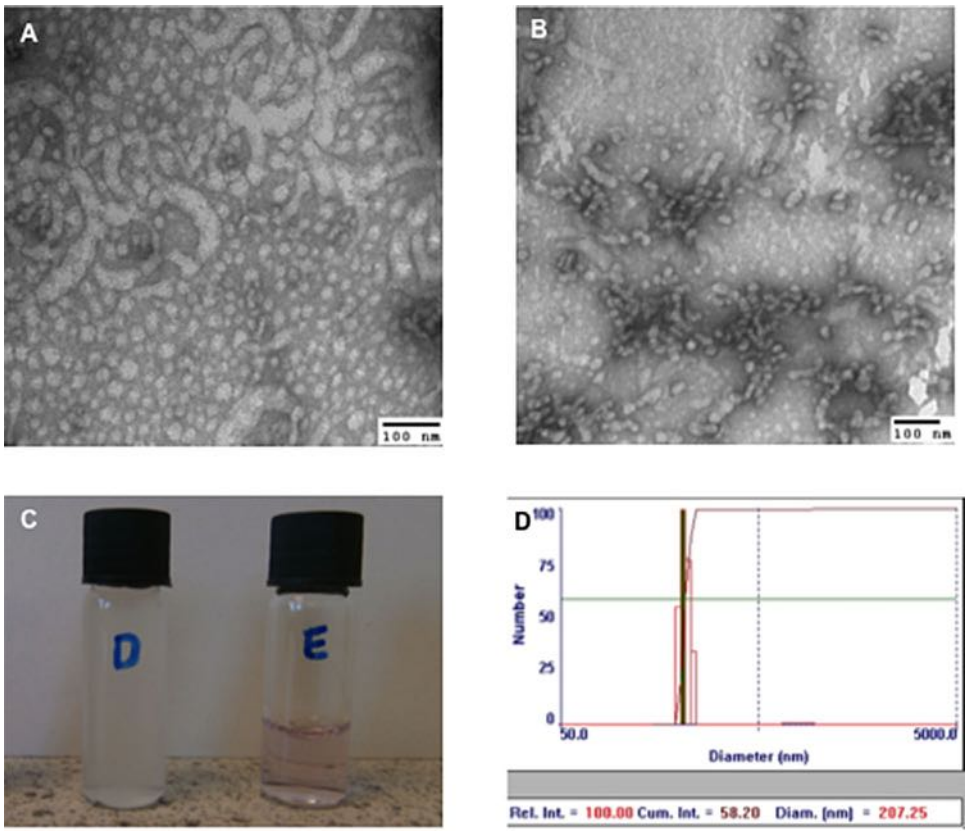

Figure 1.5: Self-assembly of Poly(glutamate)-*b*-Poly(Z-L-lysine)(PLG-*b*-PZLL). (A) TEM of PLG_{50}-*b*-$PZLL_{25}$; (B) TEM of PLG_{50}-*b*-$PZLL_{50}$; (C) encapsulation assay with the hydrophobic dye Nile red presence in self-assembled nanostructures of PLG_{50}-*b*-$PZLL_{50}$ (left – without, and right with Nile red); (D) DLS data of the self-assembled nanoparticles[53].

1.3.2 Surface functionalization

Also surface functionalization of solid nanoparticles is an important tool for cancer therapy and cancer targeting. Therefore, inorganic material such as silica, or iron oxide nanoparticles can be specifically functionalized to impart bio functionality and a

hydrophilic character, e.g. for dissolution in aqueous media. In particular, inorganic-organic materials based on silica nanoparticles find applications in biomedical devices as drug delivery systems[54], diagnostic and screening devices[55], as well as anti-microbial agents[56]. By grafting from a 3-aminopropyltrimethoxysilane (APTS) modified silica nanoparticle PBLG, PZLL, and *S*-*tert*-butyl protected polycysteine (PtBLC) polypeptides were successfully covalently bonded on the silica nanoparticle surfaces[57]. By varying the monomer:substrate ratios, different grafting degrees were achieved, resulting in longer or shorter polymer chains that directly influence the grafted particle size. Conjugation of fluorescent protein, or encapsulation of rhodamine in the polymer chains illustrate potentials for both, cell targeting, and drug delivery, respectively.

Furthermore, magnetic iron nanoparticles depict another suitable substrate for polypeptide grafting and biomedical application. Particles can be used for magnetic resonance imaging. Another interesting feature of iron oxide particles below 30 nm is the property of hyperthermia and tissue thermal ablation[58]. Interestingly, their magnetic character can be used for specific guidance and targeting towards desired tissue[59]. Therefore it is crucial to keep nanoparticles in solution without aggregation. Here surface grafting of polypeptide can improve the desired properties. Similar to silica grafting, APTS modified particles were used to graft polypeptides. In one particular example, additional glycosylation in the site chains of the polypeptide ensures increased hydrophilic character (Figure 1.6)[60].

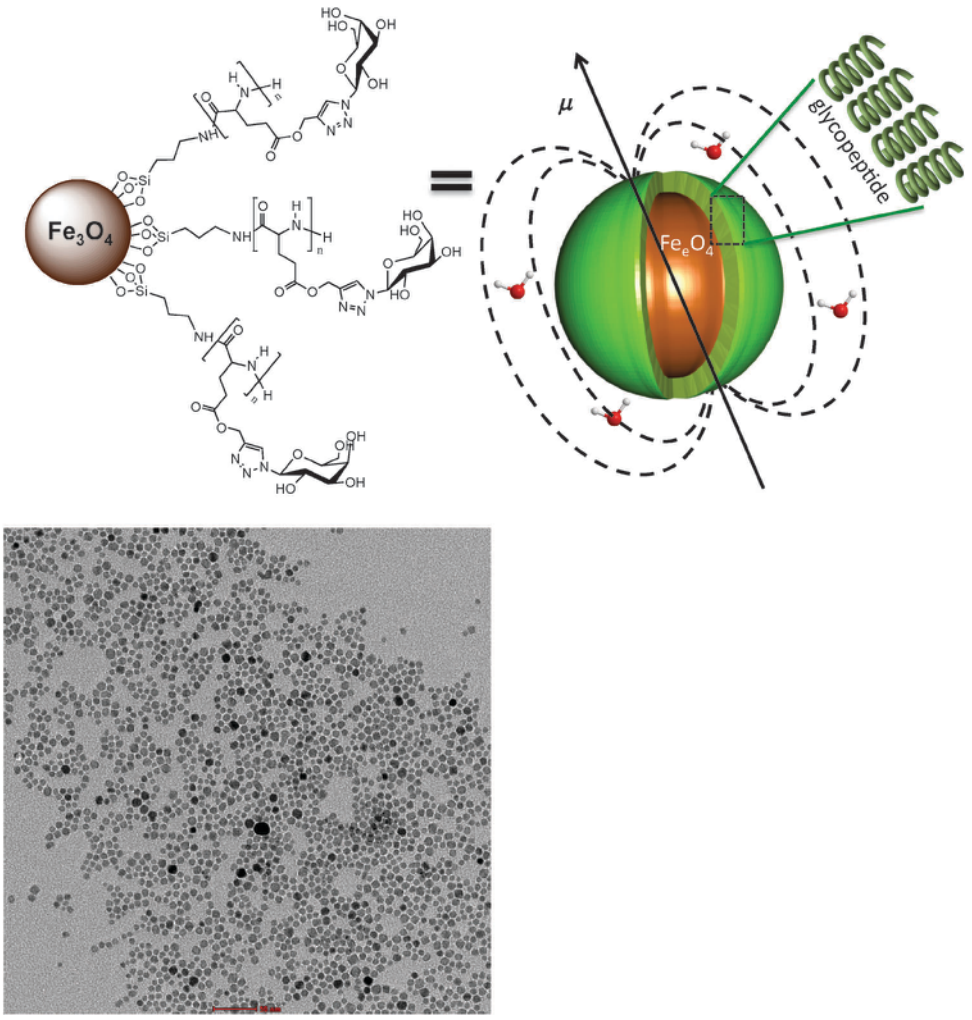

Figure 1.6: Synthetic glycopeptides, grafted on magnetic nanoparticles enable these particles to stay in solution[60]

1.3.3 Planar surface functionalization

Among surface grafting of polypeptides from spherical substrates also grafting from planar substrate raised high interests for medical materials, stabilization of dispersions, coatings protection, biosensors or adhesion material production[61],[62]. In addition it is believed that due to the optical properties of PBLG, its dipole moment of 8000 D and its hyperpolarization β of 5 x 10^{-28} esu[63] application in liquid crystal display can be achieved[64]. Grafted monolayers of PBLG were successfully obtained using *grafting to* and *grafting from* approaches. *Grafting from* approaches, using PBLG raised high interest and is discussed in several publications[65],[66]. While researchers concluded a lower polymer density using the *grafting* to approach, a thickness of 12 ± 3 Å was achieved using a *grafting from* approach[67]. A higher density of polymer material was achieved by improving the accessibility of the initiator. A mixed monolayer of CH3- and

amine-terminated alkyltrichlorosilanes were successfully attached to the surface yielding in optimized layer thickness of 50 Å[68]. Klok and coworker introduced a monolayer of poly(N^{ε}-(monomethoxy-oligo(ethylene glycol)succinate))-L-lysine brushes on silicon wafer surfaces. These brushes have a α-helix formation and are stable between pH 4 and 9 which makes them preventing any nonspecific protein adsorption on surfaces[69].

Although the polypeptide monolayer grafting offers the ability to introduce additional functionality to surfaces, the grafting process allows only formation of full-covered surfaces unless patterning approaches for the deposition of the initiator are applied. Therefore, it would be interesting if polypeptide grafting could also be performed in a locally selective manner. This approach is already known as photolithography and implies photoinitiated cationic and radical polymerizations.

1.4 Photoinitiated polymerizations

Photoinitiation of cationic and radical polymerization finds applications not only in coating, adhesion, and inks, but also in stereolithography, nanotechnology, laser imaging and 3D printing.

In case of radical polymerization, the initiator is excited by light irradiation towards its singlet or triplet state, in most approaches resulting in the creation of two reactive radical species. The monomers, limited to olefin double bond compounds are attacked by the active radical initiator, undergoing polymerization into a macromolecule (Figure 1.7). Here, it has to be noted, that both, inactive initiator and monomers are in close environment, not able to undergo polymerization, unless light irradiation is applied.

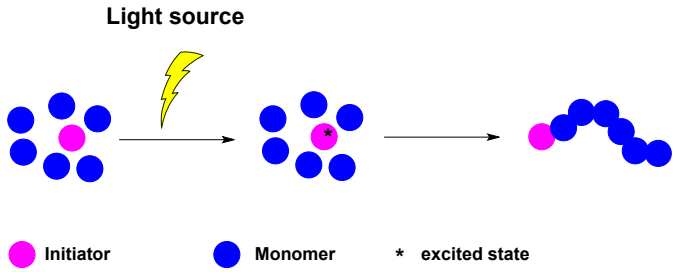

Figure 1.7: Schematic photoinitiated radical polymerization. After light irradiation, the initiator is in its excited state, able to attack monomer molecules triggering propagation.

The radical initiator molecules can be classified into two types, cleavage, and H-abstraction initiators, type I, and type II, respectively[70],[71]. The initiator forms a radical short after light exposure and propagation rates of the radical polymerization yields in the formation of the macromolecule. Using narrow laser beams as light source, surface-

initiated polymerization allows tailoring of the surface, resulting in functionalized, shaped, and featured disposition. One important aspect is the inter-feature spacing, finding applications in sensors[72], nanofluidic devices[73], and protein-affinity separation approaches[74].

Surface-initiated UV-polymerization is well-documented, including different strategies as chemical lithography, electron-beam lithography, scanning probe lithography, and two-photon photopolymerization[75]. The latter approach is applied for fabrication of narrow complexes in two- and three-dimensional structures. For instance, Scott and coworkers used a two-color single-photon photoinitiation system to obtain well-defined polymer structures on surfaces. While one wavelength is initiating the polymerization of triethylene glycol dimethacrylate (TEGDMA) by selectively activating ethyl 4-(dimethylamino)benzoate (EDAB), the second wavelength is causing absorption and activation of an inhibiting species, tetraethylthiuram disulfide (TED). The results is a well-defined polymer gelation material, with a thickness of around 50 -100 nm (Figure 1.8).[76]

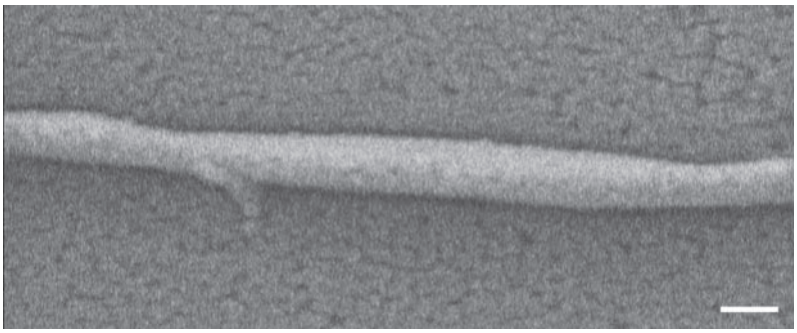

Figure 1.8: Radical photoinitiated of TEGDMA on a glass slide. EDAB was selectively irradiated at a wavelength of 364 nm, while the inhibitor TED was activated with a wavelength of 473 nm, obtaining a narrow gelated polymer column with a thickness between 50-100 nm. Scale bar, 200 nm[76]

The use of light masks allows formation of surface topologies; certain surface regions are hold in dark, therefore the initiation event is avoided, whereas regions, uncovered, undergo initiation and polymerization due to light exposure. Using the above described two-color single-photon initiation approach high quality stamps can be produced (Figure 1.9).

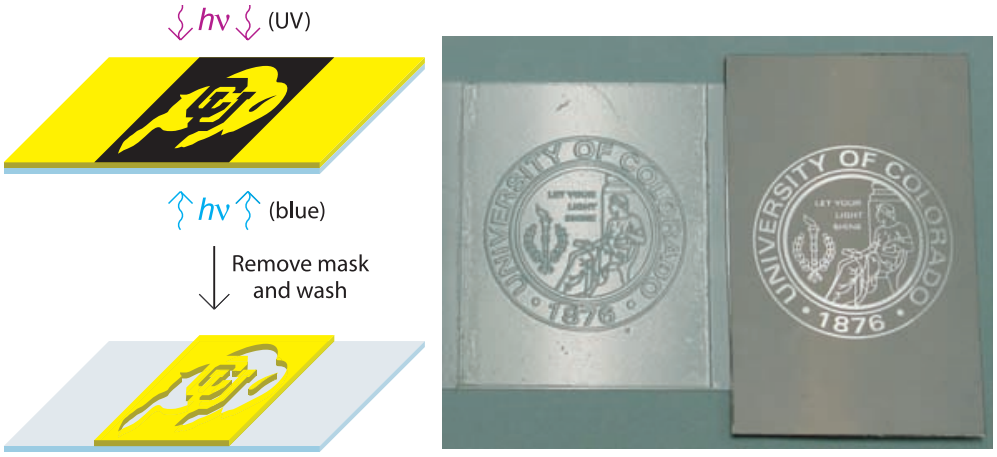

Figure 1.9: Schematic illustration of the use of light mask in a photo-initiation-photoinhibition system. The result is a nearly identical print from the original motif[76]

As Scott and coworker successfully demonstrated, light is a powerful tool to allow a locally selective polymerization of monomers. The crucial point is the activation of the photoinitiator by the light exposure. While photopolymerization is mainly applied to radical and cationic polymerization, in principle, other polymerization mechanism could be amended to a photopolymerization. The breakdown event of the photoinitiator as such is crucial, while monomer material, and its propagation has a minor relevance for the successful development of such as process. This lead to the postulation that photopolymerization of NCA monomers might be possible. As mentioned above, NCA initiation is caused by the presence of a basic or nucleophilic species. If the light trigger would result in the formation of a nucleophilic compound, it was hypothesized that a photopolymerization process might be possible.

1.5 Photobase generators

The concept of to create polypeptide material by light initiation is based on the use of polymerization initiators that bear a photochemical labile protection group. As mentioned above, either a nucleophile or a base is required to initiate a ROP of NCAs either via the NAM or AMM mechanism. Initiator molecules that deliver a nucleophilic compound as breakdown product of a light triggered photo cleavage reaction, are known as photobase generators. The photochemical generation of such active species is of high interest in polymer application such as coatings and imaging. In the following these compounds are briefly introduced.

1.5.1 Different types of photobase generators

In microlithography, organic acid photogeneration created high interest in the 1990s[77]. Mainly onium salts and nitrobenzyl esters were used[78]. More recently, new photoacid generators were investigated containing a sulfonium salt[79]. Photobase generated active species has received less attention. However, those active species bear large potential in various fields. Photobase generators can be classified by their functional structure, including carbamates, *O*-acyloximes, ammonium salts, sulfonamides, formamides, nifedipines, amineimide, α-aminoketones, and amidines (Figure 1.10). The most important classes, i.e. carbamates, *O*-acyloximes, and ammonium salt-based photobase generators are discussed in the following, particularly focusing on their specific breakdown mechanism.

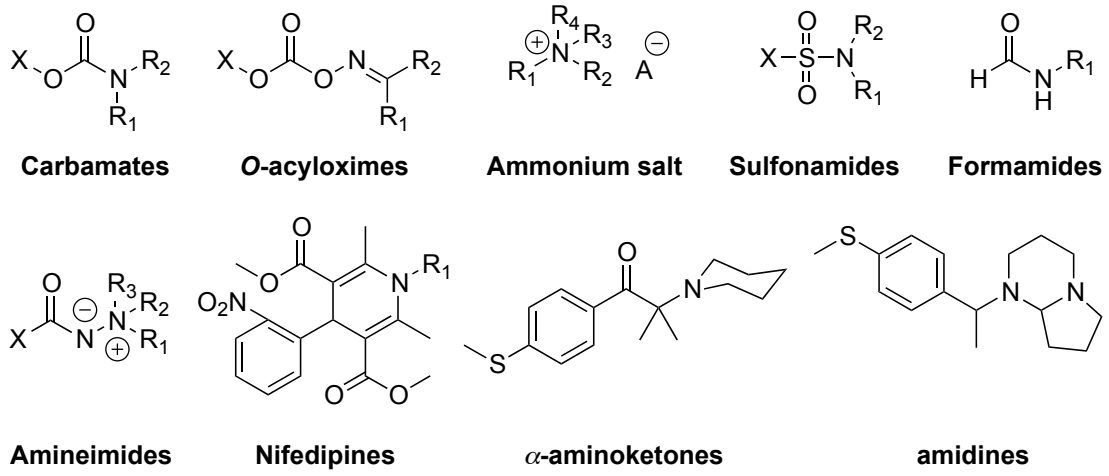

Figure 1.10: Chemical structures of different photobase generator types

Carbamates are protected amines, which, once they are irradiated by light, release primary and secondary amines. The pioneers in the synthesis of photobase generators in microlithography are James Cameron and Jean J.M. Fréchet. They mainly concentrated on carbamate photoproduct (Figure 1.11).

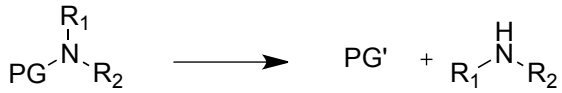

Figure 1.11: Schematic formation of an amine-based photoproduct (PG: protection group)

The photolabile base generator is readily synthesized by the linkage of a primary alcohol and an isocyanate compound[80], where cyclohexyl isocyanate bears the resulting base moiety(Figure 1.12).

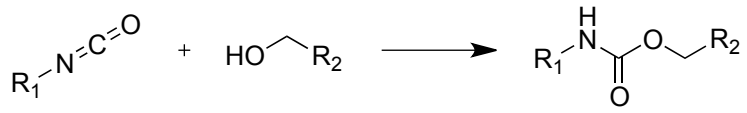

Figure 1.12: General synthesis of a carbamate-based photobase generator. The alcohol undergoes nucleophilic attack under basic conditions, resulting in the formation of a carbamate

Here, it has to be noted that the alcohol compound introduces the chromophoric group, while the protected base is integrated in the isocyanate compound. Once irradiated by light, carbamate-based photobase generators undergo decarboxylation, releasing the former isocyanate amine as a primary amine, while the carbon and oxygen, together with the alcohol oxygen is decarboxylating[81].

O-acyloximes also generate primary and secondary amines, however, an additional step is required involving the presence of water, since an intermediate imine is formed during the radical reaction. The water causes the breakdown of the imine into a ketone and primary amine compound ([82].

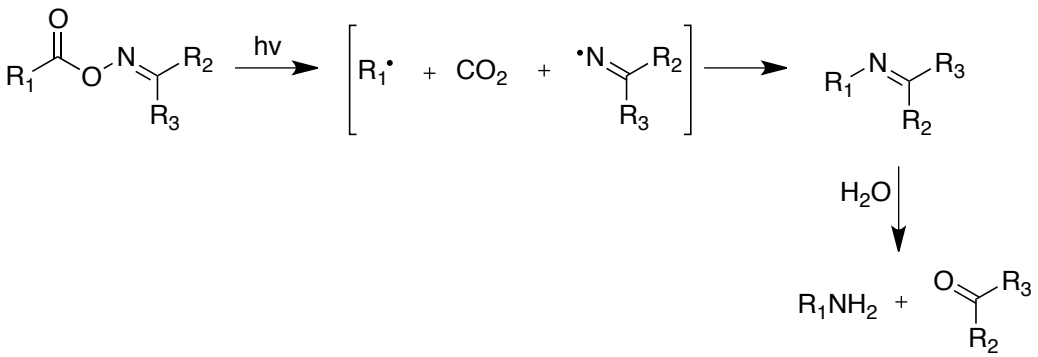

Figure 1.13: *O*-acyloximes breakdown via UV irradiation leads to the decarboxylation and the imine formation. An additional step involving water is required to obtain the desired primary amine compound

Ammonium salts release amines after UV irradiation. In contrast to O-acyloximes, these photobase generators show generally no side reaction. In one approach quaternary ammonium salts and borate anions are utilized to form a tertiary amine. By starting with a single electron transfer from the anion to the cation, followed by an C-N bond cleavage and a final second single electron transfer, a radical and the resulting amine is formed (Figure 1.14)[83].

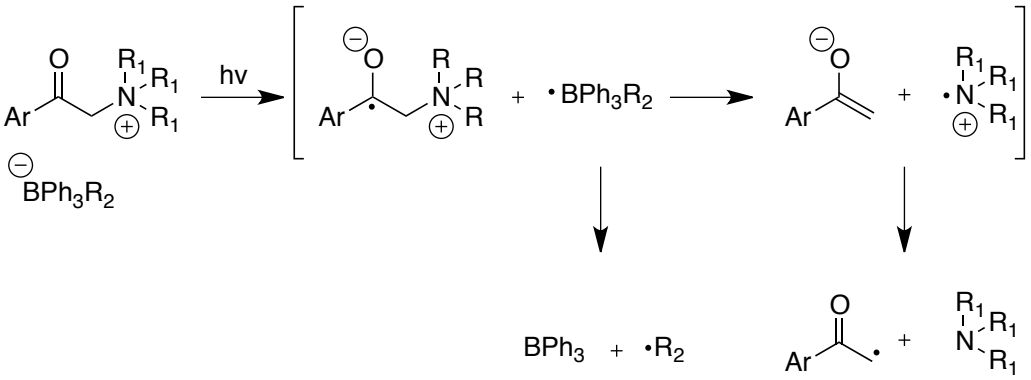

Figure 1.14: Tertiary amine formation by UV exposure to an ammonium salt

Sulfonamides and formamides are barely used in photochemical approaches. Nifedipines, *α*-aminoketones, and amidines are believed to undergo an AMM-based NCA ROP and therefore are not suitable for the desired NCA ROP photopolymerization system. Amineimide are known to be thermal unstable.

For the interest of a photoinitiated NCA ROP, the priority is set for primary amines. Carbamates and *O*-acyloximes photobase generators release primary amines, however, it has to be noted that the latter needs the presence of water. The presence of water could interfere with the initiation of NCA ROP, which leads to the conclusion that carbamates would be the first choice to develop a photoinitiated NCA ROP.

1.5.2 Chromophoric protection groups for photobase generators

As described above, the carbamate-based photobase generator is formed by a nucleophilic attack of a chromophoric alcohol on an isocyanate under basic conditions. Most popular wide spread chromophoric compounds for photobase generators are *o*-nitrobenzyl alcohols, originally pioneered by Woodward and coworkers[84]. In these benzyl rings a nitro substitution group is present on the *ortho* position to the CH_2OH group. The presence of the nitro group introduces a new photocleavable mechanism, in which the initial nitro compound is converted into an *o*-nitrosobenzylaldehyde. In *o*-nitrobenzyl chromophoric groups, it is the nitro group, which undergoes excitation, which is characterized as low-lying excited state[85],[86]. Nitrogen and double bonded oxygen are considered to have an *sp*-configured molecule orbital (Figure 1.15). Once the molecule is irradiated, it undergoes an $n - \pi^*$ excitation, in which one electron of the electron pair in the *n* orbital is translocated in the higher π^* orbital. The *sp* orbital consideration favors the stabilization of the unpaired electron with electron in the *s* binding orbital between the nitrogen and single bonded oxygen. (red dotted line).

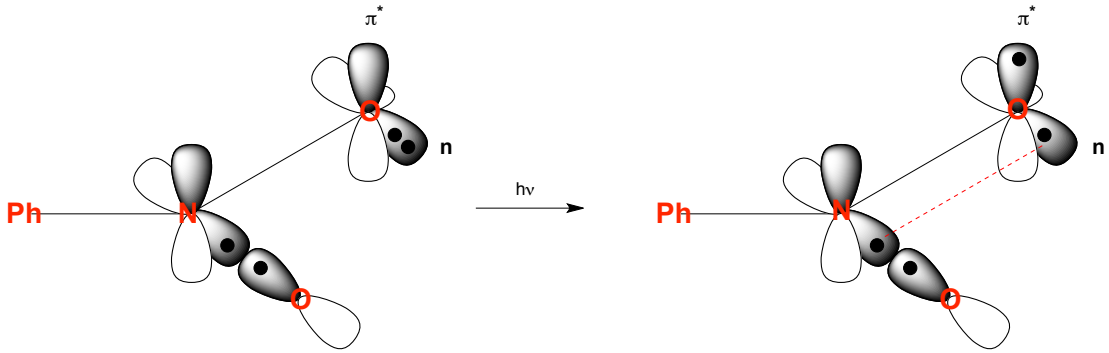

Figure 1.15: *sp* molecule orbital consideration of the nitro group of an *o*-nitrobenzylalcohol. After excitation, the unpaired electron is stabilized by the electron in the *s*-binding orbital between nitrogen and single-bonded oxygen.

Once the oxygen radical is formed, the proximity to the alcoholic CH_2 allows the abstraction of a proton. This leads to two radicals, on two groups, *ortho* to each other in the aromatic ring. In the following an electron rearrangement results in the loss of the two radicals, together with the loss of the conjugated system in the aromatic ring. The drive, to recover the aromaticity is the formation of a five-membered ring by the nucleophilic attack of the negative charged oxygen of the protonated nitro group, followed by an electron rearrangement. The final step towards the photo cleavage is the decarboxylation, the formation of the aldehyde and the release of the primary amine as generated base or nucleophile (Figure 1.16).

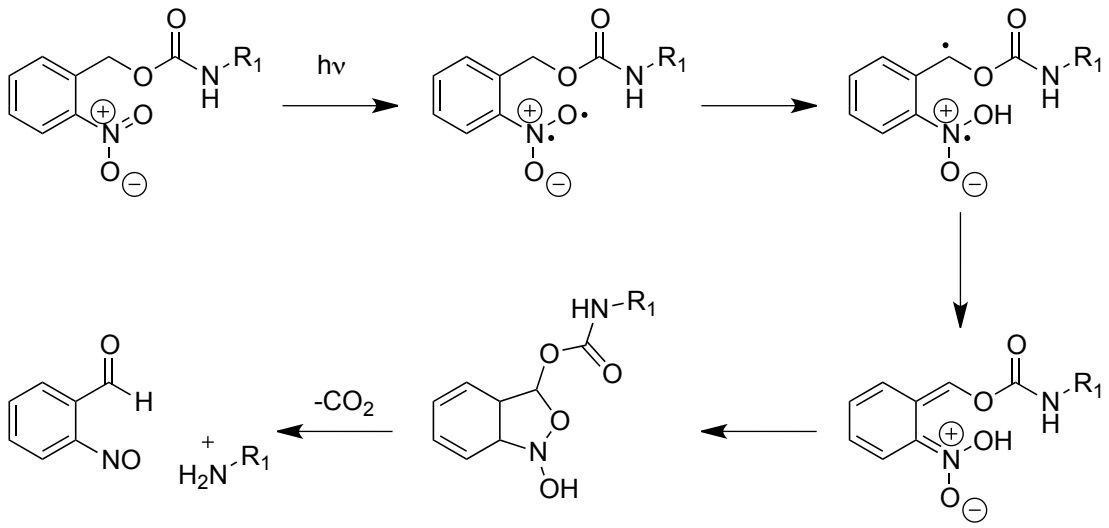

Figure 1.16: Intramolecular rearrangement, after two radicals are formed via light energy absorption. The nitro carbamate compound is, releasing a primary amine compound and a nitroso aldehyde compound.

Fréchet and Cameron investigated the improvement of this mechanism by modifying the benzyl ring by substitutions on different positions. For example, a second nitro group of the second *ortho* position to the CH_2OH group was believed to increase to probability to undergo the above-explained radical mechanism. Indeed, by introducing a further nitro

group the hydrogen abstraction was more capable[87]. A quantum yield boost from 0.13 to 0.62 was recorded. However, when amine and aldehyde was formed, previous studies of Fréchet also indicated that imine formation was favored[88]. An introduction of a bulky group on the α position, starting from a methyl up to a phenyl group could prevent this undesired side reaction, since ketones are less reactive towards amine than aldehydes. However, a lower quantum yield of 0.11 was recorded. Also the introduction of a second 2,6-dinitrobenzyl moiety on the α position did not fulfill expected quantum yield improvement. Therefore, the researchers concluded, that a combination of factors has influence on the quantum yield, therefore on the success of the photocleavage: next to electronic also steric effect and the statistic of hydrogen abstraction are responsible for the quantum yield.

The quantum yield is a scale that indicates how efficient a photobase generator can be photocleaved. This factor has to be considered when deciding, which doses of photo energy can be applied to the system. Next to the efficiency, also the variability in the absorption spectrum is of high interest, since different photo systems can be assembled using light sources with different emissions. Introduction of substituents in the benzyl ring on either the *para* or *meta* positions have influence on the electronic effect. The either electron-withdrawing or electron-donating features of the substituent have direct influence on the absorption spectrum of the chromophore. Introduction of a methoxy substituent would result in an electron–donating effect. This substitution is shifting the absorption spectrum of the chromophore from the deep UV region into a higher wavelength region[89]. While reducing the benzyl ring to a mono-nitro-substitution, the introduction of two methoxy groups in the para and meta position shifted the absorption maximum (λ_{max}) from 254 to 350 nm [90].

Next to *o*-nitrobenzyl-based photobase generators, photobase generators can be synthesized with various photolabile chromophoric groups, summarized in Table 1.1.

Table 1.1: Summary of photolabile groups, used in photolytic approaches. These groups can be used for the synthesis of photobase generators. The chromophoric groups are sorted by their absorption maximum (λ_{max})

Compound	λ_{max} (nm)	reference
2-nitrobenzyl chloroformate	254	[87]
2,6-dinitrobenzenemethanol	254	[87]
2,6-dinitro-*α*-methylbenzenemethanol	254	[87]
2-nitro-*α*-(2'-nitro- phenyl)benzenemethanol	254	[87]
2,6-dinitro-*α*-(2',6'-dinitrophenyl)benzenemethanol	254	[87]
Benzophenone oxime	254	[91]
3,5-dimethoxy-(*α*-benzyol)benzenemethanol	254	[92]
3,4-diemthoxy-*α*-diemthylbenzenemethanol	261	[93]
3,4,5-triemthoxy-*α*-diemthylbenzenemethanol	270	[93]
3.5-Dimethoxybenzenemethanol	276	[94]
2-acetonaphthone oxime	283	[95]
9-fluorenone oxime	300	[96]
N-hydroxynaphtalimide	333	[95]
3,5-dimethoxy-2-nitrobenzenemethanol	364	[97]
7-*N*,*N*-Diethylamino-4-hydroxymethyl coumarin	412	[98]
7-hydroxy-4-methylcoumarin	474	[99]
6-chloro-7-hydroxy-4-methylcoumarin	474	[99]
6-bromo-7-hydroxy-4-methylcoumarin	474	[99]
3,6-dibromo-7-hydroxy-4-methylcoumarin	498	[99]

Benzenemethanol-based photobase generators were analyzed in detail by Fréchet and coworkers. It was shown that especially the photobase generator including 2,6-dinitrobenzenemethanol[87] has the highest quantum yield and therefore is favored for photolytic experiments.

The synthesis of a coumarin[99] protected photobase generator includes several steps as selenium oxide-based oxidation and final carbamate formation with an isocyanate[98]. Together with 3,5-dimethoxy-2-nitrobenzenemethanol, these two chromophoric groups were converted in their photobase generators by introducing a triethoxysilane moiety. By combining the carbamate with a triethoxysilane moiety, it was possible to incorporate the photobase generators on silicon wafer surfaces[100] The λ_{max} value of the two photobase generators differs between 345 nm and 412 nm, therefore the creation of a photosystem with "two independent wavelength-selective functional levels" was

possible. Using a Polychrome V system, it was possible to irradiate the samples with two monochromatic wavelengths (345, and 412 nm) and to customize a photolithographical pattern in a two steps approach (Figure 1.17 a). After the light irradiation with the first monochromatic wavelength, deprotected amines were assembled with fluorescent dye, before the second monochromatic wavelength was applied, followed by assemble with a second fluorescent dye. The result is a pattern, indicating that the two photobase generators were successfully cleaved selectively (Figure 1.17 b). These data are promising results for the proposed photoinitiated NCA ROPs, since assembly with fluorescent dye is the proof of primary amine accessibility on silicon wafers. The presence of the primary amines can act as nucleophilic initiator causing a polymerization reaction according to the NAM mechanism.

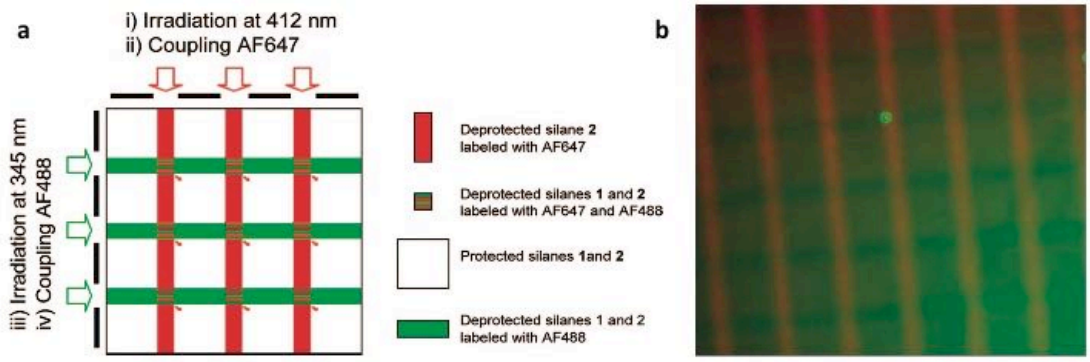

Figure 1.17: Set-up of a photosystem with two independent wavelengths to photo cleaves silane based photobase generator **1,** 3,5-dimethoxy-2-nitrobenzenemethanol, and **2**, 7-*N*,*N*-Diethylamino-4-hydroxymethyl coumarin. (a) Schematic pattern, (b) fluorescent microscope images of the substrate. After the first light irradiation at 412 nm, the deprotected amines were assembled with the fluorescent dye AF647. After the second irradiation at 345 nm, the deprotected amines were assembled with the fluorescent dye AF488[100].

1.6 Aim of this thesis

The aim of this thesis is to demonstrate a successful photoinitiated NCA ROP by photobase generators. This should include a selective photo-triggered initiation, since it is believed that light irradiation could also cause side reactions in this polymerization approach. Moreover, it should be demonstrated that the NCA photopolymerisation process can be utilized to make advanced materials either by surface polymerization or complex polymer architectures. According to these aims the thesis is structured into the following chapters.

In Chapter 2 the focus is on the proof of principle of photoinitiated NCA ROP. 2,6-dinitrobenzylcyclohexylcarbamate is chosen, since it is known to have the highest quantum yield in photocleavage. A further optimization of the photosystem with 4,5-

dimethoxy-2-nitrobenzylcyclohexylcarbamate is used for significant reduction of side reactions. MALDI-Tof-MS are performed for end-group analysis of the polymer chains, while Real-Time FT-IR monitors NCA ROP by following monomer consumption and polymer creation. Photo-initiated polymerization of both poly(benzyl-L-glutamate) and poly(Tfa-L-lysine) are investigated to demonstrate that photo-initiated NCA ROP can be performed for different monomers.

Chapter 3 discusses the influence of two factors, the irradiation time and the light intensity, on the photo-triggered NCA ROP. Gel permeation chromatography analysis is performed on all polypeptide products, obtained by varying the irradiation time from 5 – 60 minutes, as well the light source distances from 2 – 20 cm. In addition, a hybrid block copolymer is synthesized using hydrophobic poly(dimethylsiloxane)-based photobase generator as macroinitiator.

Applications of the novel photo-initiation system can be found in Chapter 4. Photo-initiated grafting of poly(benzyl-L-glutamate) is performed from spherical substrates (silica nanoparticles), as well as from planar substrate (silicon wafer). A number of analysis methods was applied to verify successful grafting, including thermalgravimetric analysis, UV-Vis spectroscopy, dynamic light scattering, contact angle measurements, and ellipsometry, but also elemental analysis as X-ray photoelectron spectroscopy and time-of-flight secondary ion mass spectroscopy.

Chapter 5 focuses on the synthesis of a novel amphiphilic block copolypeptide, poly(benzyl-L-glutamate)-*b*-Poly(L-arginine). The polypeptide is obtained by the synthesis of a precursor block-copolypeptide, followed by four modification steps. Final self-assembly into a nanoparticle macromolecule is investigated by dynamic light scattering and transmission electron microscopy. In addition, the chapter discusses the formation of the block copolypeptide by initiation with a carboxylic acid- and side chain-protected serine amino acid for potential *graft onto* approaches on solid nanoparticles.

1.7 References

[1] E. D. Korn, *Science* **1966**, *153*, 1491-1498.
[2] G. A. Di Lullo, S. M. Sweeney, J. Körkkö, L. Ala-Kokko and J. D. San Antonio, *Journal of Biological Chemistry* **2002**, *277*.
[3] T. B. Tomasi and H. M. Grey, *Prog Allergy* **1972**, *16*, 81-213.
[4] Q. Huang, H. Y. Yu and Q. Ru, *Journal of Food Science* **2009**, *75*, 50 - 57.
[5] S. H. Bakhru, S. Furtado, A. P. Morello and E. Mathiowitz, *Adv Drug Deliv Rev* **2013**, *65*, 811-821.
[6] R. B. Merrifield, *Journal of the American Chemical Society* **1963**, *85*, 2149-&.
[7] M. Amblard, J. A. Fehrentz, J. Martinez and G. Subra, *Mol Biotechnol* **2006**, *33*, 239-254.
[8] D. A. Tirrell, M. J. Fournier and T. L. Mason, *MRS Bull.* **1991**, *16*, 23.
[9] H. Leuchs, *Berichte Der Deutschen Chemischen Gesellschaft* **1906**, *39*, 2641-2643.
[10] T. Curtius and W. Sieber, *Ber. Dtsch. Chem. Ges. B* **1921**, *54*, 1430-1437.
[11] a) T. Curtius and W. Sieber, *Ber. Dtsch. Chem. Ges. B* **1922**, *55*, 1543-1558; b) T. Curtius, K. Hochschwender, H. Meier, W. Lehmann, A. Benckiser, M. Schenck, W. Wirbatz, J. Gaier and W. Müllhäusser, *J. Prakt. Chem.* **1930**, *125*, 211-302.
[12] F. Wessely, *Z. Physiol. Chem.* **1925**, *146*, 72-90.
[13] F. Wessely and F. Sigmund, *Z. Physiol. Chem.* **1926**, *159*, 102-119.
[14] a) F. Sigmund and F. Wessely, *Z. Physiol. Chem.* **1926**, *157*, 91-105; b) F. Wessely and J. Mayer, *Monatsh. Chem.* **1928**, *50*, 439-448.
[15] N. Hadjichristidis, H. Iatrou, M. Pitsikalis and G. Sakellariou, *Chem Rev* **2009**, *109*, 5528-5578.
[16] H. R. Kricheldorf, *Angew Chem Int Ed Engl* **2006**, *45*, 5752-5784.
[17] N. M. B. Smeets, P. L. J. van der Weide, J. Meuldijk, J. A. J. M. Vekemans and L. A. Hulshof, *Organic Process Research & Development* **2005**, *9*, 757-763.
[18] F. Cornille, J.-L. Copier, J.-P. Senet and Y. Robin in *Process for the preparation of amino acid N-carboxyanhydrides*, *Vol.* **2002**.
[19] T. J. Deming, *Nature* **1997**, *390*, 386-389.
[20] a) I. Dimitriov and H. Schlaad, *Chemical communications* **2003**, 2944 - 2945; b) W. Vayaboury, O. Giani, H. Cottet, A. Deratani and F. Schué, *Macromolecular rapid communications* **2004**, *25*, 1221- 1224.
[21] T. J. Deming, *Wiley Interdiscip Rev Nanomed Nanobiotechnol* **2014**, *6*, 283-297.
[22] A. C. Farthing and R. J. W. Reynolds, *Nature* **1950**, *165*, 647-647.
[23] F. Fuchs, *Berichte Der Deutschen Chemischen Gesellschaft* **1922**, *55*, 2943-2943.
[24] W. H. Daly and D. Poche, *Tetrahedron Letters* **1988**, *29*, 5859-5862.
[25] H. Eckert and B. Forster, *Angewandte Chemie-International Edition in English* **1987**, *26*, 894-895.
[26] A. C. Farthing, *Journal of the Chemical Society* **1950**, 3213-3217.
[27] A. Nagai, D. Sato, J. Ishikawa, B. Ochiai, H. Kudo and T. Endo, *Macromolecules* **2004**, *37*, 2332-2334.
[28] E. Peggion, Terbojev.M, A. Cosani and Colombin.C, *Journal of the American Chemical Society* **1966**, *88*, 3630-&.
[29] M. Goodmann and J. Hurtchison, *J. Am. Chem. Soc.* **1966**, *88*, 3627-3630.
[30] H. Lu and J. J. Cheng, *Journal of the American Chemical Society* **2007**, *129*, 14114-+.
[31] H. Lu and J. J. Cheng, *Journal of the American Chemical Society* **2008**, *130*, 12562-+.
[32] D. G. H. Ballard and C. H. Bamford, *Journal of the American Chemical Society* **1957**, *79*, 2336-2338.
[33] D. G. H. Ballard and C. H. Bamford, *Journal of the Chemical Society* **1956**, 381-387.
[34] H. R. Kricheldorf and R. Mulhaupt, *Makromolekulare Chemie-Macromolecular Chemistry and Physics* **1979**, *180*, 1419-1433.
[35] M. A. Alousi, L. A. Ballard, J. V. Reilly and S. S. Alousi, *Acta Cytologica* **1967**, *11*, 132-&.

[36] M. Rothe and D. Mühlhausen, *Angewandte Chemie* **1976**, *88*, 338-339.
[37] T. J. Deming, *Nature* **1997**, *390*, 386-389.
[38] Y.-L. Peng, S.-L. Lai and C.-C. Lin, *Macromolecules* **2008**, *41*, 3455 - 3459.
[39] G. J. M. Habraken, M. Peeters, C. H. J. T. Dietz, C. E. Koning and A. Heise, *Polymer Chemistry* **2010**, *1*, 514 - 524.
[40] J. Li, S. Xu, J. Zheng, Y. Pan, J. Wang, L. Zhang, X. He and D. Liu, *European Polymer Journal* **2012**, *48*, 1696 - 1708.
[41] T. Xing, B. Lai and Y. L., *Macromolecular Chemistry and Physics* **2013**, *214*, 578 - 588.
[42] Y. Shen, X. Fu, W. Fu and Z. Li, *Chem Soc Rev* **2015**, *44*, 612-622.
[43] Y. Kuroyanagi, K.-Y. Kim, M. Seno and T. Kawai, *Polymer Chemistry* **1983**, *21*, 1289 - 1303.
[44] H. R. Kricheldorf and D. Mueller, *Macromolecules* **1983**, *16*, 615 - 623.
[45] M. Yu, A. P. Nowak and T. J. Deming, *J. Am. Chem. Soc.* **1999**, *121*, 12210 - 12211.
[46] Z. Li and T. J. Deming, *Soft Matter* **2010**, *6*, 2546 - 2551.
[47] Z. Tian, M. Wang, A. Y. Zhang and Z. G. Feng, *Polymer* **2008**, *49*, 446 - 454.
[48] K. Miyata, R. J. Christie and K. Kataoka, *Reactive & Functional Polymers* **2011**, *71*, 227 - 234.
[49] H. Arimura, Y. Ohaya and T. Ouchi, *Macromolecular rapid communications* **2004**, *25*, 743 - 747.
[50] J. Rao, Z. Luo, Z. Ge, H. Liu and S. Liu, *Biomacromolecules* **2007**, *8*, 3871 - 3878.
[51] J. Jacobs, N. Gathergood and A. Heise, *Macromolecular rapid communications* **2013**, *34*, 1325 - 1329.
[52] R. P. Johnson, Y.-I. Jeong, E. Choi, C.-W. Chung, D. H. Kang, S.-O. Oh, H. Suh and I. Kim, *Advanced Functional Materials* **2012**, *22*, 1058 - 1068.
[53] T. Stukenkemper, A. Dose, M. Caballo Gonzalez, A. J. Groenen, S. Hehir, V. Andres-Guerrero, R. Herrero Vanrell and N. R. Cameron, *Macromol Biosci* **2015**, *15*, 138-145.
[54] D. J. Bharali, I. Kleijbor, E. K. Stachowiak, P. Dutta, I. Roy, N. Kaur, E. J. Bergey, P. N. Prasad and M. K. Stachowiak, *Proceedings of the National Academy of Sciences of the United States of America* **2005**, *102*, 11539 - 11544.
[55] C. M. Stafford, A. Y. Fadeev, T. P. Russell and T. J. McCarthy, *Langmuir* **2001**, *17*, 6547 - 6552.
[56] J. Song, H. Kong and J. Jang, *Chemical communications* **2009**, 5418 - 5420.
[57] T. Borase, M. Iacono, S. I. Ali, P. D. Thornton and A. Heise, *Polymer Chemistry* **2012**, *3*, 1267.
[58] A. Cervadoro, M. Cho, J. Key, C. Cooper, C. Stigliano, S. Aryal, A. Brazdeikis, J. F. Leary and P. Decuzzi, *J. Am. Chem. Soc.* **2014**, *6*, 12939 - 12946.
[59] S. A. Corr, J. Byrne, R. Tekoriute, C. J. Meledandri, D. F. Brougham, M. Lynch, C. Kerskens, L. O'Dwyer and Y. K. Gun'ko, *J. Am. Chem. Soc.* **2008**, *130*, 4214 - 4215.
[60] T. Borase, T. Ninjbadgar, A. Kapetanakis, S. Roche, R. O'Connor, C. Kerskens, A. Heise and D. F. Brougham, *Angewandte Chemie-International Edition* **2013**, *52*, 3164 - 3167.
[61] J. Rühe, *J. Nachr. Chem. Tech. Lab.* **1994**, *42*, 1237.
[62] M. Knichel, P. Heiduschka, W. Beck, G. Jung and W. Göpel, *Sensors and Actuators B: Chemical* **1995**, *28*, 85 - 94.
[63] B. F. Levine and C. G. Bethea, *Journal of Chemical Physics* **1976**, *65*, 1989.
[64] S. Machida, T. I. Urano, K. Sano, K. Sunohara, K. Sasaki, M. Yoshiki and Y. Mori, *Langmuir* **1995**, *11*, 4838 - 4843.
[65] T. Borase and A. Heise, *Advanced Materials* **2016**, *28*, 5725 - 5731.
[66] S. H. Wibowo, A. Sulistio, E. H. Wong, A. Blencowe and G. G. Qiao, *Chem Commun (Camb)* **2014**, *50*, 4971-4988.
[67] Y. C. Chang and C. W. Frank, *Langmuir* **1996**, *12*, 5824 - 5829.
[68] A. Heise, H. Menzel, H. Yim, R. H. Wieringa, A. J. Schouten, V. Erb and M. Stamm, *Langmuir* **1997**, *13*, 723 - 728.
[69] J. Wang, M. I. Gibson, R. Barbey, S.-J. Xiao and H.-A. Klok, *Macromolecular rapid communications* **2009**, *30*, 845 - 850.

[70] H. F. Gruber, *Progress in Polymer Science* **1992**, *17*, 953 - 1044.
[71] H. J. Hagemann, *Progress in Organic Coatings* **1985**, *13*, 123 - 150.
[72] R. C. Bailey and J. T. Hupp, *Anal Chem* **2003**, *75*, 2392 - 2398.
[73] D. J. Beebe, J. S. Moore, Q. Yu, R. H. Liu, M. L. Kraft, B.-H. Jo and C. Devadoss, *Proceedings of the National Academy of Sciences of the United States of America* **2000**, *97*, 13488 - 13493.
[74] N. Nath and A. Chilkoti, *Advanced Materials* **2002**, *14*, 1243 - 1247.
[75] P. J. Campagnola, D. M. Delguidice, G. A. Epling, K. D. Hoffacker, A. R. Howell, J. D. Pitts and S. L. Goodman, *Macromolecules* **2000**, *33*, 1511 - 1513.
[76] T. F. Scott, B. A. Kowalski, A. C. Sullivan, C. N. Bowman and R. R. McLeod, *Science* **2009**, *324*, 913 - 917.
[77] a) B. Amit, U. Zehavi and A. Patchorn, *Journal of Organic Chemistry* **1974**, *39*, 192 - 196; b) U. Zehavi, *Advances in Carbohydrate Chemistry and Biochemistry* **1988**, *46*, 179-204.
[78] K. Mizoguchi and E. Hasegawa, *Polymers for Advanced Technologies* **1996**, *7*, 471-477.
[79] J. B. Yoo, S.-W. Park, H. N. Kang, H. S. Mondkar, K. Sohn, H.-M. Kim, K.-B. Kim and H. Lee, *Polymer* **2014**, *55*, 3599 - 3604.
[80] J. F. Cameron and J. M. J. Frechet, *Journal of Organic Chemistry* **1990**, *55*, 5919-5922.
[81] J. F. Cameron and J. M. J. Fréchet, *Journal of Photochemistry and Photobiology a-Chemistry* **1991**, *59*, 105 - 113.
[82] J. Lalevee, X. Allonas, J. P. Fouassier, H. Tachi, A. Izumitani, M. Shirai and M. Tsunooka, *Journal of Photochemistry and Photobiology a-Chemistry* **2002**, *151*, 27-37.
[83] A. M. Sarker, Y. Kaneko and D. C. Neckers, *Journal of Photochemistry and Photobiology a-Chemistry* **1999**, *121*, 83-90.
[84] A. Patchornik, B. Amit and R. B. Woodward, *J. Am. Chem. Soc.* **1970**, *92*, 6333 - 6335.
[85] E. Reichmanis, C. W. Wilkins and E. A. Chandross, *Journal of Vacuum Science & Technology* **1981**, *19*, 1338.
[86] H. Barzynski and D. Sänger, *Macromol. Mater. Eng.* **1981**, *93*, 131 - 141.
[87] J. F. Cameron and J. M. J. Frechet, *Journal of the American Chemical Society* **1991**, *113*, 4303-4313.
[88] J. E. Beecher, J. F. Cameron and J. M. J. Frechet, *Journal of Materials Chemistry* **1992**, *2*, 811-816.
[89] H. Lutz, E. Breheret and L. Lindqvist, *The Journal of Physical Chemistry* **1973**, *77*, 1758 - 1762.
[90] J. F. Cameron, J. M. J. Fréchet, M.-K. Leung, C.-P. Niesert, S. A. MacDonald and C. G. Willson in *Photoresist composition with photosensitive base generator Vol. 5,545,509* USA, **1996**.
[91] K. H. Chae, J. C. Gwark and T. Chang, *Macromolecular rapid communications* **2000**, *21*, 1007 -1012.
[92] A. Del Campo, D. Boos, H. W. Spiess and U. Jonas, *Angewandte Chemie-International Edition* **2005**, *44*, 4707 - 4712.
[93] G. W. Kabalka, N. K. Reddy and C. Narayana, *Tetrahedron Letters* **1993**, *34*, 7667 - 7668.
[94] C. Birr, W. Lochinger, G. Stahnke and P. Lang, *Liebigs Ann. Chem.* **1972**, *763*, 162 - 172.
[95] K. Suyama, S. Nakao and M. Shirai, *Journal of Photopolymer Science and Technology* **2005**, *18*, 141 - 148.
[96] G. Bucher, J. C. Scaiano, R. Sinta, G. Barclay and J. Cameron, *J. Am. Chem. Soc.* **1995**, *117*, 3848 - 3855.
[97] M. Kessler, R. Glatthar, B. Giese and C. G. Bochet, *Org. Lett.* **2003**, *5*, 1179 - 1181.
[98] V. R. Shembekar, Y. Chen, B. K. Carpenter and G. P. Hess, *Biochemistry* **2005**, *44*, 7107 - 7114.

[99] T. Furuta, S. S.-H. Wang, J. L. Dantzker, T. M. Dore, W. J. Bybee, E. M. Callaway, W. Denk and R. Y. Tsien, *Proceedings of the National Academy of Sciences of the United States of America* **1999**, *96*, 1193 - 1200.
[100] P. Stegmaier, J. M. Alonso and A. D. Campo, *Langmuir* **2008**, *24*, 11872-11879.

2. Photo-initiated polymerization of N-carboxyanhydrides

2.1 Introduction

An approach that has not been explored to date is light-induced polymerization of NCAs. A successful development would open up, for the first time, the possibility of exploiting spatially controlled lithographic methods to prepare functional polypeptide-grafted surface features in the sub 100 nm size ranges for next-generation bio-interfaces and nano-fluidics. The digital nature of the initiation stimulus could also be exploited in any number of spatially challenging *in situ* technological applications requiring amino acid NCA polymerization once light can be introduced, e.g. by optical fiber. The potential of light-induced NCA polymerization could be analogous to that realized in vinyl polymerization, where UV-induced processes have created significant (commercial) impact from coatings to nano-lithography[1]-[3]. Conventional photopolymerization systems are mainly based on either cationic or radical polymerizations. In radical polymerization, the light beam excites the initiator, resulting in the formation of the initiating radical. This principle has been applied broadly from coatings to biomedical materials. It has further been used to produce structured surfaces and three-dimensional objects by stereolithography[1]-[3]. Most recently, photoinitiation has also been added to the techniques of controlled radical[4]-[8] and ring-opening polymerisations (ROP) of lactones[9]. These techniques have been utilised to fabricate three-dimensional (nano) objects and patterned surfaces as well as well-defined macromolecular structures.

Either a nucleophile or a base initiates the conventional NCA ROP polymerizations. A successful photoinitiation of NCAs would require the light-triggered formation of a nucleophile, preferably a primary amine. Such compounds have been pioneered by Cameron and Fréchet as photobase generators in microlithography[10],[11]. They are based on carbamate containing photo cleavable products such as nitrobenzyl compounds[12]. Unlike conventional photoreactions such as acrylate curing in which the monomers form a reactive diluent so that the reaction can be performed in bulk, a light induced polymerization of NCAs would require the presence of a reaction medium in which monomer and initiator are dissolved. Ideally, an aprotic, polar solvent with its UV cut-off should not interfere with the absorption of the photoinitiator to guarantee the maximum energy transfer from the light source on the photoinitiator. It is crucial to determine a suitable system, which satisfies

ideal conditions for both, a light-triggered formation of a nucleophile, and a controlled NCA ROP polymerization.

In this chapter, we report the first example of UV-initiated polymerization of NCAs. The particular emphasis of this initial work was the proof of concept and the demonstration that the initiation process is selective and the polymers are structurally well defined.

2.2 Experimentals

Materials

2,6-Dinitrobenzaldehyde 98%, cyclohexyl isocyanate 98%, α-pinene, benzyl-L-glutamate, triphosgene, methyllithium solution (1,6 M in diethyl ether), sodium borohydride, sodium hydroxide, trans-2-[3-(4-tert-butylphenyl)-2-methyl-2-propenylidene]malononitrile (DCTB), magnesium sulfate, and 1-Methyl-2-pyrrolidinone were purchased from Sigma-Aldrich. Tfa-L-lysine was supplied by Novabiochem, N,N-Dimethylformamide (dry, septa) was purchased from Merck, and 2-Isopropylthioxanthone was supplied by TCI chemicals. THF, Ethyl acetate and n-heptane were inhibitor-free and collected from an SPS-800 solvent purification system, equipped with a mole sieve and Al2O3 column.

General methods

Samples for absorption measurement were dissolved in acetonitrile and measured in quartz cuvettes with a path length of 10 mm. The spectra were measured on a PerkinElmer Lamda 35 UV/Vis spectrophotometer. The absorption range was set from 200 – 800 nm, slit width 2 nm, scan speed 480 nm min-1, lamp change at 326 nm. Data were analyzed by PerkinElmer UV WinLab software.

Photo-induced polymerizations were carried in NMP under stirring. The reactions were carried out in a quartz cuvette with a path length of 10 mm (Quartz SUPRASIL®, Hellma Analytics) with 0,02 mol eq. and 0,01 mol eq. of photoamine generator and sensitizer, respectively. Negative controls, in absence of UV irradiation were carried out in glass Schlenk tubes. As light source (254 nm) the H-bulb lamp (Nordson, UV MAC) was used.

Matrix assisted laser desorption/ionization-time of flight-mass spectroscopy (MALDI-ToF-MS) was carried out on an ultrafleXtreme™ MALDI-TOF/TOF-MS (Bruker Daltonics, Bremen, Germany). The system features a frequency-tripled Nd:YAG laser, producing a wavelength of 355 nm and a 2 kHz repetition rate (Smartbeam-II™). flexControl (Bruker Daltonics) software was used for data acquisition. As matrix material DCTB (20 mg ml^{-1}) was used. Potassium trifluoroacetic acid (KTFA) was added as cationic ionization agent (10 mg ml^{-1}). Poly(ethylene glycol) (Mw 1.000, 2.500, 5.000, 10.000) was used as reference. The polymer material was dissolved in HFIP or THF (10 mg ml^{-1}). Matrix material, ionization agent and polymer sample were mixed (20:1:3) and placed on the target steal plate. The solvent was vaporized before measurement.

Size exclusion chromatography (SEC) was performed on a system equipped with a Waters 2414 refractive index detector (40 °C), PSS PFG guard column followed by a 2PFG-linear-XL (7 µm, 8 x 300 mm) columns in series at 40 °C, Waters 1515 isocratic HPLC pump, and a Waters 2707 autosampler. HFIP in presence of potassium trifluoroacetate (3 g L^{-1}) was used as eluent at a flow rate of 0.8 ml min^{-1}. Poly(methyl methacrylate) was used as standards (Polymer Laboratories MP = 580 Da up to MP = 7.1 x 106 Da).

FT-IR was measured on a PerkinElmer Spectrum 100 FT-IR Spectrometer, equipped with a Universal ATR Sampling Accessory. Spectra were analyzed with the PerkinElmer Spectrum software, version 10.5.2. Data were collected from wavenumber 4000 – 650 cm^{-1}, 4 scans per sample.

Real-time infrared spectroscopy was performed on a Bruker Vertex 70 spectrometer equipped with a GladiATR accessory (PIKR technologies). Samples were irradiated by a Dr. Hönle Bluepoint 4 UVC light source. The light guide (UVC 8mm/1,5m) was positioned directly above the ATR crystal by an adjustable holder, with a distance of 1,0 cm.

Synthesis

Synthesis of γ-benzyl-L-glutamate (BLG) N-carboxyanhydride

γ-benzyl-L-Glutamic acid (4,8 g, 20,2 mmol) was transferred into a already preflashed 3-neck round bottom flask. 30 ml of anhydrous THF was added and stirred under nitrogen flow at 60 °C. Alpha-pinene (9.64 ml, 60,7 mmol) was added to the suspension. Triphosgene (3,48 g, 11.7 mmol) was dissolved in 20 ml of anhydrous THF, transferred into a funnel and added drop wise to the reaction mixture. The suspension was stirred under nitrogen atmosphere at 60 °C under reflux until it turned into a clear yellowish solution (~3 hours). The solution was concentrated to 2/3 by vacuum evaporation before 50 ml of anhydrous n-heptane was added for crystallization. The NCA was recrystallized twice, dried under vacuum and stored under -20 °C for further use. Yield 3.833 g, 14,56 mmol, 72 %.

^{1}H-NMR (300 MHz, $CDCl_3$, δ, ppm): 2,11 (m, 1H, CHCH_2), 2,24 (m, 1H, CHCH_2), 2,56 (t, 2H, OCOCH_2, J = 6,87 Hz), 4,35 (t, 1H, CHCH_2, J = 6,03 Hz), 5,12 (s, 2H, ArCH_2), 6,56 (broad, s, 1H, NH), 7,33 (m, 5H, ArH). ATR-IR (cm^{-1}): 3334, 1881 (C=O amide), 1782 (C=O anhydride), 1720 (C=O ester), 1397, 1252, 1188, 931, 737.

Synthesis of 5-tert-O-butyl L-glutamate (TLG) N-carboxyanhydride

5-tert-O-butyl L-glutamic acid (3,0 g, 14,76 mmol) was transferred into an already preflashed 3-neck round bottom flask. 20 ml of anhydrous ethyl acetate was added and stirred under nitrogen flow at 65 °C. Alpha-pinene (14,06 ml, 89 mmol) was added to the suspension. Triphosgene (2,54 g, 8,56 mmol) was dissolved in 10 ml of anhydrous ethyl acetate, transferred into a funnel and added drop wise to the reaction mixture. The suspension was stirred under nitrogen atmosphere at 65 °C under reflux until it turned into a clear yellowish solution (~3 hours). The solvents were vaporized under vacuum and taken over into hexane. It was heated up to 50 °C, before 1/3 of hexane volume of dichloromethane was added to turn the suspension into a clear solution. This procedure was repeated for recrystallization once more to obtain the white pure product. Yield 1,52 g, 6,65 mmol, 45 %.

^{1}H-NMR (300 MHz, $CDCl_3$, δ, ppm): 1,43 (s, 9H CH_3), 2,04 (m, 1H, CHCH_2), 2,23 (m, 1H, CHCH_2), 2,44 (t, 2H, OCOCH_2, J = 6,68 Hz), 4,34 (t, 1H, CHCH_2, J = 5,88 Hz), 6,36 (broad, s, 1H, NH). ATR-IR (cm^{-1}): 3338, 1859 (C=O amide), 1792 (C=O anhydride), 1696 (C=O ester), 1455, 1370 (C-H methyl), 1098, 923, 739 cm^{-1}

Synthesis of Nε-trifluoroacetyl-L-lysine N-carboxyanhydride

Nε-Trifluoroacetyl-L-lysine (3,0 g, 12,39 mmol) was transferred into an already preflashed 3-neck round bottom flask. 40 ml of anhydrous ethyl acetate was added and stirred under nitrogen flow at 105 °C. Alpha-pinene (4,13 ml, 26,0 mmol) was added to the suspension. Triphosgene (1,838 g, 6,19 mmol) was dissolved in 10 ml of anhydrous ethyl acetate, transferred into a funnel and added drop wise to the reaction mixture. The suspension was stirred under nitrogen atmosphere at 105 °C under reflux until it turned into a clear yellowish solution (~3,5 hours). The solution was concentrated to 2/3 by vacuum evaporation before anhydrous n-heptane was added for crystallization. The NCA was recrystallized twice, dried under vacuum and stored under -20 °C for further use. Yield 1,42 g, 5,32 mmol, 43%.

^{1}H-NMR (300 MHz, DMSO, δ, ppm): 1,36 (m, 2H, CHCH_2), 1,49 (m, 2H, CHCH*2*CH_2), 1,73 (m, 2H, NHCH_2CH_2), 3,17 (q, 2H, NHCH_2, *J* = 6,24 Hz), 4,43 (t, 1H, CHCH_2, *J* = 5,88 Hz), 9,09 (broad, s, 1H, NHCO), 9,42 (broad, s, 1H, NHCH). ATR-IR (cm^{-1}): 3311, 2945, 1855 (C=O amide), 1777 (C=O anhydride), 1704, 1559, 1155 (C-F), 919

Synthesis of β-tert-O-butyl-L-aspartic acid N-carboxyanhydride

β-tert-O-butyl-L-aspartic acid (2,0 g, 10,57 mmol) was transferred into a already preflashed 3-neck round bottom flask. 10 ml of anhydrous THF was added and stirred under nitrogen flow at 68 °C. Alpha-pinene (5,04 ml, 31,7 mmol) was added to the suspension. Triphosgene (1,82 g, 6,13 mmol) was dissolved in 5 ml of anhydrous THF, transferred into a funnel and added drop wise to the reaction mixture. The suspension was stirred under nitrogen atmosphere at 68 °C under reflux until it turned into a clear yellowish solution. Anhydrous n-heptane was added for crystallization. The NCA was filtrated and recrystallized twice to obtain the pure white crystal. Yield 1,901 g, 8,83 mmol, 84 %.

^{1}H-NMR (300 MHz, DMSO, δ, ppm): 1,38 (s, 9H, CH_3), 2,67 (dd, 1H, CHCH_2, J = 4,56 Hz, 17,46 Hz), 2,92 (dd, 1H, CHCH_2, J = 4,08 Hz, 17,44 Hz), 4,61 (t, 1H, C*H*CH2, J = 4,28 Hz), 8,99 (broad, s, 1H, N*H*). ATR-IR (cm^{-1}): 3246, 2970, 1845 (C=O amide), 1754 (C=O anhydride), 1715, 1370, 1233, 1098.

Synthesis of β-benzyl-L-aspartic acid N-carboxyanhydride

β-benzyl-L-aspartic acid (2,0 g, 8,96 mmol) was transferred into a already preflashed 3-neck round bottom flask. 25 ml of anhydrous THF was added and stirred under nitrogen flow at 68 °C. Alpha-pinene (8,54 ml, 53,8 mmol) was added to the suspension. Triphosgene (1,542 g, 5,20 mmol) was dissolved in 5 ml of anhydrous THF, transferred into a funnel and added drop wise to the reaction mixture. The suspension was stirred under nitrogen atmosphere at 68 °C under reflux until it turned into a clear yellowish solution. Anhydrous n-heptane was added for crystallization. The NCA was filtrated and recrystallized twice to obtain the pure white crystal. Yield 1,05 g, 4,23 mmol, 47 %.

^{1}H-NMR (300 MHz, DMSO, δ, ppm): 2,89 (dd, 1H, CHCH_2, J = 4.2 Hz, 17,86 Hz), 3,08 (dd, 1H, CHCH_2, J = 4,76 Hz, 17,84 Hz), 4,68 (t, 1H, C*H*CH2, J = 4,48 Hz), 5,12 (s, 2H, ArCH_2), 7,36 (m, 5H, Ar*H*). ATR-IR (cm^{-1}): 3305, 1831 (C=O amide), 1783(C=O anhydride), 1724 (C=O ester), 1496, 1398, 1108, 924, 749.

Synthesis of 2,6-dinitrobenzenemethanol

2,6-dinitrobenzaldehyde (0,5 g, 2,55 mmol) was added to a round bottle flask before methanol (25 ml) was added. The reaction mixture was stirred and warmed up in a 40 °C

water bath until the whole reagent was dissolved. The following reaction was hold into an ice bath.

Sodium borohydride (37,0 mg, 0,981 mmol) was dissolved in a 0,2 M aqueous solution of sodium hydroxide (1,6 ml) before it was added drop wise to the reaction mixture. The reaction mixture turned from light yellow to dark purple and was stirred in the ice bath for 1 hour, before it brought up to room temperature for another 2 hours. For the workup, the solvent was removed by rotor evaporation. In the following, 10 ml of H_2O was added and liquid and formed dark crystals were transferred into a separation funnel. An excess of diethyl ether was added and washed 3 times. The solvent was dried by $MgSO_4$ and vaporized. The brown crystals were recrystallized in chloroform to obtain the yellow crystals of 2,6-dinitrobenzenemethanol. Yield 0.441 g, 2,226 mmol, 87 %.

^{1}H-NMR (300 MHz, $CDCl_3$, δ, ppm): 2,58 (broad, s, 1H, O*H*), 4,93 (s, 2H, CH_2OH), 7,64 (t, 1H, p-Ar*H*, *J* = 8,16 Hz), 8,08 (d, 2H, m-Ar*H*, *J* = 8,16 Hz). ^{13}C-NMR: (100MHz, $CDCl_3$, δ, ppm): 57,08 (1C), 128,29 (1C), 129,74 (3C), 151,01 (2C). ATR-IR (cm^{-1}): 3525, 3418 (O-H, alcohol), 3083, 1608, 1579 (aromatic), 1524, 1350 (N-O nitro), 1024, 891

Synthesis of 2,6-dinitrobenzyl cyclohexylcarbamate 2.1

2,6-dinitrobenzenemethanol (0,4 g, 2,02 mmol) was dissolved in anhydrous tetrahydrofuran (7 ml) at room temperature under nitrogen atmosphere. An ethereal solution of methyllithium (1,6 M, 0,126 ml, 0,202 mmol) was added drop wise to the reaction solution and was stirred under these condition for 4 hours. The reaction mixture then was treated drop wise with cyclohexylisocyanate (0,258 ml, 2,02 mmol) diluted in THF (5 ml) and stirred under reflux at 68 °C for 12 hours, cooled to room temperature and concentrated under vacuum. The residues was washed several times in ether and water, dried with MgSO4 and concentrated under vacuum. The brown orange oil was transferred on a column for flash chromatography (ethyl acetate / hexane: 20 / 80). The solution mixture was vaporized and after recrystallization in diethyl ether:hexane 1:5 the yellow crystals were obtained. Yield 314,7 mg, 0,973 mmol, 48,2%.

^{1}H-NMR (300 MHz, $CDCl_3$, δ, ppm): 1,01 – 1,84 (m, 10H, p-, o-, m-cyclo*H*), 3,35 (m, 1H, NHC*H*), 4,52 (broad, s, 1H, N*H*), 5,50 (s, 2H, CH_2OC(O)), 7,61 (t, 1H, p-Ar*H*, *J* = 8,16 Hz), 7,98 (d, 2H, m-Ar*H*, *J* = 8,16 Hz). ^{13}C-NMR (100 MHz, $CDCl_3$, δ, ppm): 24.88 (cyclohexyl *C meta* to substituent), 25.56 (cyclohexyl *C*, *para* to substituent), 33.34 (cyclohexyl *C*, *ortho* to

substituent), 50.28 (cyclohexyl *C*, *ipso* to substituent), 58.36 (*C*H_2), 127.32 (ipso to $CH_2OC(O)$), 127.82 (para to $CH_2OC(O)$), 129.85 (meta to $CH_2OC(O)$), 151.11 (ipso to NO_2), 154.46 (*C*(O)) . ATR-IR (cm^{-1}): 3525, 3418 (O-H, alcohol), 3083, 1608, 1579 (aromatic), 1524, 1350 (N-O nitro), 1024, 891.

Synthesis of benzyl cyclohexylcarbamate 2.2

Benzyl alcohol (1 ml, 9,62 mmol) was diluted in 15 ml of acetonitrile and transferred into an already preflashed 3-neck round bottom flask. 1-methyl-1H-imidazole (0,066 ml, 0,804 mmol) was added via syringe and the reaction mixture was hold at room temperature while stirring. Cyclohexylisocyanate (1,02 ml, 7,99 mmol) was diluted into 5 ml of acetonitrile before it was added drop wise to the reaction mixture. It was stirred under nitrogen and at 37 °C for 14 hours.

The reaction mixture was tested on TLC before the solvent was vaporized. The crude oil was loaded on column (EOAc/Hep 5/2). The solvents were vaporized obtaining white crystals, benzyl cyclohexylcarbamate.

^{1}H-NMR (300 MHz, $CDCl_3$, δ, ppm): 1,07 – 1,96 (m, 10H, p-, o-, m-cyclo*H*), 3,51 (s, 1H, NHC*H*), 4,65 (broad, s, 1H, N*H*), 5,10 (s, 2H, CH_2OC(O)), 7,33 (m, 5H, Ar*H*).

NCA ring-opening polymerization

1.5 g of NCA was transferred into a preflashed Schlenk tube. The solid monomer was dissolved in DMF (5,7 molar), and 0,02 mol eq. cyclohexylamine was added. The reaction mixture was stirred under inert atmosphere for 3 hours and precipitated into an excess of diethyl ether, followed by two reprecipitation steps in THF / diethyl ether.

Real-time FTIR polymerization

NCAs of TLL (0.373 mmol) and BLG (0.38 mmol) were dissolved in NMP (1 ml) with 0,02 mol eq. photoamine generator and 0,01 mol eq. ITX sensitizer. Two drops of the reaction mixture were directly placed on the ATR crystal. Samples were covered by a quartz plate to prevent evaporation during irradiation. The sample was monitored 25 s by RT-IR, before irradiation for 35 s with a scan each 0.1 s. The polymerization was monitored for further 180 min., taking one scan per minute.

Photo-initiated polymerization for MALDI-ToF

100 mg of NCA was added to a quartz cuvette and 0,02 mol eq. 2,6-dinitrobenzylcyclohexylcarbamate 1 and 0,01 mol eq. 2-isopropylthioxanthone added. After complete dissolution in anhydrous NMP (0.181 molar), the cuvette was vertically exposed to the light source (H-bulb) for 2 min. under stirring. After irradiation, the samples were covered in aluminum foil, and stirred for 2 h at room temperature. The reaction mixture was added drop wise into an excess of diethyl ether for precipitation, followed by one precipitation step in THF / diethyl ether. The white solid product was filtrated and dried under vacuum.

2.3 Results and discussion

2.3.1 Selection of NCAs and photobase generators by initial screening experiments

A range of amino acid NCAs was synthesized as shown in Scheme 1. These were selected due to their different side groups in order to investigate their behavior in the light-induced polymerization. *γ*-benzyl-L-glutamate (BLG) is the most commonly used NCA monomer in NCA ROP, however it bears an aromatic ring in its side chain. Since it was believed that the absorption of the aromatic ring could interfere with the photoinitiation, also 5-*tert*-butyl-L-glutamate (TBA) NCA was synthesized that included a non-light-absorbing protecting group. Further diversity in the choice of NCA monomers was introduced by adding the aspartate analogous molecules. Introduction of variety in the polarity of the NCA monomers was achieved by successful synthesis of N_ε-trifluoroacetyl-L-lysine. All primary monomers for the polymerization of NCAs are synthesized by the same general procedure (Scheme 2.1) following the Fuchs-Farthing method[13]. The various side-chain protected amino acids were converted into the five-membered ring structures by the reaction with triphosgene in either THF or ethyl acetate. In this process the ring-formation is initiated by a nucleophilic attack of the primary amine on the triphosgene, that results in the consumption of triphosgene and the formation of HCl. Alpha-pinene acts as a HCl scavenger, taking up the hydrochloride side-product at the expense of the double bond in the six-membered ring. All NCA monomers were obtained as white crystals and purity was determined by NMR and ATR-FTIR analysis.

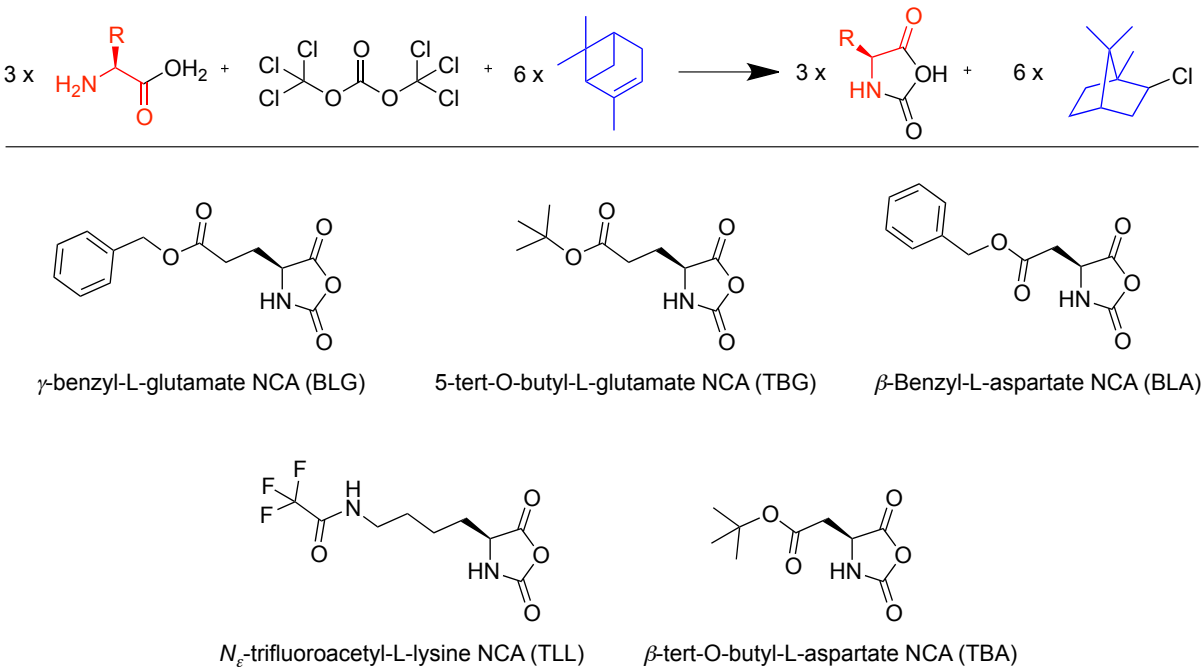

Scheme 2.1: Overall amino acid conversion into a five ring N-carboxyanhydride (NCA). Various NCAs were synthesized from different amino acids.

Either nucleophiles or basic compounds initiate the polymerization of NCA monomer into polypeptides. The majority of polypeptides reported in the literature are initiated by primary[14], secondary amines[15], or even by non-peptide synthetic polymers with an amine terminus[16]. This polymerization offers control over the molecular weight through the amine/NCA ratio as well as low polydispersity. It was hypothesized that the photogeneration of a primary amine in the presence of NCA could be utilized to achieve a polymerization following the same mechanism. Frechét and coworkers showed the photo-induced breakdown of a carbamate compound into products that bear primary amines such as cyclohexylamine. Therefore, different potential photoamine generators were synthesized (Scheme 2.2). The first two compounds **2.1** and **2.2** were anticipated to initiate a ring-opening polymerization via the NAM mechanism similar to conventional primary amines after the photo cleavage of the chromophoric protection group.

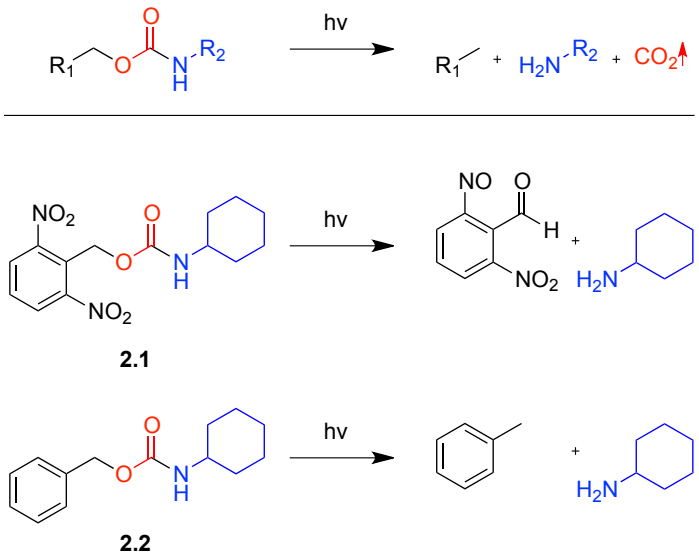

Scheme 2.2: Overall photo reaction and breakdown of carbamate compounds. Cleavage by light irradiation resulting in decarboxylation and formation of primary amines 2,6-dinitrobenzyl cyclohexylcarbamate (**2.1**) and benzyl cyclohexylcarbamate (**2.2**).

The first two photoamine generators were synthesized by the same route, where an isocyanate and alcohol are dissolved in acetonitrile. The isocyanate is nucleophilically attacked by a deprotonated alcohol in presence of the soft base 1-methyl imidazole. Both carbamates, **2.1** and **2.2** were synthesized in quantitative yield (Scheme 2.3). The shift and full disappearance of the α-CH_2 protons from the alcohol compound at 4.93 ppm to the carbamates at 5.5 and 5.1 ppm, respectively, confirmed successful carbamate formation. The resulting carbamate compounds can easily break down at CH_2-O- under UV irradiation due to the electron rich and chromophoric benzyl ring. Addition of electron withdrawing

groups (NO_2) in the *ortho* position, electron donating groups in the *meta* position influence the breakdown and quantum yield of the photo-cleavage effectively[11],[10].

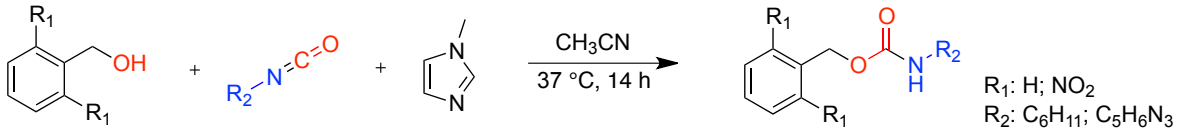

Scheme 2.3: Synthesis of a carbamate by the use of an alcohol and an isocyanate under basic conditions.

In the initial experiments, feasibility of the different NCA monomers were investigated for their ability to be converted into polypeptides in the presence of a conventional nucleophilic initiator, cyclohexylamine. The NCA to initiator ratio was set to 20 or 50, respectively. The NCA monomers were dissolved in anhydrous DMF, before the initiator was added. After a reaction time of 4 hours, FTIR analysis confirmed full conversion of the reactions, before it was precipitated in diethyl ether. Additional reprecipitation ensured complete purification of the polymer material. The solid products were dissolved in HFIP and analyzed by SEC. Polymerization of benzyl-L-glutamate (BLG) NCA showed a controlled conversion into its polypeptide poly(benzyl-L-glutamate) (PBLG) (Table 2.1) with a close agreement to the targeted molecular weight. Similar results were obtained in the polymerization of benzyl-protected aspartate (BLA) NCA with a low polydispersity, however the targeted molecular weight was not achieved. In contrast to the benzyl protected amino acid, controlled polymerization of the *tert*-butyl protected NCAs was barely achievable. After initiator addition the reaction precipitated, ruling out any controlled polymerization. The precipitate was removed from the reaction solution before any analysis was performed. Secondary structure formation at low degree of polymerization is presumed to have caused the precipitation.

Table 2.1: SEC results of NCA polymerization of PBLG, PTLG, PBLA, PTLA, and PTLL. All reactions were carried out for four hours, in presence of cyclohexylamine with various monomer:initiator ratios. After precipitation samples were measured by HFIP-SEC, calibrated with PMMA standard.

Polymer	M:I	M_n^{th} (g/mol)	M_n^{GPC} (g/mol)	*Đ*
Poly(benzyl-*L*-glutamate) (PBLG)	50	11,200	9,900	1,1
Poly(*tert*-butyl-*L*-glutamate) (PTLG)	20	3800	50400*	1.1*
Poly(benzyl-*L*-aspartate) (PBLA)	50	10350	6932	1.1
Poly(*tert*-butyl-*L*-aspartate) (PTLA)	20	3520	1561*	1.6*
Poly(Tfa-*L*-lysine) (PTLL)	20	2509	4334	1.6

* precipitation during reaction. This sample was filtrated before further work-up

Polymerization of Tfa-L-lysine was also achieved without any visual precipitation. The polydispersity is somewhat broader and there is some discrepancy from the targeted molecular weight but it has to be noted that the reaction conditions where not optimized. Based on the screening results BLG and TLL NCA were selected for the photopolymerisation experiments.

2.3.2 Light source emission vs. component absorption

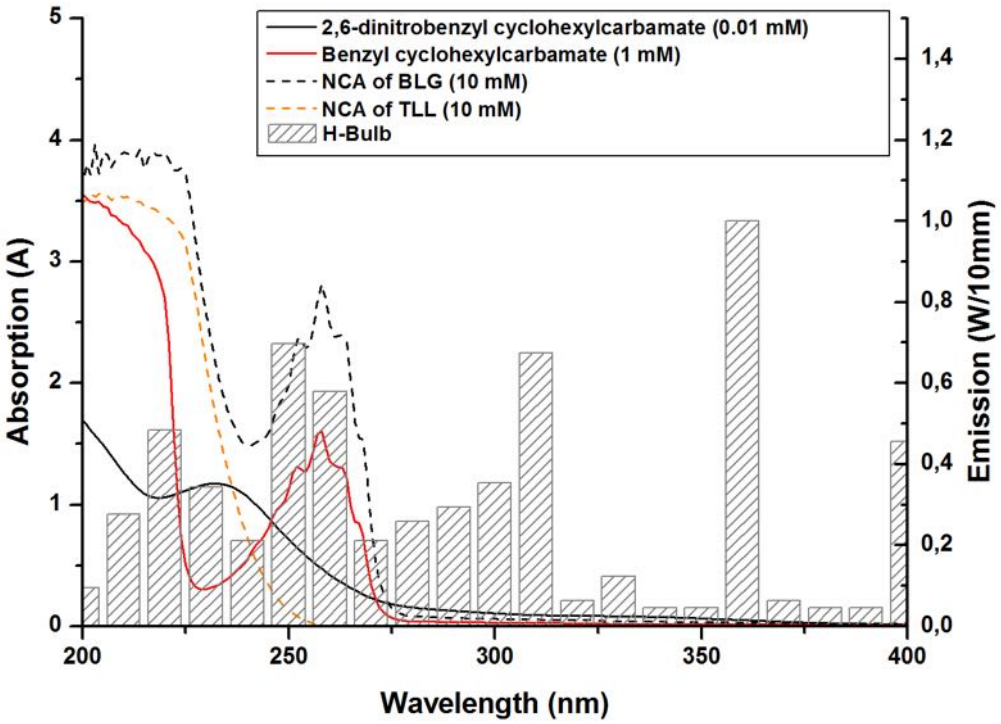

Figure 2.1: UV-Vis absorption spectra of two different photoamine generators, NCA monomers (BLG, TLL), and emission spectrum of the H blub lamp. All samples were dissolved in acetonitrile at different concentrations.

It is essential to introduce the light energy of the irradiated UV light source into the chemical reaction. Ideally, the emission of the light source should overlap with the absorption of the chromophore group of the photoamine generator. The emission of the H-bulb lamp has a broad emission band in deep UV, starting from 220 to 300 nm, as well as at 360 nm (Figure 2.1). For the absorption measurements the photoamine generators and TLL- and BLG-NCA were dissolved in acetonitrile due to its low UV cutoff (190 nm). Benzyl cyclohexylcarbamate and 2,6-dinitrobenzyl cyclohexylcarbamate have different chromophoric groups; therefore also their absorption maxima are different, at 258 and 232 nm respectively. The presence of the strongly electron withdrawing group NO_2 influence the electron occupancy in the aromatic ring and changes the absorbance maximum. For both investigated initiators a good overlap of their absorption spectra with the emission spectrum of the H-bulb lamp was found, which is believed to cause a breakdown of the photo-initiators into their corresponding nucleophilic breakdown product.

To investigate if the monomer could interfere with the light absorption of the photoamine generator, their absorption was measured as well. BLG-NCA with it benzyl ester in the side

chain shows an absorption maximum in the same wavelength range as benzyl cyclohexylcarbamate. In contrast, TLL does not include any chromophoric group and does not show any light absorbance in the crucial UV wavelength region, which might result in a more efficient photocleavage event and cleaner photopolymerization. However, since BLG is the most commonly used NCA monomer, it also will be considered in the following photopolymerization, next to TLL NCA.

2.3.3 Preliminary photoinitiator breakdown analysis

The key for a photo-induced ring opening polymerization is the release of primary amines as a breakdown product of the photoamine generator. As already depicted in Scheme 2.2, the breakdown follows a decarboxylation. This decarboxylation can be monitored by RT-IR spectroscopy since the decarboxylation should lead to a decrease of the carbamate carbonyl vibration. Therefore, carbonyl vibrations at 1682 cm^{-1} for benzyl cyclohexylcarbamate, and at 1714 cm^{-1} for 2,6-dinitrobenzyl cyclohexylcarbamate were monitored (Figure 2.2). For the measurement, the initiators **2.1** and **2.2** were dissolved in acetonitrile (7,7 and 10,1 mmolar, respectively). The cuvette was placed vertically under the H-bulb lamp. After every 30 s irradiation time, the cuvette was removed and one drop of the reaction mixture analyzed by ATR-FTIR. Then the cuvette was again placed under the H-bulb for further irradiation. This procedure was repeated until an irradiation time of 240 s was reached.

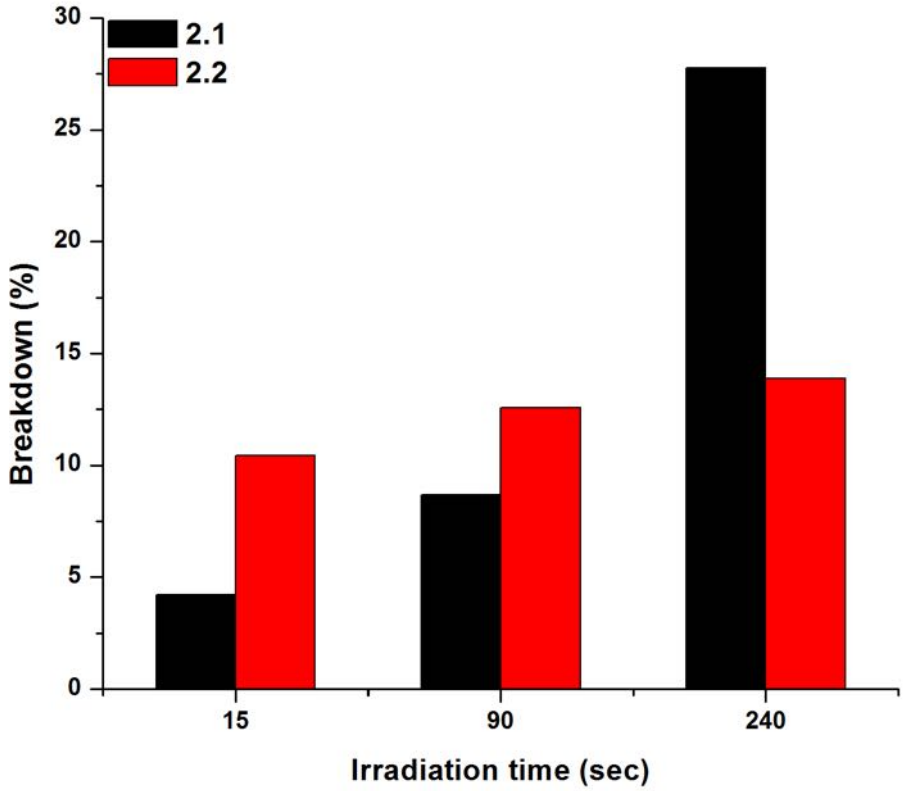

Figure 2.2: ATR-FTIR monitoring of the carbonyl vibration at 1714 cm^{-1} and 1682 cm^{-1} of the carbamate compounds **2.1** (black) and **2.2** (red), respectively, as a function in response of time. The peak integral at t=0 was used as reference and was set to zero. The reduction of the integral in time was compared to the reference to calculate the breakdown in percentage. The sample was measured after 15, 90, and 240 sec.

The breakdown percentage was calculated by dividing the integrated peak area of the respective diagnostic peak by the integrated peak area at t=0. It has to be noted that even incomplete breakdown of the photoamine generator might still achieve full conversion of the monomer into polymer material and is common in acrylate-based photo polymerizations[17]. In acrylate systems photoinitiation rate profiles revealed that breakdown rates are depending on the irradiation gradient and the thickness of medium, however, always reveal full conversion of the monomer. Photoinitiation is a result of the balance between bleaching rate and light attenuation degree of the light. Breakdown percentage of benzyl cyclohexylcarbamate (**2.2**) is observed at 10 % in the first 15 s, and with longer irradiation time, the breakdown process reaches 14% at 240 s. 2,6-Dinitrobenzyl cyclohexylcarbamate (**2.1)** shows an increased breakdown process: in the first 90 s a reduced breakdown is observed compared to **2.2**. However, after 240 s, a breakdown of 28% is monitored, which is twice the amount as **2.2** showed after this irradiation time. This significant increased breakdown percentage led to the decision to choose **2.1** for further photo-triggered experiments.

2.3.4 Solvent screening

Irradiation can cause a range of side reactions among the reaction components. Most prominent is the formation of radicals that can either directly or via secondary reactions create unwanted reaction species interfering with the polymerization. As one of the major components in the system, the solvent stability under those conditions is critical. While identifying side products of solvents under irradiation was beyond the scope of this project, in the first instance various organic solvents were screened for their general suitability in NCA ring-opening polymerization. DMF is by far the most established solvent in ring-opening polymerizations of NCA, because of its aprotic and polar nature thus preventing hydrogen bonding and secondary structure formation of the resulting polypeptide. Solvents with the same characteristics were selected and tested in model polymerizations using BLG-NCA and cyclohexylamine as initiator (Table 2.2). Suitable solvents were defined as those in which the polymer remained soluble during the polymerization.

Table 2.2: Different polar aprotic solvents that were used for polymerization of BLG using cyclohexylamine as initiator. In all reactions the same monomer:initiator ratio (20:1) was used.

Solvent	UV cutoff (nm)	Behavior of polymer
DMF	268	in solution
THF	212	precipitation
HFIP	n.n.	precipitation
Ethyl acetate	256	precipitation
Acetonitrile	190	precipitation
Dioxane	215	precipitation
Propylene Carbonate	220	precipitation
Methylpyrrolidone	285	in solution
Pyridine	390	precipitation

Unsurprisingly, the polymerization in DMF showed no precipitation. The same result was observed for methylpyrrolidone (NMP). DMF and NMP, on molecular level, have similar functional moieties. Adjacent to the tertiary amine, both molecules have a carbonyl group. The main difference of the molecules is the linear structure of DMF and the cyclic structure of NMP. All other solvents showed either precipitation before addition of the initiator or

shortly after the initiation of the polymerization. Therefore, it was obvious that only two solvent systems would be suitable for further investigations.

2.3.5 Photopolymerization of NCA using photoamine generator 2.1

The step from a conventional initiation system to a photo-cleavage initiation bears many risks of side reactions. Irradiating solvents such as DMF and NMP with their own UV absorption in the deep UV wavelength range could cause undesired radicals. These radicals could form various nucleophilic or basic species, which would result in an undesired, uncontrolled polymerization. Furthermore, thermal polymerizations of the monomer could also lead to a side reaction. It is known that NCA monomers can form cyclic oligopeptides, although at high temperature[18]. On the other hand, labile photoamine generators could break down without UV light absorption, leading to an initiation, independent of UV irradiation. Therefore, reaction optimization was approached systematically to undoubtedly prove the occurrence of a photoinduced process. The approach is based on different negative controls performed with each polymerization. Each reaction set consisted of four reaction samples that were performed for each photo-induced polymerization:

1) Monomer, in present of the **2.1**, with UV irradiation (denoted as +2.1/+UV)
2) Monomer, in absence of the **2.1**, with UV irradiation (denoted as -2.1/+UV)
3) Monomer, in presence of the **2.1**, without UV irradiation (denoted as +2.1/-UV)
4) Monomer, in absence of the **2.1**, without UV irradiation (denoted as -2.1/-UV)

If the polymerization is truly photo-triggered a polypeptide should only be obtained in experiment 1) (+1/+UV) while being absent in all negative controls (2-4).

The first set of polymerizations was performed with BLG-NCA as monomer, and **2.1** as photoamine generator in NMP. The sensitizer, 2-isopropylthioxanthone (ITX), was added to the reaction to overcome light cut-off of the solvent (Note: It was later found that the addition of a sensitizer had no effect on the polymerization). All polymerization reactions were carried out with an initiating UV exposure under a H-bulb lamp of 2 minutes at room temperature. After the reaction was continued for 24 hours in the dark, a sample was withdrawn from each reaction for attenuated total reflectance infrared (ATR-IR) measurements. This technique allows to distinguish between the NCA monomer and the polypeptide. While BLG-NCA is characterized by strong peaks at 1786 and 1853 cm^{-1} (C=O

groups of the anhydride), presence of poly(benzyl-L-glutamate) is evident from the polypeptide amide II peak at 1548 cm^{-1} in the polymer backbone[19]. Comparing the FTIR spectra in Figure 2.3A reveals the presence of strong NCA signals for all three negative controls, while in the +2.1/+UV experiment the intensity of these signals is significantly reduced. Coincidently, this sample also displays the characteristic amide II peak at 1548 cm^{-1}, which is absent in all negative controls. This provides clear evidence that NCA polymerization occurred in this sample and polypeptide was formed while that is not the case in the negative controls. To prove that the lack of NCA conversion in the negative control is due to the absence of an initiation process and the NCA is indeed still active, cyclohexylamine was added to those reactions. After additional stirring for one day, also in those samples NCA consumption and polymer formation was observed highlighted by the reduced vibration at 1853 cm^{-1} and the new appearance of vibrations at 1548 cm-1 (Figure 2.3B). The results clearly demonstrated a successful photo polymerization of BLG NCA, while in the absence of either light energy or initiator no polymerization was observed.

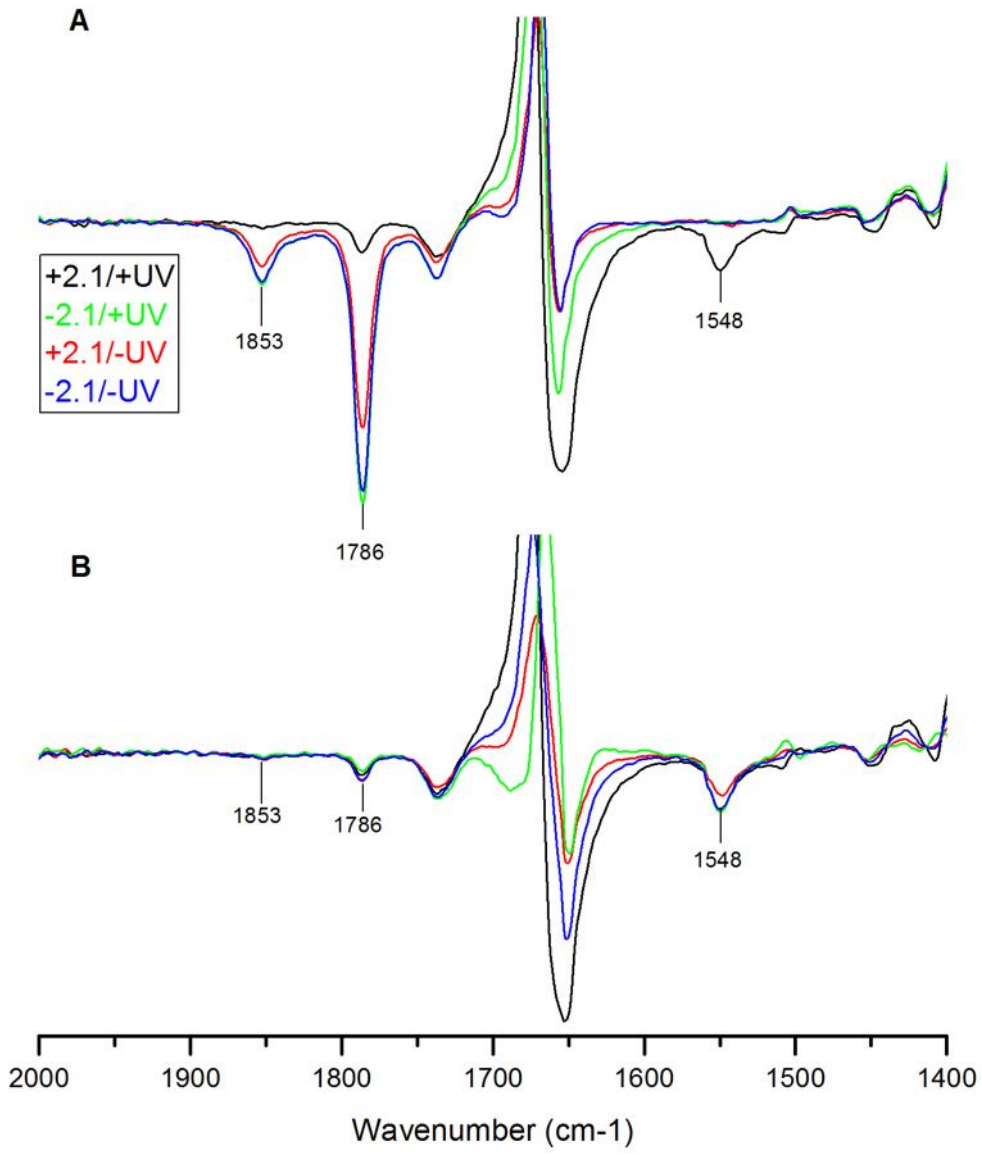

Figure 2.3: FT-IR spectra of photo-initiated polymerization of BLG NCA in NMP. A set of four samples (3 negative controls) was measured by a drop of the reaction mixture directly placed on the ATR crystal. A: After a reaction time of 24 hours. B: After addition of cyclohexylamine to reaction set A and additional reaction time of 24 h.

While ATR-IR measurements provide insight into the polymerization end-point, real-time FT-IR bears the potential of a time-resolved analysis of the process, i.e. the exact moment of the initiation event as well as information about the kinetics of a reaction. In order to explore this, a drop of the reaction mixture was placed onto the ATR crystal and covered with a glass lid. The light source was equipped with a light guide and placed directly above the drop at a distance of 1 cm (Figure 2.4). After 25 s equilibration time, UV irradiation was applied for 35 s. RT-IR spectra were recorded at a scan frequency of 0.1 s for 10 min.

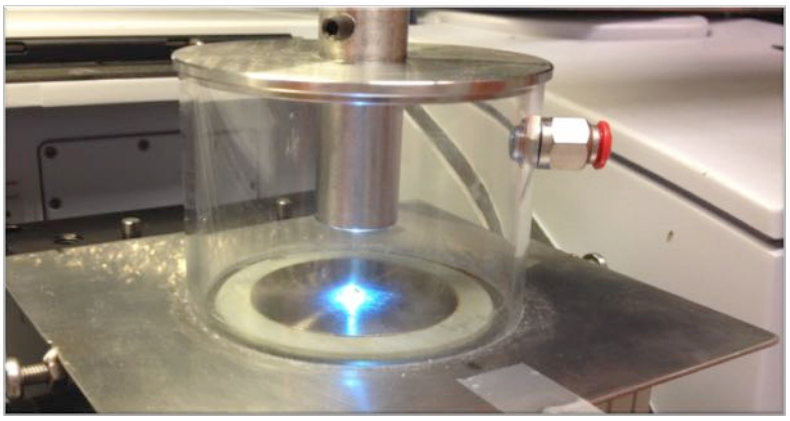

Figure 2.4: Set-up of the real-time infrared spectrometer. At a distance of 1 cm above the ATR-crystal the lamp was positioned.

From the real-time spectra the monomer conversion could be monitored by following the decreasing NCA carbonyl stretching bands at 1786 cm^{-1}, while polymer formation was apparent from the increasing amide II bands of the polypeptide at 1548 cm^{-1}. The negative control experiments confirmed no significant NCA was consumed over a period of 100 s under these conditions in the absence of UV light with or without **2.1** present (+2.1-UV, and -2.1-UV), respectively. Moreover, in both cases no polymer formation is observed, which is consistent with the absence of NCA conversion. On the other hand, in the +2.1+UV experiment a decrease of relative NCA concentration is evident shortly after irradiation was applied. This coincides with an increase of the amide II band providing evidence that the NCA consumption is due to polypeptide formation. The initial apparent increase of the NCA concentration between 30 and 40 s is considered an artifact of the measurement probably caused by the rapid CO_2 formation leading to some solvent removal. In the -2.1+UV experiment a slight decrease of the NCA concentration and an increase of PBLG formation was also observed. It is suggested that heat generation caused by the light source could lead to this effect. Kricheldorf showed spontaneous polymerizations of various NCAs at 60 °C, including cyclic oligopeptide formation, initiation of dimethylamine, and N-formyl terminal formation[20]. Moreover it has to be considered that optimal reaction conditions, which include an inert nitrogen atmosphere, are not present on the ATR crystal. It is suggested that atmospheric water could also interfere during initiation. This fact could explain further the overall slight increase of amide II bands in all samples. When the polymerizations were carried out with TLL NCA, similar results were obtained in the RT-FTIR experiment highlighting the monomer variability of this process (Figure 2.5).

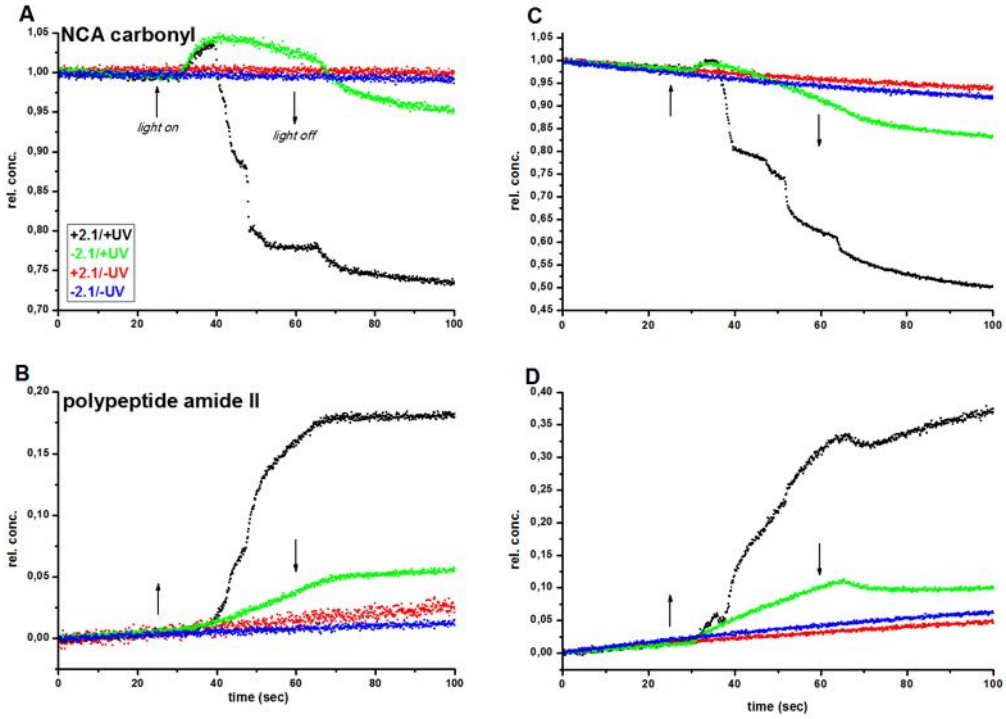

Figure 2.5: Real-time FTIR results of BLG NCA polymerization with and without photoamine generator and UV light following the NCA carbonyl band at 1782 cm^{-1} and the polypeptide amide II band at 1548 cm^{-1}.

2.3.6 Characterization of photo-initiated polypeptides

In order to gain information on the end-group fidelity of this process, the reactions were repeated in a cuvette for subsequent MALDI-ToF-MS analysis. The cuvettes were placed vertically in front of the light source to ensure the stirring of the reaction mixture and the homogenous creation of the reactive species. Photo-induced polymerization of BLG and of TLL were performed in 0.18 M monomer solutions in NMP with 0.02 mol eq. of photoamine generator corresponding to a 50:1 monomer:initiator ratio. After addition of photoamine generator and ITX in the dark, the reaction mixtures were irradiated with UV light for 2 min and left to react in the dark for 3 h (+2.1+UV). The same three control experiments, as described earlier, were also undertaken. At the end of the reaction, a sample was taken from the reaction mixture and analyzed by MALDI-ToF-MS. Initially the sample obtained from conventional cyclohexylamine initiated PBLG material was investigated. The two dominating peak series (peaks A and B in Figure 2.6a, structure A and B Figure 2.7) can be assigned to PBLG initiated by cyclohexylamine terminated with an amine or pyroglutamate end-group (through intramolecular end-group cyclization), respectively.

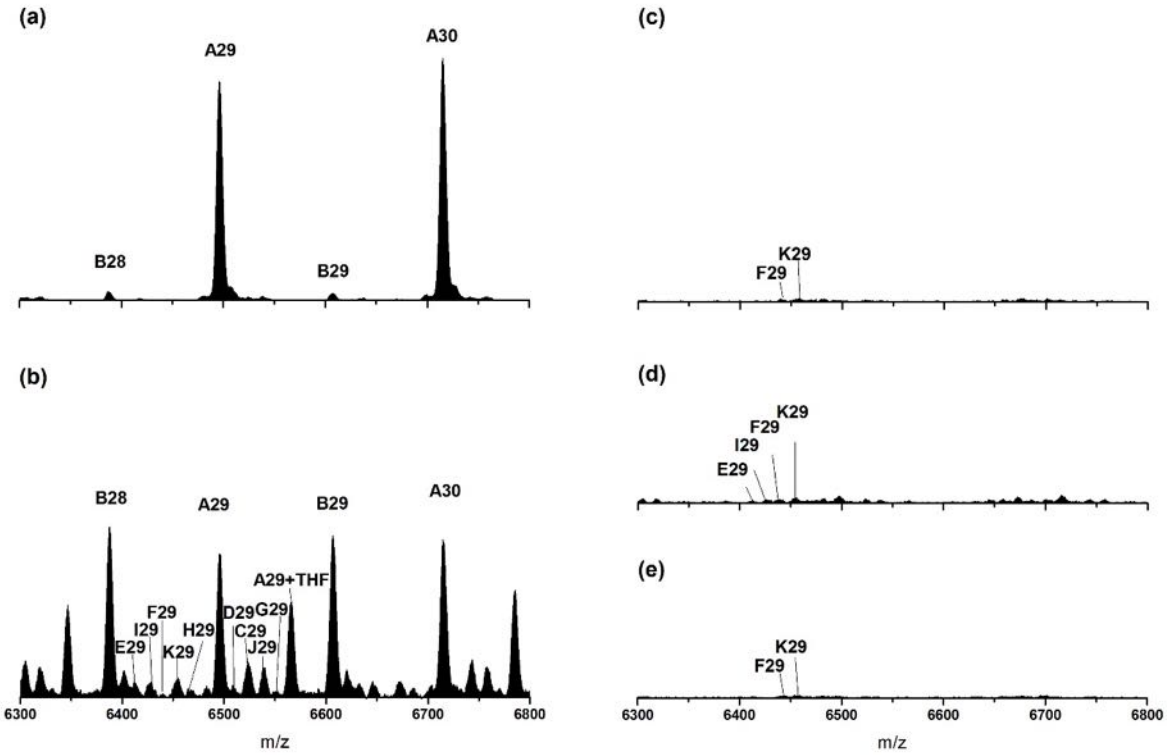

Figure 2.6: MALDI-ToF-MS results of conventional initiated PBLG polymerization (a), photo-initiated PBLG polymerization (b), and negative controls (c-e). Letters depict structures shown in Figure 2.7; the numbers refer to the degree of polymerization. All samples were dissolved in HFIP, with addition of potassium trifluoroacetic acid (KTFA).

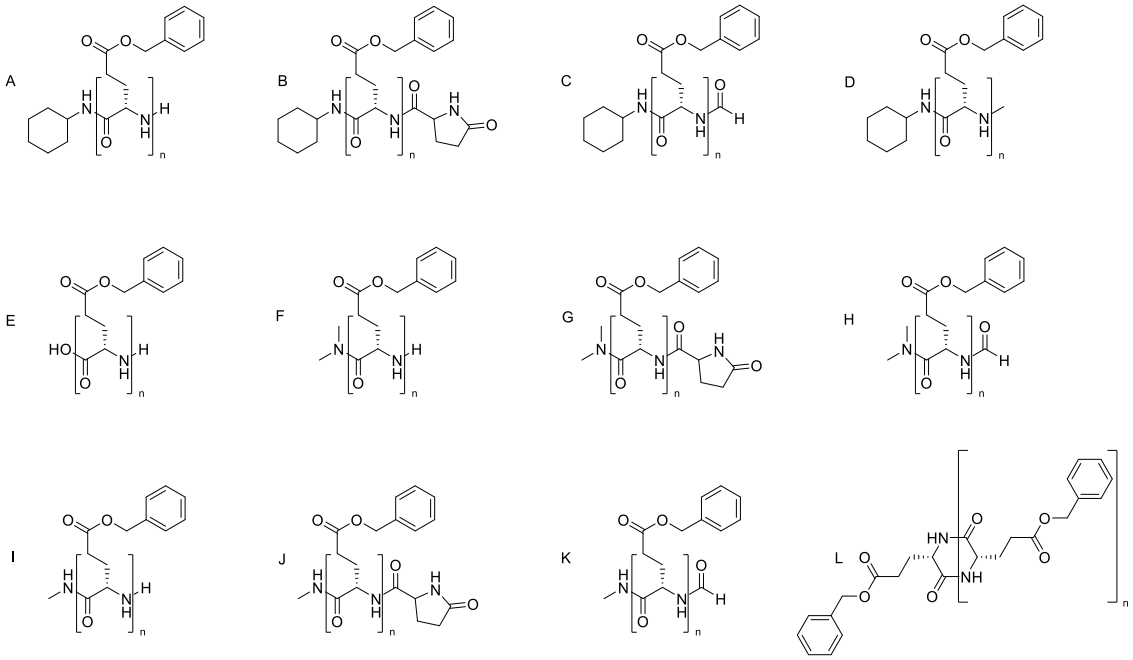

Figure 2.7: Various identified PBLG polymerization product species, assigned to MADLI-ToF-MS spectrum peaks shown in Figure 2.6. Species series include cyclohexylamine initiated (A-D), mono- and dimethylamine initiated (F-K), water initiated (E) polymer chains, as well as cyclic products (L).

When the same polymerization was carried out under +2.1+UV conditions, the same two peak series can be identified as the major products (Figure 2.6b). The relatively higher concentration of pyroglutamate end-groups in the case of photoinitiation probably also arises due to heating effects by the lamp; this reaction is known to be more prominent at higher temperatures[2]. In addition, a range of other structures is present including cyclohexylamine initiated, N-formyl and N-methyl terminated polymers as well as water (structure E), base, and di-, and monomethylamines initiated polypeptides (structure F-K Figure 2.7). Some of those structures are thought to be a consequence of the UV-mediated decomposition of the reaction components including the solvent NMP. No significant amounts of polymer were detected in any of the control experiments (Figure 2.6 c, d, and e). Critically, peaks of cyclohexylamine initiated PBLG are absent in all UV controls. Traces of ring formation (structure L) of the oligopeptide are found in the negative controls at smaller mass values (m/z = 3108, data not shown).

For comparison the reaction was then carried out with TLL NCA. The MALDI-ToF-MS spectrum of the product obtained from the photo-induced polymerization of TLL NCA with **2.1** is almost identical with the polypeptide from the conventional initiation (Figure 2.8).

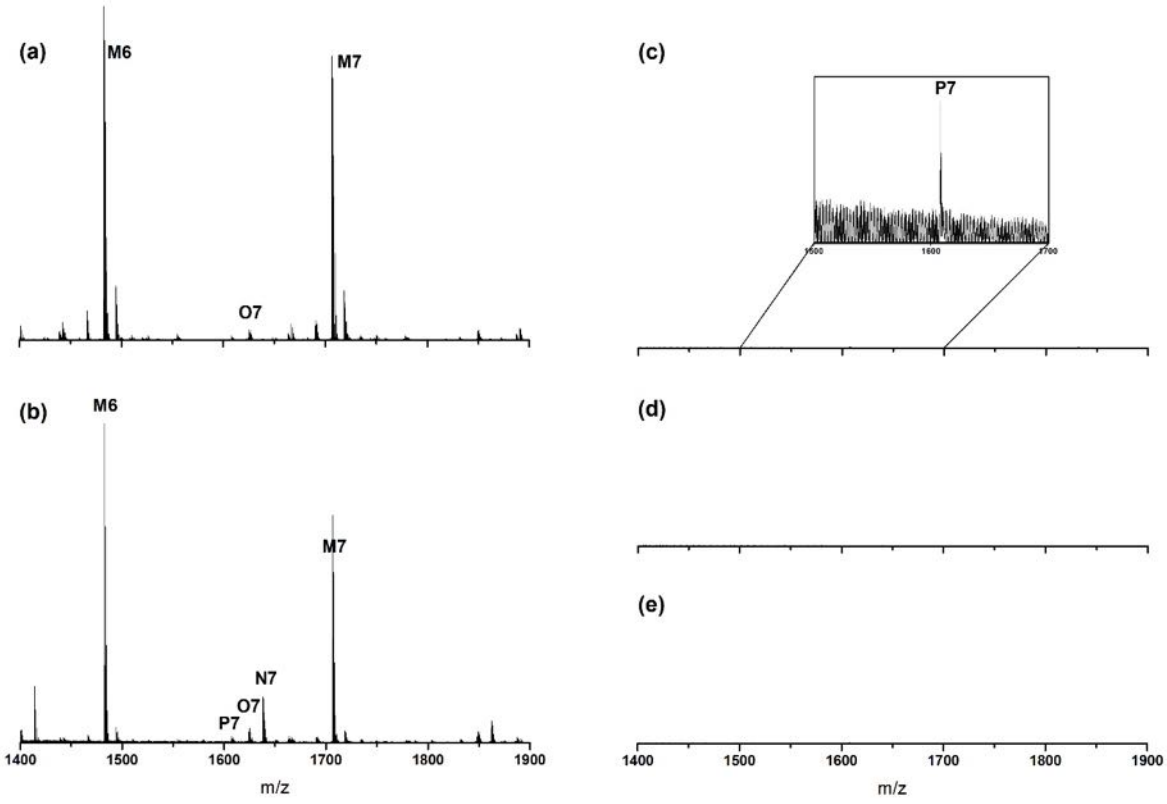

Figure 2.8: MALDI-Tof-MS result of conventional polymerization (a), photo-initiated polymerization (b), and negative control (c-e) of PTLL. Letters depict structures shown in Figure 2.9; the numbers refer to the degree of polymerization. All samples were dissolved in HFIP, with addition of potassium trifluoroacetic acid (KTFA).

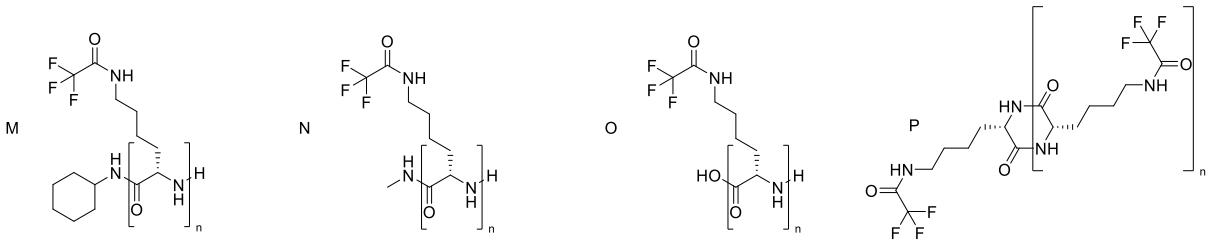

Figure 2.9: Various identified PTLL polymerization product species, assigned to MADLI-ToF-MS spectrum peaks shown in Figure 2.8. Species series include cyclohexylamine initiated (M), methylamine initiated (N), water initiated (O) polymer chains, as well as cyclic products (P).

All negative controls show the absence of cyclohexylamine-initiated polymer. Small traces of the cyclic polypeptide (structure P, Figure 2.9) can be detected in -2.1+UV. It is noticeable that fewer side-reactions occur than in the BLG NCA polymerization. One factor is the absence of a "backbite" reaction between the terminal primary amine and the adjacent side chain, as in the pyroglutamate formation, which reduces the number of possible end-group structures in the TLL case. One can also speculate that the absence of a chromophore such as the benzyl group in BLG might reduce undesired side-reactions. The MALDI-ToF-MS analysis clearly demonstrates that UV-generated cyclohexylamine is the initiating species in both BLG and TLL NCA polymerizations and that the NAM mechanism is the dominant polymerization mechanism.

Side reactions as observed in Figure 2.6a can influence the polymerization control and therefore increase the polydispersity of the overall polymerization product. Thus, molecular weight analysis by size exclusion chromatography (SEC) was performed on a set of polypeptides. The photoreaction was performed inside a quartz cuvette, light was exposed vertically, allowing stirring of the reaction solution inside the cuvette. SEC chromatograms of PBLG and PTLL were obtained from the initiation using photoamine generator **2.1** (solid lines) and cyclohexylamine (dot lines) as conventional reference. FT-IR analysis was used to confirm full conversion of the NCA monomers by the disappearance of the NCA carbonyl band. All polymer samples were precipitated to obtain pure material. SEC data from all polymerizations are summarized in Table 2.1. Theoretical and measured molecular weights are in good agreement in most samples although it has to be noted that all samples were measured against PMMA standards. Comparison should be viewed with caution.

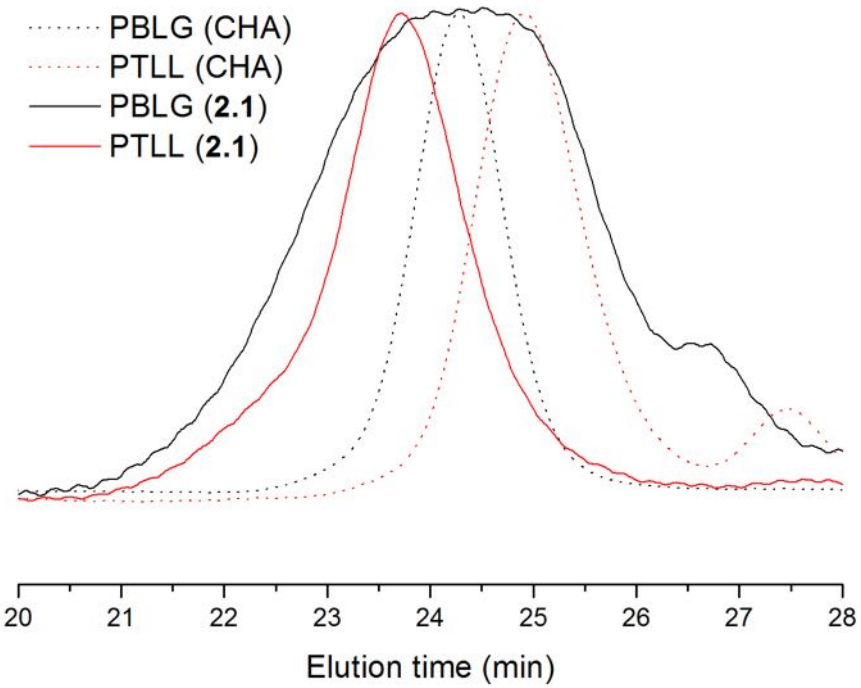

Figure 2.10: SEC chromatograms of PBLG (black) and PTLL (red), initiated by conventional initiation with cyclohexylamine (CHA) and by photoinitiation by photoamine generator (**2.1**). Conventional initiations are shown as dotted lines, photoinitiations are shown in solid lines.

In case of polydispersity, there is an increase between conventional initiation and photoinitiation of PBLG. While the chromatogram shows a narrow peak in the cyclohexylamine-initiated reaction, a broader peak is observed in the photo-initiated reaction. It has to be noted that there is a significant difference in the presence of active species during initiation events, when both reactions are compared. In the conventional initiation 100% of the amine of cyclohexylamine is accessible at the point when it is added to the reaction. All polymer chains start propagation at the same time point. In case of the photo-initiation, the initiator has to be generated first during the light exposure of 2 min. Polymer chains therefore start propagation at different time points. In addition the increase in polydispersity was expected due to the side reaction that were detected in MALDI-Tof. A shoulder at the lower molecular weight end also contributes to the increasing polydispersity. One could speculate that a lower propagation rate of one of the MALDI-Tof detected polymer species could be the reason. Another hypothetical reason could be a non-linear breakdown of the photo-initiator.

When polymerization was carried out with TLL similar results were obtained (Figure 2.10, red lines). Although an unexpected bimodal distribution is observed in the conventional distribution, the peak of the majority population shows a low polydispersity. This is also the case for the photo-initiated polymerization. A monomodal distribution is observed. In

addition, the low polydispersity confirms the results obtained from MALDI-Tof experiments. The reduction of the side reactions is suggested to cause the lower polydispersity obtained by SEC.

Table 2.3: SEC results of NCA polymerization of BLG and TLL. Conventional initiation with cyclohexylamine is denoted as CHA, photoinitiation was preformed with 2.**1**. All reactions contain a monomer:initiator ratio of 50:1, dissolved in NMP.

Initiator	PBLG			PTLL		
	$M_n^{th(a)}$ (g/mol)	M_n^{GPC} (g/mol)	*Đ*	$M_n^{th(a)}$ (g/mol)	M_n^{GPC} (g/mol)	*Đ*
CHA*	11.100	14.500	1,1	11.300**	10477	1.1
2.1*	11.100	11.000	1,8	11.300	19.500	1,3
2.1	11.100	10.100	1,8	11.300	13.800	1,6

* shown in Figure 2.10. ** bimodal distribution. [(a)] calculated by initiator to NCA ratio

2.4 Conclusion

The first photopolymerization of NCAs was successfully demonstrated. In this process the active initiator cyclohexylamine was produced in situ by the UV-induced breakdown of photoamine generator 2,6-dinitrobenzylcarbamate. Real-time FTIR and MALDI-ToF-MS analyses provide clear evidence for the proposed photoinitiation mechanism as well as the attachment of the active initiator to the polypeptide chain. Using two different NCA monomers, which differ in size and polarity, there is strong evidence that in theory, the photoinitiation does not have any other limits than the conventional initiation of NCAs. The one exception is the probably the ability to obtain polymers with narrow molecular weight distribution as the initiation step in the photoprocess is slow compared to the conventional polymerization. This proof of concept generates new possibilities for designing polypeptides both in solution and on surfaces. In particular, for surface-initiated processes the possibilities for spatial organization, on the nanometer scale (though masking strategies) coupled with control over polypeptide composition[19] open us exciting new possibilities for bio-functionalized surfaces.

2.5 References

[1] Y. Yagci, S. Jockusch and N. Turro, *Macromolecules* **2010**, *43*, 6245 - 6260.
[2] F. P. Melchels, J. Feijen and D. W. Grijpma, *Biomaterials* **2010**, *31*, 6121-6130.
[3] J. P. Fouassier, X. Allonas and D. Burget, *Progress in Organic Coatings* **2003**, *47*, 16 - 36.
[4] S. Dadashi-Silab, M. A. Tasdelen and Y. Yagci, *Journal of Polymer Science Part a-Polymer Chemistry* **2014**, *52*, 2878 - 2888.
[5] A. Anastasaki, V. Nikolaou, F. Brandford-Adams, G. Nurumbetov, Q. Zhang, G. J. Clarkson, D. J. Fox, P. Wilson, K. Kempe and D. M. Haddleton, *Chem Commun (Camb)* **2015**, *51*, 5626-5629.
[6] X. Pan, N. Malhotra, A. Simakova, Z. Wang, D. Konkolewicz and K. Matyjaszewski, *J Am Chem Soc* **2015**, *137*, 15430-15433.
[7] J. Xu, K. Jung, A. Atme, S. Shunmagam and C. Boyer, *J. Am. Chem. Soc.* **2014**, *136*.
[8] S. Dadashi-Silab, S. Doran and Y. Yagci, *Chem Rev* **2016**, *116*, 10212-10275.
[9] C. Fu, J. Xu and C. Boyer, *Chem Commun (Camb)* **2016**, *52*, 7126-7129.
[10] J. F. Cameron and J. M. J. Frechet, *Journal of the American Chemical Society* **1991**, *113*, 4303-4313.
[11] J. F. Cameron and J. M. J. Frechet, *Journal of Organic Chemistry* **1990**, *55*, 5919-5922.
[12] N. J. Turro, Y. J. Li, S. Jockusch, Y. Hagiwara, M. Okazaki, R. A. Mesch, D. I. Schuster and C. G. Wilson, *Journal of Organic Chemistry* **2013**, *78*, 1735-1741.
[13] A. C. Farthing, *Journal of the Chemical Society* **1950**, 3213-3217.
[14] J. Huang and A. Heise, *Chem Soc Rev* **2013**, *42*, 7373-7390.
[15] H. Lu and J. Cheng, *J Am Chem Soc* **2007**, *129*, 14114-14115.
[16] G. J. Habraken, A. Heise and P. D. Thornton, *Macromol Rapid Commun* **2012**, *33*, 272-286.
[17] C. V. G.F. Arenas, *European Polymer Journal* **2009**, *45*, 515-522.
[18] A. Kricheldorf, C. V. Lossov, N. Lomadze and G. Schwarz, *Polymer Chemistry* **2008**, *46*, 4012 - 4020.
[19] T. Borase, M. Iacono, A. S.I., P. D. Thornton and A. Heise, *Polymer Chemistry* **2012**, *3*, 1267.
[20] H. Kricheldorf, C. von Lossow and G. Schwarz, *Macromolecules* **2005**, *38*, 5513 - 5518.

3. Optimization and characterization of the photo-initiated polymerization system

3.1 Introduction

As described in Chapter 2.3, a selective initiation process of a light-initiated NCA ROP polymerization was achieved. However, various side-reactions were determined that could affect the purity of the reaction product and limit the applicability of the process. Finding condition that reduces those side reactions is thus desirable. It is suggested that heat creation of the powerful H-bulb lamp is the origin of the formation of thermal side products in the photo-initiated polymerization, besides other reactions caused by radical reactions. It was hypothesized that a substitution of the current light source with one that is less heat emitting might reduce the formation of side products. The blacklight lamp Vilber Lourmat VL-215.L is commonly used in electrophoresis techniques. It has the advantage of a reduced heat output due to a reduced intensity with a maximum emission at 365 nm. To ensure an efficient initiation, the photoamine generator should match the emission spectrum of this new light source. The absorption of the photoamine generator is depends on the nature and position of functional groups in the benzyl ring, enabling absorption spectra from 250 to 420 nm[1]. Studies of Patchornik, Amit and Woodward showed that introduction of two methoxy groups in the chromophore shifts the absorbance in wavelengths beyond than 320 nm[2]. This could enable the dispensation of the UV sensitizer as well as shifting the photoreaction away from the solvent's UV cutoff.

In this chapter we report the successful optimization of a photo-initiated NCA polymerization by replacing the light source emitting in the near UV-A wavelength range as well as the photoamine generator to match its absorption spectrum with the emission of the light source. The replacement solved two problems: (1) the light energy transfer in the solvent cutoff range was prevented, thus omitting the need for a UV sensitizer. (2) The light source did not emit as much heat as the previous source, resulting in a significant reduction of side reaction and reduction of undesired polymer species. The new system permitted the control of the polymer molecular weight through reaction parameters, i.e. irradiation time and distance between light source and reactor. In addition, a block copolymer was successfully synthesized by using a macromolecular photoamine generator. This achievement shows the flexibility of the photopolymerization system as in conventional NCA ROP polymerization.

3.2 Experimentals

Materials

Cyclohexyl isocyanate 98%, α-pinene, benzyl-L-glutamate, triphosgene, dibutyltin dilaurate, trans-2-[3-(4-tert-butylphenyl)-2-methyl-2-propenylidene]malononitrile (DCTB), and potassium trifluoroacetate 98% were purchased from Sigma-Aldrich. 4,5-dimethoxy-2-nitrobenyl alcohol was supplied by Alfa Aesar. Anhydrous DMF was purchased from Acros Chemicals. THF, ethyl acetate, and n-heptane were inhibitor-free and collected from a SPS-800 solvent purification system, equipped with a mole sieve and Al2O3 column. HFIP was supplied from unknown commercial source and distilled before use. Acetonitrile was purchased from VWR.

General methods

Samples for absorption measurement were dissolved in acetonitrile and measured in quartz cuvettes with a path length of 10 mm. The spectra were measured on a PerkinElmer Lamda 35 UV/Vis spectrophotometer. The absorption range was set from 200 – 800 nm, slit width 2 nm, scan speed 480 nm min-1, lamp change at 326 nm. Data were analyzed by PerkinElmer UV WinLab software.

Photo polymerizations were carried out in NMP under stirring. The reactions were carried out in a quartz cuvette with a path length of 10 mm (Quartz SUPRASIL®, Hellma Analytics). The cuvette was placed vertically in front of the light source in a distance of 3 cm. In all reactions a blacklight lamp Vilber Lourmat VL-215.L was used.

Photo-initiation for distance and time measurements

Each photo-initiation for a certain distance and time was carried out in a triple set. BLG NCA and 0.05 mol eq. of 4,5-dimethoxybenzylcyclohexylcarbamate 2 were dissolved in anhydrous NMP (7.7 mmolar). The solution was transferred into a quartz cuvette, before it was vertically exposed to the blacklight lamp. For distance-dependent measurements an exposure time of 60 min was chosen. In case of time-dependent measurements a distance of 2.5 cm were chosen. After exposure all samples were covered in aluminum foil and stirred for 46 hours at room temperature. Precipitation in diethyl ether, filtration and drying under vacuum revealed the solid white product.

MALDI-ToF

Matrix assisted laser desorption/ionization-time of flight-mass spectroscopy (MALDI-ToF-MS) was carried out on an ultrafleXtreme™ MALDI-TOF/TOF-MS (Bruker Daltonics, Bremen,

Germany). The system features a frequency-tripled Nd:YAG laser, producing a wavelength of 355 nm and a 2 kHz repetition rate (Smartbeam-II™). flexControl (Bruker Daltonics) software was used for data acquisition. As matrix material DCTB (20 mg ml-1) was used. Potassium trifluoroacetic acid (KTFA) was added as cationic ionization agent (10 mg ml-1). Poly(ethylene glycol) (Mw 1.000, 2.500, 5.000, 10.000) was used as reference. The polymer material was dissolved in HFIP or THF (10 mg ml-1). Matrix material, ionization agent and polymer sample were mixed (20:1:3) and placed on the target steal plate. The solvent was vaporized before measurement.

SEC

Size exclusion chromatography (SEC) was performed on a system equipped with a Waters 2414 refractive index detector (40 °C), PSS PFG guard column followed by a 2PFG-linear-XL (7 µm, 8 x 300 mm) columns in series at 40 °C, Waters 1515 isocratic HPLC pump, and a Waters 2707 autosampler. HFIP in presence of potassium trifluoroacetate (3 g L-1) was used as eluent at a flow rate of 0.8 ml min-1. Poly(methyl methacrylate) was used as standards (Polymer Laboratories MP = 580 Da up to MP = 7.1 x 106 Da).

FT_IR

FT-IR was measured on a PerkinElmer Spectrum 100 FT-IR Spectrometer, equipped with a Universal ATR Sampling Accessory. Spectra were analyzed with the PerkinElmer Spectrum software, version 10.5.2. Data were collected from wavenumber 4000 – 650 cm-1, 4 scans per sample.

Synthesis

Synthesis of 4,5-dimethoxy-2-nitrobenzylcyclohexylcarbamate 3.1

4,5-dimethoxy-2-nitrobenzylalcohol (0,25 g, 1,173 mmol) was transferred into a preflashed round bottom flask, under nitrogen atmosphere. 5 ml of $CHCl_3$ was added before cyclohexyl isocyanate (0,136 ml, 1,066 mmol) was added drop-wise to the reaction mixture. A catalytic amount of triethylamine (0,016 ml, 0,117 mmol) was added to the reaction mixture. It was stirred under equal conditions for 3 days. The reaction was terminated by transferring the reaction mixture into an excess of diethyl ether for precipitation, obtaining the pure white solid product, 76 %. ^{1}H-NMR (300 MHz, $CDCl_3$, δ, ppm): 1.08 – 1.95 (m, 10H, p-, o-, m-cyclohexyl *H*), 3,47 (m, 1H, NHC*H*), 3,92 – 3,94 (ds, 6H, CH_3O), 4,76 (s, 1H, N*H*), 5,71 (2H, CH_2OC(O)), 6,97 (s, 1H, C*H* ortho to NO_2), 7,67 (s, 1H, C*H*, ortho to CH_2O). ^{13}C-NMR: (100MHz, $CDCl_3$, δ, ppm): 24,9 (cyclohexyl *C meta* to substituent), 25,6 (cyclohexyl *C*, *para* to substituent), 33,6 (cyclohexyl *C*, *ortho* to substituent), 50,2 (cyclohexyl *C*, *ipso* to substituent),

56,6 (*C*CH_3O), 63.5 (*C*H_2O) 108,6 (*C*H, *ortho* to NO_2), 110,5 (*C*H, *ortho* to CH_2O), 128,5 (*ipso* to CH_2O), 140,1 (*C*NO_2), 148,1 (*C*, *meta* to NO*2*), 153,7 (*C, para* to NO_2), 155,2 (*C*(O)).

Synthesis of Poly(dimethylsiloxane)propyl isocyanate

Triphosgene (1,484 g, 5 mmol) was transferred in an already preflashed double neck round bottom flask. Anhydrous toluene (50 ml) was added to dissolve the substrate. Poly(dimethylsiloxane)propylamine (1,075 ml, 1mmol) was added drop wise, before the reaction was heated up to reflux. The reaction was set under inert atmosphere, before it was stirred under these conditions for 92 hours. Under inert atmosphere the mixture was transferred to a round bottom flask before the solvent was vaporized. The remaining oil product was used as such for further use.

Synthesis of 4,5-dimethoxy-2-nitrobenzyl-Poly(dimethylsiloxane) carbamate

Poly(diemthylsiloxane)propyl isocyanate (1,015 g, 1 mmol) was used as such from the previous reaction, It was dissolved in 7,5 ml of deuterated chloroform to follow the reaction by NMR. 4-5-dimethoxy-2-nitrobenzyl alcohol was dissolved in 2,5 ml deuterated chloroform before it was added to the reaction mixture. The flask was hold under inert atmosphere. Dibutylyin dilaurate (30 µl, 50 µmol) was added directly. The reaction mixture was stirred at room temperature and under inert atmosphere overnight. The crude oil was purified by column chromatography, using the solvent system EtOAc/heptane 1/1. The solvents were vaporized, yielding the yellowish oil, 4,5-diemthoxy-2-nitrobenzyl-Poly(dimethylsiloxane) carbamate (0,888 g, 0,723 mmol, 72,3 % yield). ^{1}H-NMR (300 MHz, $CDCl_3$, δ, ppm): 0,01 – 0,1 (m, 72 H, SiC*H*$_3$), 0,47 – 0,55 (m, 4 H, C*H*$_2$Si), 0,83 (t, 3H, C*H*$_3$(CH_2)$_3$Si), 1,23 (m, 4H, CH_3(C*H*$_2$)$_2$$CH_2$Si), 1,77 (m, 2H, Si$CH_2$C*H*$_2$$CH_2$NH), 3,17 (m, 2H, C*H*$_2$NH), 3,92 – 3,94 (ds, 6H, OC*H*$_3$), 4,88 (s, 1H, N*H*), 5,48 (s, 2h, C(O)OC*H*$_2$), 6,98 (s, 1H, C*H* ortho to NO_2), 7,69 (s, 1H, C*H*, ortho to CH_2O). ^{13}C-NMR: (100MHz, $CDCl_3$, δ, ppm): 1,1 (Si*C*H_3), 14,0 (*C*H_3(CH_2)$_3$Si), 18,2 (Si*C*H_2(CH_2)$_2$NH), 25,6 (CH_3(CH_2)$_2$*C*H_2Si), 25,7 (CH_3CH_2*C*H_2CH_2Si), 29,2 (CH_3*C*H_2(CH_2)Si), 29,4 (SiCH_2*C*H_2CH_2NH), 44,3 (*C*H_2NH), 56,6 (O*C*H_3), 63,6 (C(O)O*C*H_2), 108,4 (ortho to CH_2O), 110,5 (ortho to NO_2), 138,9 (C(O)OCH_2*C*), 144,7 (*C*NO_2), 148,4 (C(NO2)CH*C*OCH_3), 153,7 (CCH*C*OCH_3), 156,1 (*C*(O)O).

3.3 Results and discussion

3.3.1 Second generation photoamine generator

To synthesize the photoamine generator 4,5-dimethoxy-2-nitrobenzylcyclohexyl carbamate **3.1**, the same synthetic reaction conditions were performed as for 2.1 (Scheme 3.1). The nitro group on the *β*-position to the benzyl carbamate ensures the same molecular breakdown mechanism as discussed for the previous photoamine generator, the Norrish-type II reaction[3]. The methoxy-groups are strongly electron donating groups changing the electron state in the conjugated aromatic ring. The inductive effect is strong especially due to the substitution in the *para* position[4] and shifts the absorption spectrum into the UV-A wavelength region[5].

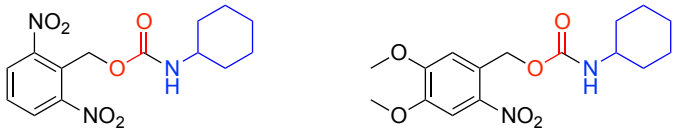

2.1 **3.1**

Scheme 3.1: chemical structure of photoamine generator **2.1**, 2,6-dinitrobenzylcyclohexyl carbamate (left) and photoamine generator **3.1,** 4,5-dimethoxy-2-nitrobenzylcylcohexyl carbamate

The absorption spectrum of **3.1** highlights this (Figure 3.1). While this photoamine generator still has an absorption in the UV-C wavelength region at 240 nm (red line), another absorption region in the UV-A wavelength region (350 nm) is observed due to the presence of the methoxy-groups. The H-bulb light source (green columns), which had an ideal absorption/emission overlap for **2.1**, does not cover its absorption in this higher wavelength region. However, the emission of the blacklight Vilber Lourmat VL-215.L (brown columns) is well overlapping with the absorption in this higher wavelength region.

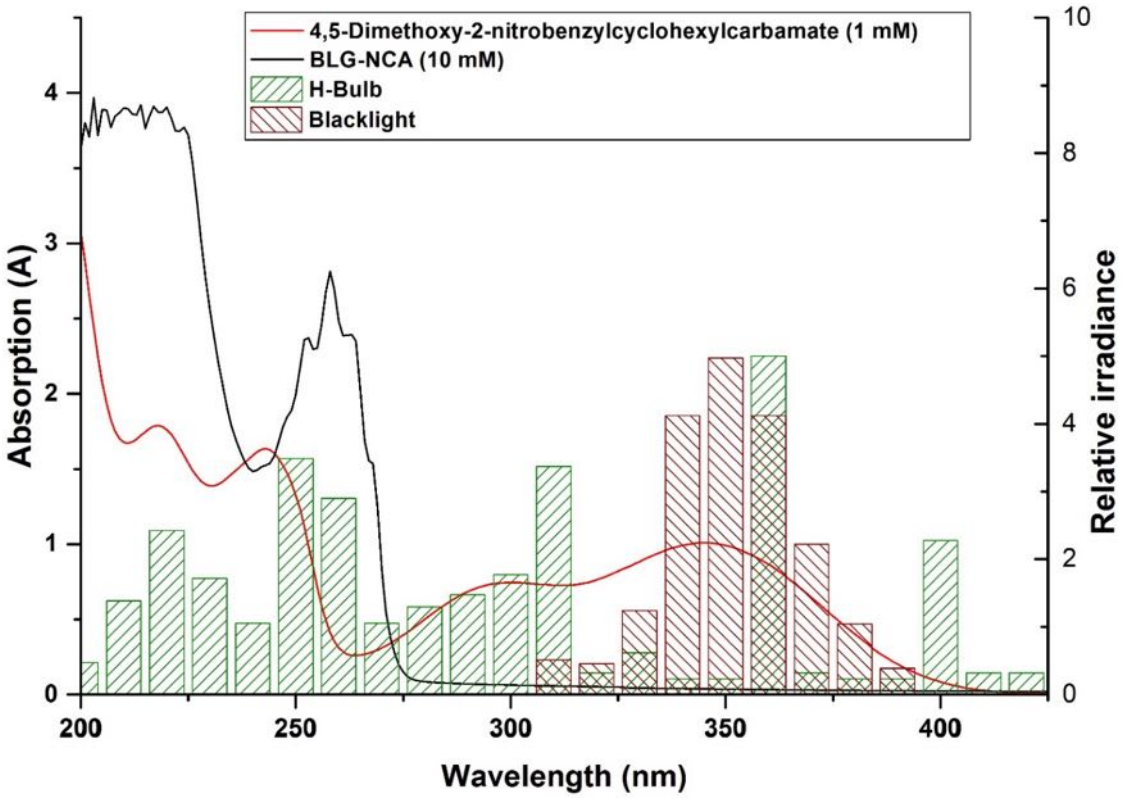

Figure 3.1: UV-Vis absorption spectra of photoamine generator **3.1** and BLG NCA monomer (lines), and the emission spectra of the H-bulb lamp (green columns), and the blacklight lamp Vilber Lourmat VL-215.L (brown columns)

For the reactions, quartz cuvettes were equipped with magnetic stirring bars and positioned directly above a magnetic stirring plate in a vertical position, allowing the stirring of the reaction mixture in the cuvettes. The Vilber Lourmat VL-215.L lamp was places in front of the cuvettes. The set-up allowed irradiation of several samples (e.g. at different distances) at the same time (Figure 3.2). In the following, all photo-induced polymerization of BLG and of TFLL were performed in 0.18 M monomer solutions in NMP with 0.02 mol eq. of photoamine generator corresponding to a 50:1 monomer:initiator ratio.

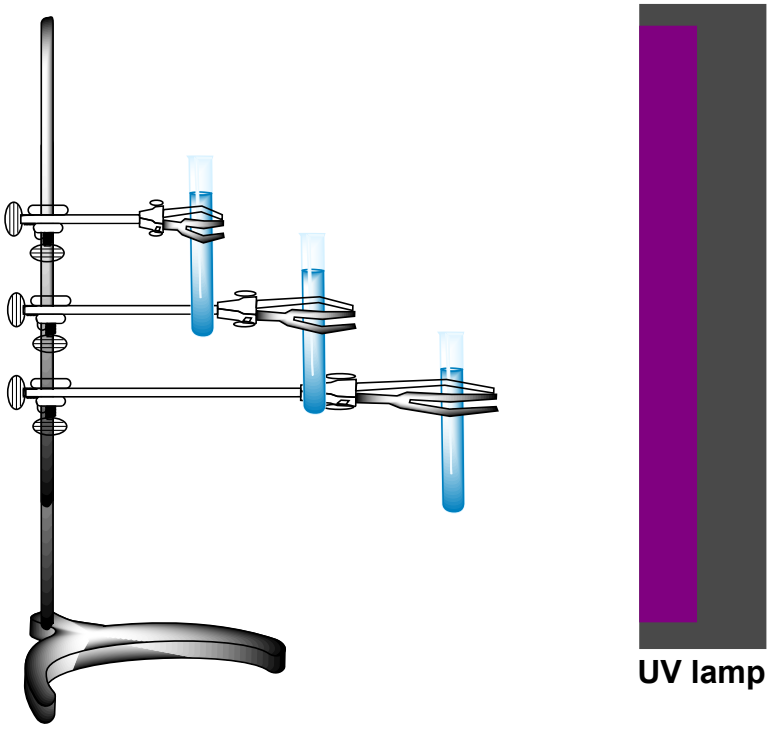

Figure 3.2: Set up of the photo-initiation of BLG with photoamine generator **3.1** and the light source Vilber Lourmat VL-215.L. The cuvettes are hanged above a magnet stirring plate in vertical direction, equipped with a magnetic stirring bar. The cuvettes can be hanged in various distances from the light source.

3.3.2 Optimization of photopolymerization with 3.1

Monomer and photoamine generator **3.1** were added in a 50:1 ratio. The quartz cuvette was placed vertically approx. 3 cm in front of the light source, allowing the reaction mixture to stir during the 60 min. light exposure. Afterwards, the cuvette was covered in aluminum foil for further 46 hours at room temperature. FT-IR measurement confirmed full conversion of the NCA monomer after that time. A negative control, **+3.1**/-UV was performed in the same fashion except for the exposure to light to investigate the stability of the initiator. Next to the negative control, a conventionally cyclohexylamine initiated polymerization was carried out as reference.

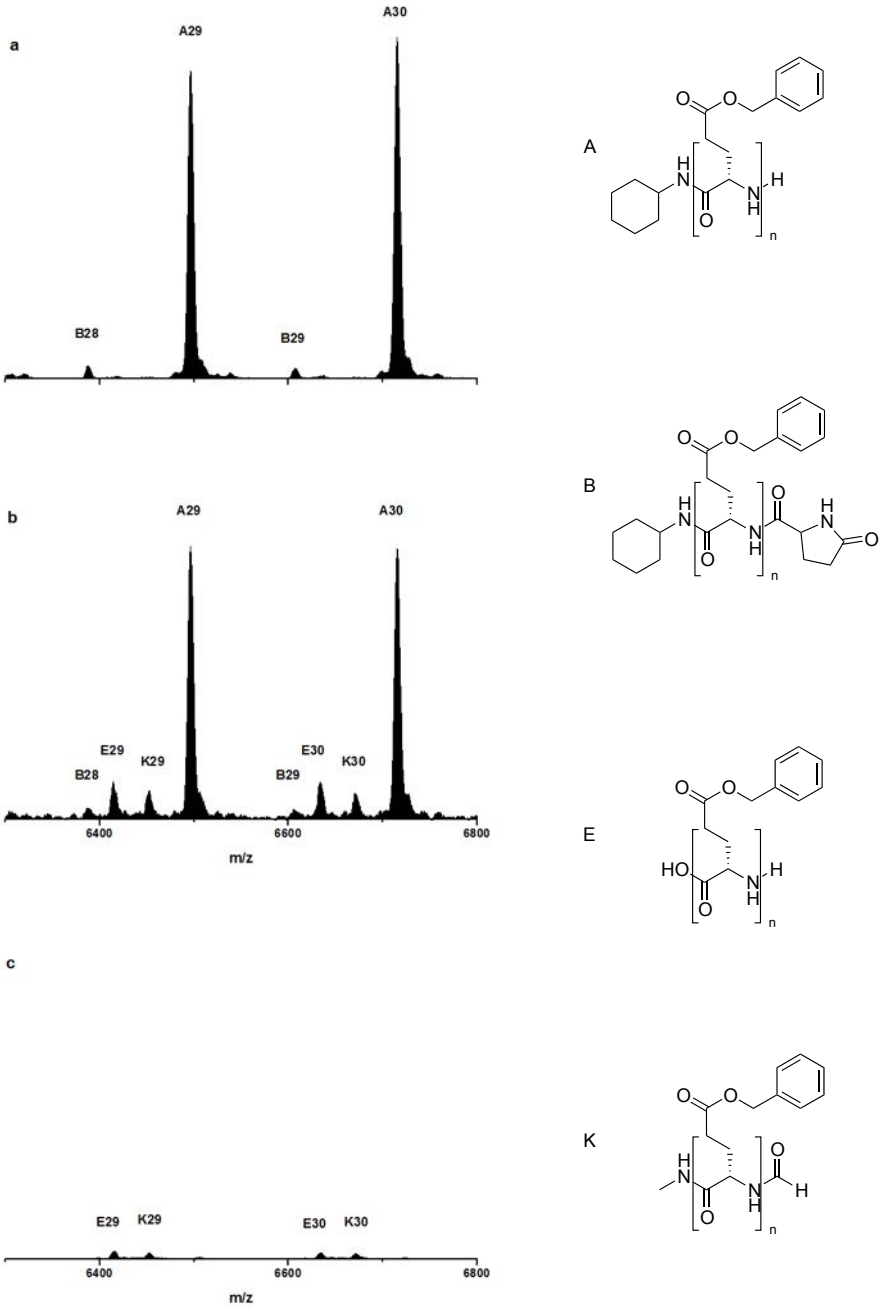

Figure 3.3: Comparison of MALDI-Tof-MS results between conventional and photo-initiated PBLG polymerization. (a) Results of a conventional initiated polymerization, using cyclohexylamine, (b) photo-initiated polymerization by photoamine generator **3.1**, (c) a negative control without UV irradiation. All spectra were normalized to the same peak intensity. Letters depict structures shown on the right. The numbers refer to the degree of polymerization. All samples were dissolved on HFIP, with addition of potassium trifluoroacetic acid (KTFA).

The success of the photopolymerization system was confirmed by MALDI-Tof-MS analysis of the PBLG product in DMF. As expected, two distinctive cyclohexylamine-initiated polymer species, A and B, terminated with an amine and pyroglutamate, respectively, were detected

in the MALDI-ToF-MS spectrum for the conventional polymerization (Figure 3.3 a). Similar results were obtained by the photo-initiated polymerization with **3.1** (Figure 3.3 b). Almost exclusively cyclohexylamine-initiated species, structure A, next to a minor presence of species B was found. Low intensity series of side products, structure E and K, were also observed, which represent structures initiated by water and methylamine, respectively. In comparison to the MALDI-Tof results in Chapter 2 (Figure 2.6 b), a significant reduction of side-reactions is observed. Neither dimethylamine initiated nor cyclic polymer products could be identified. The absence of the latter species is rationalized with the significant heat reduction during light exposure using the Vilber Lourmat VL-215.L lamp[6]. However, methylamine initiated polymer products could not be prevented. This is possibly caused by the breakdown of DMF into methylamine due to UV light exposure. After precipitation, the negative control showed only traces of solid product. These traces were collected and analyzed by MALDI-ToF-MS (Figure 3.3 c). The sample shows no cyclohexylamine-initiated species, confirming the stability of the chromophoric protecting group of the cyclohexylamine. Low-level detection of the same side product as in the photo-initiated polymerization supports the claim that those species are formed by the instability of the solvent. The overall MALDI-Tof spectrum of the photo-initiated polymerization (Figure d) depicts a good agreement with a controlled NCA-ROP polymerization.

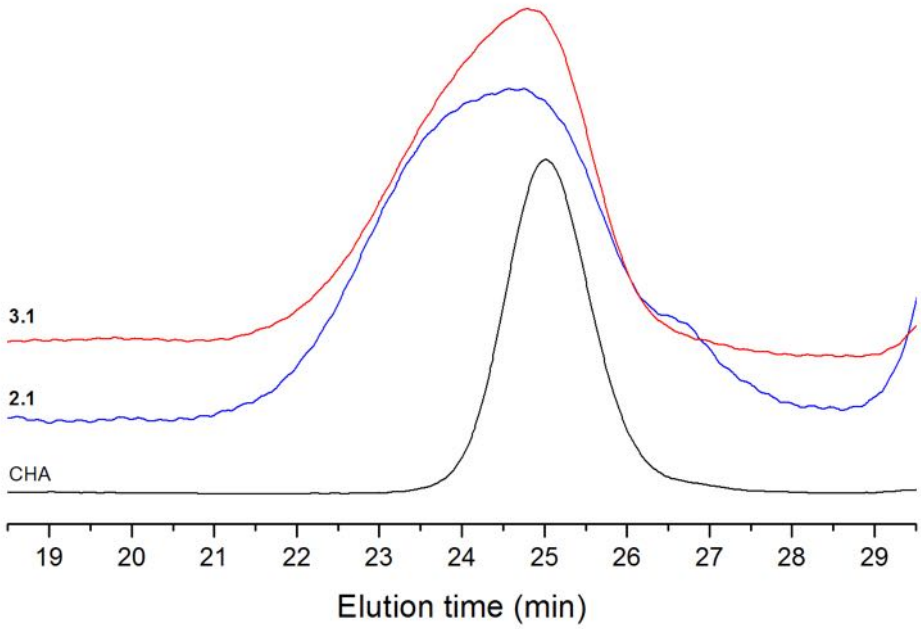

Figure 3.4: SEC chromatograms of PBLG, initiated by conventional initiation with cyclohexylamine (black), photo-initiated by photoamine generator **2.1** (blue) and by photoamine generator **3.1** (red).

SEC analysis provided additional insights into the optimized photopolymerization system. As previously, a conventional cyclohexylamine-initiated polymerization was used as reference (indicated as CHA), next to the **2.1**-initiated PBLG product (Figure 3.4). All three reactions had the same monomer:initiator ratio of 50:1. SEC data from all polymerizations are summarized in Table 3.1. The cyclohexylamine-initiated sample displays the lowest polydispersity of about 1.1 in comparison to both photo-initiated polymerization. This is in agreement with what is typically achievable in this type of reactions. Polydispersities of PBLG obtained with both photoinitiators are higher and around 1.5 (Table 3.1). It appears that monomodality was improved by using photoinitiator **3.1**. Notable is the absence of a shoulder in the chromatogram of PBLG from **3.1**, compared with the product obtained from the **2.1**-initiated polymerization (Figure 3.4). This shoulder might be caused by the much larger amount of side-products evident from the MALDI-ToF analysis as discussed in Chapter 2.3 but this remains speculative without further studies.

It was further investigated whether the molecular weight could be controlled by the monomer to initiator ratio. Polymerizations with ratios of 20:1, 40:1 and 60:1 were performed (Table 3.1). It was observed that the polydispersities in these reactions barely varied. Moreover, theoretical and measured molecular weights were not in a good agreement. In addition, reactions with the same monomer:initiator ratio show significant variation in molecular weights. While all reactions were carried out under similar condition, with the same irradiation time of 60 min and a reaction time of 48 hours it cannot be guaranteed that all samples were positioned at exactly the same distance to the light source. It is not believed, however, that this would cause the molecular weight variations observed in these experiments. The results rather underline a characteristic and potentially a dilemma of the photopolymerization system: To increase the yield of cyclohexylamine by the breakdown of the photoamine generator a longer irradiation period is necessary. A longer irradiation period has the consequence that the initiating amine is formed over a longer period. As a result chain initiation occurs over a longer time span, which must increase the polydispersity. In contrast, in a conventional polymerization the initiator is injected into the reaction medium and all initiator molecules are available immediately.

While molecular weight control by the conventional variation of monomer to initiator ratio seems challenging, this does not mean the reaction is uncontrolled. MALDI-ToF results clearly demonstrate end-group fidelity, which is key to the design of polymer architectures and surface polymerization. Considering that this novel photopolymerization system could

have high potential for surface coating and photolithography, the highest priority was to minimize the side reactions to ensure high degree of (surface) initiator attachment.

Table 3.1: SEC results of NCA polymerization of BLG. Conventional initiation with cyclohexylamine is denoted as CHA, photoinitiation with either photoamine generator **2.1**, or **3.1**.

Initiator	M:I	$M_n^{th(a)}$ (g/mol)	M_n^{GPC} (g/mol)	$Đ$
CHA*	50	11.100	14.500	1,1
2.1*	50	11.100	11.000	1,8
3.1*	50	11.100	12.000	1,5
3.1	20	4.500	13.300	1,4
3.1	20	4.500	24.800	1,5
3.1	40	8900	14.500	1,4
3.1	40	8900	23.000	1,6
3.1	60	13.700	18.300	1,5

* analyzed by SEC and shown in Figure 3.4

3.3.3 Molecular weight control by irradiation time and distance

While molecular weight control was not achieved through the initial monomer to initiator ratio, the amount of energy applied to the system could possibly be used to modulate polypeptide molecular weights through irradiation time and sample distance. Figure 3.5 shows the light intensity reduction in dependence on the distance of the light source from a sample. The decrease is following an exponential decay, thus small variations of distances to the light source results in a significant variation of light intensity.

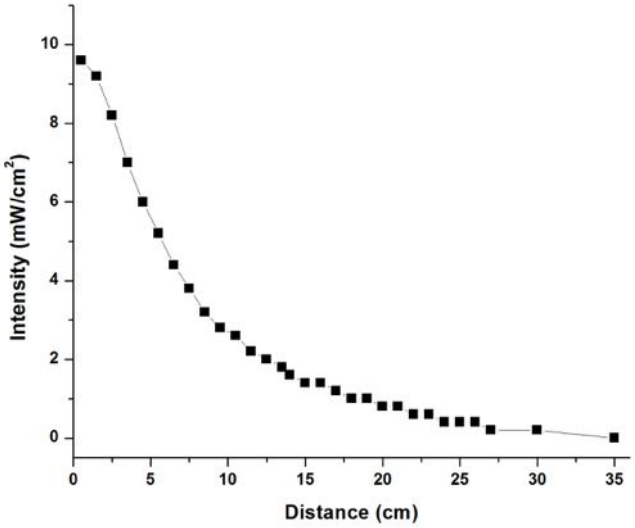

Figure 3.5: Dependence of light intensity of the Vilber-Lourmat L215-L UV lamp. The intensity was measured with Silverline Intensometer (real-time DMA setup)

Thus, it was investigated how the distance between the cuvette and the light source would influence the polymer molecular weight. The light source was installed at different distances from the cuvette, starting from 2 cm to a maximum distance of 20 cm. Polymerizations at each individual distance was performed in triplets. Individual reaction mixtures contained constant concentrations of photoamine generator **3.1** and BLG NCA (ration 1:20) and were irradiated at a constant duration of 60 min. After irradiation, the polymerization was allowed to proceed in the dark for 46 hours until full monomer conversion was reached. Complete conversion was confirmed by FT-IR, before all samples were precipitated and isolated for further analysis. Figure 3.6 b shows that the molecular weight M_n increases with an increasing light distance, i.e. less intensity, causes a reduced photoamine generator breakdown. This trend is also reflected in the corresponding GPC traces (Figure 3.6 a) where a clear shift of the traces towards higher molecular weights can be observed. With longer distances broadening of the traces becomes apparent, thus resulting in an increase of the polydispersity (PDI, Figure 3.6). It is suggested that the formation of amine initiator happens only in spontaneous events during irradiation. Lower intensity by higher distance would thus reduce the amount of amine initiator formed in the process. This creates an intrinsically higher monomer to initiator ratio at lager distances thus increasing the molecular weights.

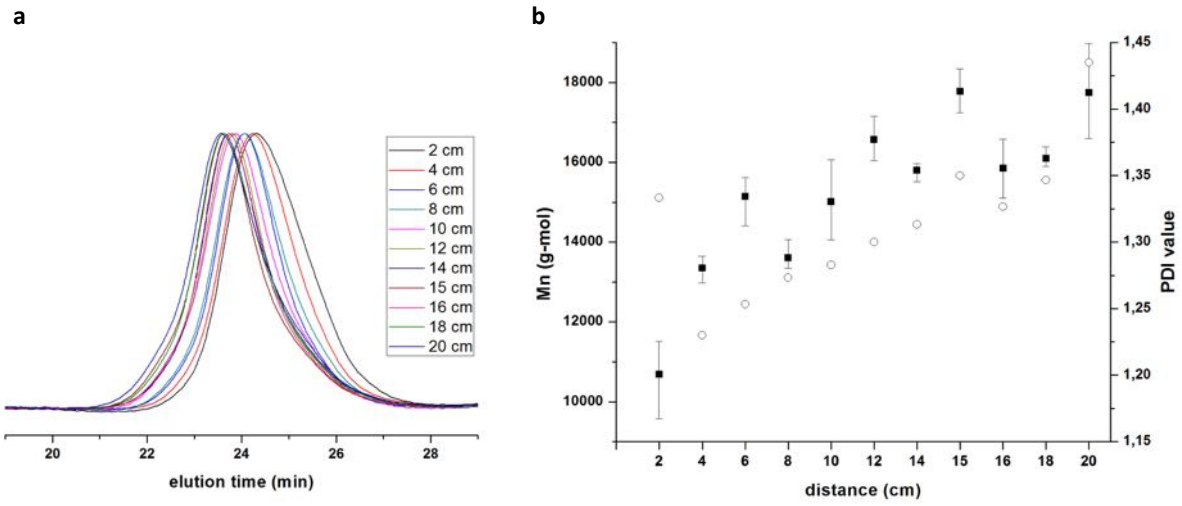

Figure 3.6: Molecular weight control by light source distance in a photoinitiation of BLG NCA with photoinitiator **3.1**. GPC traces of samples obtained from sample at different light source distances and plot of average M_n and PDI of triplicate samples. Error bars represent standard deviation.

An alternative approach to moderate the molecular weight is by varying the irradiation time at a constant distance of 2.5 cm from the cuvette. Individual reaction mixtures contained photoinitiator **3.1** and BLG NCA (ration 1:20). The polymerization was allowed to proceed in the dark for 46 hours until full monomer conversion was reached. Figure 3.7 b shows that the molecular weight of the obtained PBLG decreases with increasing irradiation time as more active initiator is generated. Closer inspection of the plot suggests an almost linear decrease on M_n for irradiation times up to 20 min from about 16000 to 12500 g/mol. while beyond this time point the decrease is less defined with higher standard deviations from the triplicate experiments. This is also reflected in the corresponding GPC traces (Figure 3.7 a) where a clear shift of the traces to lower molecular weights can be observed for the 5, 10 and 15 min. irradiation samples, respectively. At longer irradiation, increase of M_n is mainly due to trace broadening specifically at the low molecular weight side, which is also reflected in the increasing polydispersity (PDI; Figure 3.7). The scenario in these reactions is similar to a continues dosing of initiator to a controlled polymerization, which causes an increase of the molecular weight distribution due to the continuously decreasing monomer to initiator ratio. In this case, the dosing is in situ through the UV-triggered formation of amine initiator during the irradiation time. This effect is more pronounced at longer dosing (i.e. irradiation) periods. These data provide indirect proof for the controlled character of the polymerization.

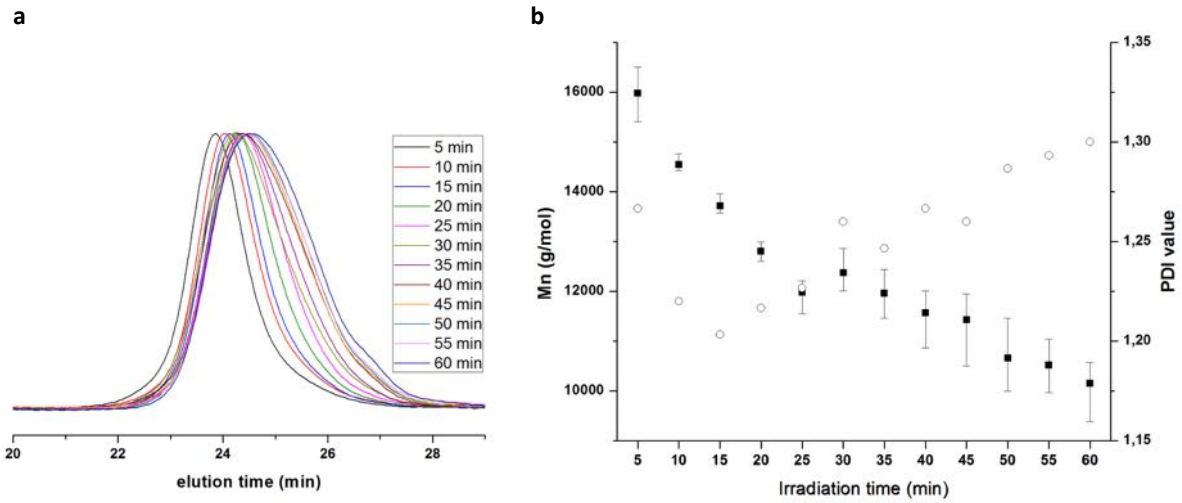

Figure 3.7: Molecular weight control by irradiation time in a photoinitiation of BLG NCA with photoinitiator **3.1**. GPC traces of samples obtained from sample at different irradiation periods and plot of average M_n and PDI of triplicate samples. Error bars represent standard deviation.

3.3.4 Macroinitiation

It was further investigated whether a block copolymer is obtainable by the photopolymerization. In the first instance it was expected that the conjugation of the polypeptide to a suitable macroinitiator could improve the solubility and facilitate SEC analysis even at small block length[7],[8] [9]. According to the synthesis of the photobase initiator by coupling of the precursor to an isocyanate, macroinitiator design requires an isocyanate functional polymer. Initially, a poly(ethylene glycol) (PEG) macroinitiator was considered, due to its established use in polypeptide hybrids[10],[11]. Unsatisfying results were obtained to convert a monoamine PEG into an isocyanate, as the first step to a carbamate-based PEG-photoamine generator. FT-IR confirmed only the presence of a primary amine and the absence of any isocyanate (data not shown). It was believed that PEG absorbs water that immediately attacks the isocyanate, which results in a decarboxylation and the formation of the initial primary amine.

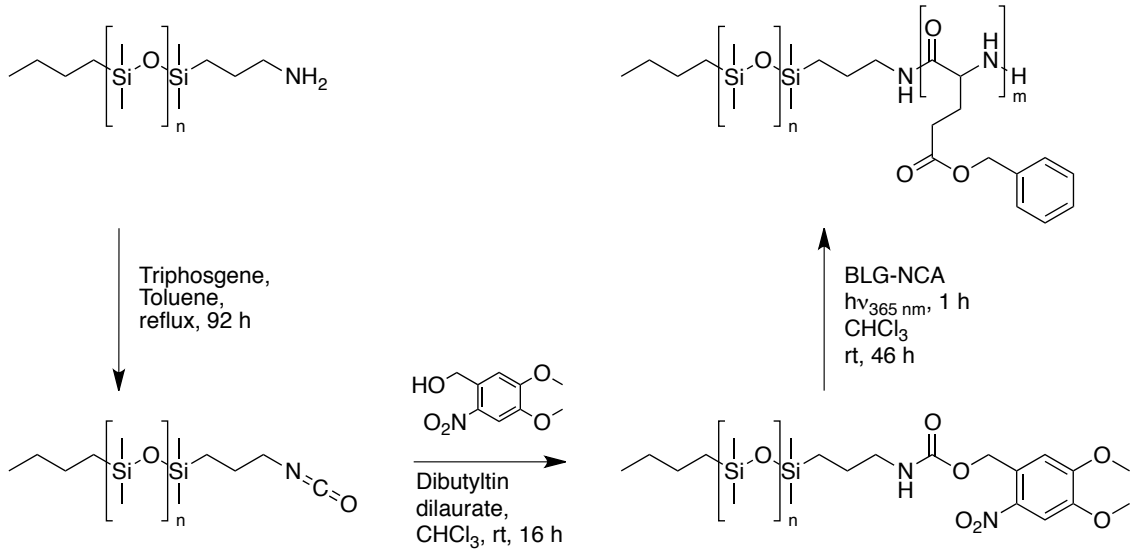

Scheme 3.2: Synthesis of the macro-photoamine generator 4,5-dimethoxy-2-nitrobenzyl-poly(dimethylsiloxane) carbamate and photopolymerization resulting in PDMS-PBLG. The first step is the conversion of the primary amine into an isocyanate, before carbamate formation is performed, adding the chromophoric alcohol in presence of dibutyltin dilaurate. In presence of light and NCA monomer the final block copolymer is formed.

Therefore the hydrophobic monoamine functionalized poly(dimethylsiloxane) (MW 1000)[12],[13] was chosen. It was believed, using this polymer, the yield in isocyanate formation would be improved. Scheme 3.2 illustrates the synthetic route, using PDMS monoamine to obtain the corresponding macro-photoamine generator. In the first step, the primary amine is converted into an isocyanate, using triphosgene. The product is directly used without any purification to form the carbamate by the addition of the chromophoric alcohol and dibutyltin dilaurate. The reaction was performed in deuterated chloroform, monitoring the C(O)OC*H*$_2$ peak which shifted from 4,93 to 5,48 ppm. Final column chromatography ensured a pure carbamate product and the removal of the tin catalyst. Due to its high hydrophobicity, photopolymerization of PDMS-PBLG polypeptide hybrid was performed in $CHCl_3$. BLG NCA:PDMS ratios of 10:1, 15:1, 20:1, and 30:1 were used to obtain PBLG blocks of different molecular weights. All reactions were irradiated for 60 min, before placing the vial in the dark for 46 hours allowing to complete the NCA conversion. Full conversion was confirmed by FT-IR. After precipitation, the polymer samples were analyzed by MALDI-Tof-MS and SEC. Figure 3.8 a, and b show MALDI-Tof-MS analysis of PDMS-PBLG$_{20}$. The overall peak ensemble consists of several peaks (Figure 3.8 b). This is the result of the diblock polymer formation, in which two polydispersities duplicate the overall number of different polymer compositions, depict as n and m for PDMS and PBLG, respectively (Scheme 3.2). Figure 3.8 b shows three peak sets that include a multitude of series. Focusing on the

left peak set, ranging from 7150 to 7200, it contains block copolymers with n= 2, 5, 8, 11, 14, and 17 with m= 31, 30, 29, 28, 27, 26, respectively, which highlights a successful polymerization initiation using the macro photoamine generator and the covalent attachment of macroinitiator to the second block, PBLG. The broad range of the peak set is explained by the additional polydispersity, which is introduced by the second block.

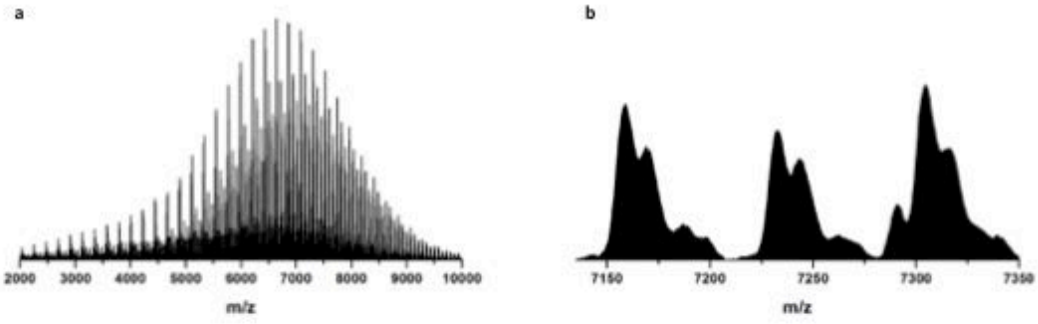

Figure 3.8: MALDI-Tof-MS analysis of PDMS-PBLG block copolymer. (a) depicts the overall polymer distribution obtained from the MALDI-ToF-MS, (b) shows a zoom-in of (a), (c) SEC traces of polyhybrids differing in the length of the PBLG block.

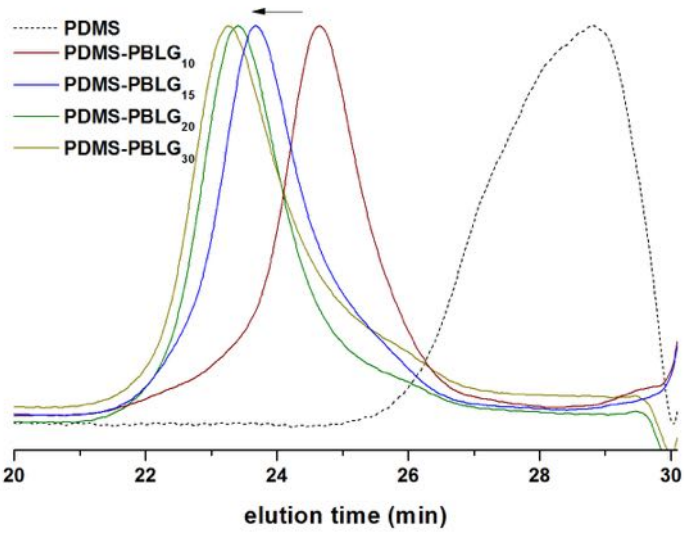

Figure 3.9: SEC analysis of PDMS-PBLG block copolymer. The macroinitiator PDMS was analyzed (dotted black line), in comparison to block copolymer with different PBLG block lengths (colored straight lines).

Table 3.2: SEC results of NCA photopolymerization of BLG using PDMS as macrophotoinitiator. Photopolymerizations with different monomer:initiator ratios were performed.

M:I	$M_n^{th(a)}$ (g/mol)	M_n^{GPC} (g/mol)	Đ
macroinitiator	1,200	1.550	1,5
10	3.200	11.210	1,3
15	4.300	15.890	1,3
20	5.400	17.830	1,4
30	7.600	15.990	1,5

Molecular weight analysis by SEC was performed on the four different block copolymer compositions (Figure 3.9). The chromatograms confirm an overall increase of molecular weight upon initiation from the PDMS macroinitiator depending on the NCA to PDMS ratio. The exception is the block copolymers with the highest NCA to PDMS ratio (30:1). While these are preliminary results on non-optimized reactions due to time constrains, these clearly demonstrate that macroinitiation by photoinitiation is possible.

3.4 Conclusion

The introduction of a new NCA photopolymerization system was demonstrated. The photoamine generator **3.1** showed absorption in the UV-A light range, shifting the photoreaction into the near visible light. This enabled the use of the blacklight lamp Vilber Lourmat VL-215.L, which, in contrast to the former H-bulb light source, had a lower intensity and lower heat creation. Especially due to the reduced heat creation higher control in case of initiation of the photopolymerization could be achieved and side reactions were significantly reduced. It was further demonstrated that molecular weight control is possible by controlling the light intensity through distance or irradiation time. The dependence of these two factors is consistent with photopolymerization as radical[14],[15] or cationic polymerizations[16],[17].

In addition, a successful photoinitiated formation of a block copolymer, using PDMS as macro-photoinitiator was demonstrated. GPC-traces showed in clear increase of molecular weight in agreement with the macroinitiation. Moreover, MALDI-Tof-MS analysis confirmed covalent attachment of the two blocks. These results open possibilities to design polypeptide architecture, for instance triblock copolypeptides and star polypeptides using diisocyanate or triisocyanate starting materials.

3.5 References

[1] C. G. Bochet, *Tetrahedron Letters* **2000**, *41*, 6341 - 6346.
[2] A. Patchornik, B. Amit and R. B. Woodward, *J. Am. Chem. Soc.* **1970**, *92*, 6333 - 6335.
[3] R. G. W. Norrish and C. H. Bamford, *Nature* **1935**, *140*, 195 - 196.
[4] S. Ando, T. Matsuura and S. Sasaki, *Polymer Journal* **1997**, *29*, 69 - 76.
[5] H. Lutz, E. Breheret and L. Lindqvist, *The Journal of Physical Chemistry* **1973**, *77*, 1758 - 1762.
[6] A. Kricheldorf, C. V. Lossov, N. Lomadze and G. Schwarz, *Polymer Chemistry* **2008**, *46*, 4012 - 4020.
[7] G. Floudas and P. Papadopoulos, *Macromolecules* **2003**, *36*, 3673 - 3683.
[8] M. Yu, A. P. Nowak and T. J. Deming, *J. Am. Chem. Soc.* **1999**, *121*, 12210 - 12211.
[9] V. Breedveld, A. P. Nowak, J. Sato and T. J. Deming, *Macromolecules* **2004**, *37*, 3943 - 3953.
[10] J. Zou, F. Zhang and K. L. Wooley, *Soft Matter* **2013**, *9*, 5951 - 5958.
[11] G. J. Habraken, A. Heise and P. D. Thornton, *Macromolecular rapid communications* **2011**, *33*, 272 - 286.
[12] E. Ibarboure, E. Papon and J. Rodríguez-Hernández, *Polymer* **2007**, *48*.
[13] T. Kumaki, M. Sisido and Y. J. Imanishi, *Journal of Biomedical Materials Research* **1985**, *19*, 785 - 811.
[14] L. Lecamp, B. Youssed and C. Bunel, *Polymer* **1997**, *38*, 6089 - 6096.
[15] S. D. Vacche, V. Geiser, Y. Leterrier and J.-A. E. Månson, *Polymer* **2010**, *51*, 334 - 341.
[16] B. Golaz, V. Michaud, Y. Leterrier and J.-A. E. Månson, *Polymer* **2012**, *53*, 2038 - 2048.
[17] C. E. Corcione, A. Greco and A. Maffezzoli, *Journal of Thermal Analysis and Calorimetry* **2003**, *72*, 687 - 693.
[18] B. Bruchmann, *Macromol. Mater. Eng.* **2007**, *292*, 981 - 992.

4. Photo-initiated polypeptide grafting from solid substrates

4.1 Introduction

Surface grafting of polypeptides resulting in the formation of thin polypeptide films on solid surfaces by NCA ROP bears possibilities for the modulation of interfaces in the field of biomaterials[1],[2]. The surface grafting of polymers can be divided into the 'grafting to' and 'grafting from' approach. The first relies on a coupling of two functional groups on the polymer and the surface, often performed via click-chemistry[3]-[5]. The latter involves the decoration of the surface with an initiating group active in the polymerization. For NCA ROP this would be a nucleophilic compound on the surface, allowing the polymerization to proceed via the NAM mechanism. Successful grafting of polypeptide from surfaces was already disclosed in literature, including grafting from silicon wafers[6], silica nanoparticles[7], magnetic Fe_3O_4 nanoparticles[8], and synthetic polymers[9]. Most of these systems employ the initiation of NCA ROP via the conventional amine-initiated mechanism (NAM) from primary amine initiators. Witte and Menzel also showed a successful surface initiation using a nickel based metal-organic catalyst[10].

An approach that has not been explored to date is light induced surface grafting of polypeptides from solid substrates. A successful development would open up, for the first time, spatially controlled lithographic methods to prepare functional polypeptide-grafted surface features for next-generation bio-interfaces, nano-fluidics and the creation of biological sensors. Creation of polypeptide patterns on surface is already possible, involving premodification reactions on the surface, in which the initiator is selectively located on the surface[11]. However, this approach involves multiple premodification steps. Direct light initiation, as proposed by us, offers the potential to draw structures through a masking process in analogy to photopolymerization of vinyl monomers[12],[13], for example acrylates[14]-[16] and would circumvent premodification steps of the surface.

In this chapter NCA photopolymerization from solid surface is described for the first time, to the best of the authors knowledge. To investigate the feasibility of the approach, the photoinduced surface grafting was performed on both spherical silica nanoparticles as well as planar silicon wafer substrates. Both substrates have their own characteristics and challenges and require individual analysis techniques to prove a successful process. As photoinitiator, the previous discussed 4,5-dimethoxy-2-nitrobenzyl chromophoric

protection group was successfully attached to a (3-aminopropyl)triethoxysilane (APTES)-based isocyanate. The carbamate product was used for surface modification of silica nanoparticles and wafers. Upon irradiation, the generated amine initiated the NCA polymerization resulting in grafted polypeptide. The grafting was confirmed by detailed surface analysis and comparison with control experiments providing clear evidence of the first UV-triggered polypeptide lithography system.

4.2 Experimentals:

Materials

Tetraethoxysilane, and 3-(triethoxysilyl)propyl isocyanate were purchased by Sigma-Aldrich. Ammonia solution, and NaOH was supplied by VWR.

Surfactant synthesis

4,5-dimethoxy-2-nitrobenzyl alcohol (1,706 g, 8,0 mmol) was transferred into an already preflashed Schlenk tube. Anhydrous THF (40 ml) was added to dissolve the alcohol, before 3-(triethoxysilyl)propyl isocyanate (1,981 ml, 8,0 mmol) was added. Dibutyltin dilaurate (40 µl, 0,067 mml) was added, before the reaction mixture was stirred at room temperature under nitrogen atmosphere for 22 hours. During reaction the conversion was analyzed by TLC plates. The crude product was concentrated under vacuum, yielding in a yellow/orange oil. It was dissolved in 2 ml DCM to load it on a column for column flash chromatography, using EtOAc/heptane in a 1/1 ration. Heptane was treated with 1% triethylamine to passivate the silica gel. After chromatography the yellow crystal, 4,5-dimethoxy-2-nitrobenzyl 3-(triethoxysilyl)propyl carbamate (3,62 g, 7,86 mmol, 98 % yield) was obtained. ^{1}H-NMR (300 MHz, $CDCl_3$, δ, ppm): 0,56 – 0,61 (t, 2H, SiCH_2, *J* = 8,1 Hz), 1,16 (t, 9H, CH_3CH_2O, *J* = 6,99 Hz), 1,59 (m, 2H, $SiCH_2CH_2$), 3,16 (m, 2H, $NHCH_2$), 3,76 (q, 6H, CH_3CH_2, *J* = 6,99 Hz), 3,90 (ds, 6H, CH_3O), 5,18 (s, 1H, N*H*), 5,43 (s, 2H, $C(O)OCH_2$), 6,95 (s, 1H, C*H ortho* to NO_2), 7,63 (s, 1H, C*H ortho* to CH_2O). ^{13}C-NMR: (100MHz, $CDCl_3$, δ, ppm): 7,78 (1C, $SiCH_2$), 18,39 (3C, CH_3CH_2), 23,40 (1C, CH_2CH_2Si), 43,64 ($NHCH_2$), 56,49, 56,50 (2C, CH_3O), 58,59 (3C, CH_3CH_2), 63,44 $C(O)OCH_2$), 108,27 (CH, *ortho* to NO_2), 110,25 (CH, *ortho* to CH_2O), 128,59 (*ipso* to CH_2O), 139,91 (CNO_2), 148,16 (*C, meta* to NO*2*), 153,64 (*C, para* to NO_2), 156,02 ($C(O)$).

Silica nanoparticle synthesis

Silica nanoparticle formation was performed according to Stöber method[17]. Tetraethoxysilane (76,0 g, 365 mmol) was transferred into a 1 l round bottom flask, before it was diluted in 738 ml pure ethanol. After 1 min stirring, ammonia (30%) (13,0 ml, 601 mmol) was added. After short stirring for 1 min the reaction mixture was left for 10 days. The initial clear solution turned into a milky hazy suspension. Subsequently the particles were obtained by several centrifugation/washing cycles in ethanol, acetone, and THF. DLS analysis provided an average particle size of 255 nm, with a PDI of 0,037.

Passivation of glassware

Glass reaction vials used for silanization were washed with THF and water, before leaving them in an oven at 120 °C overnight. After cooling under nitrogen, the vials were filled with pure HMDS. After 24 hours, the glassware was washed with THF and water, removing any unreacted HMDS.

Substrate preparation and cleaning

Silicon wafers (siltronic, 1,0,0 orientation, both side polished, undoped) were cut in 2,5 cm x 1,0 cm slides. The slides were dipped in piranha solution (H_2SO_4(conc)/H_2O_2(30 %), 5/1) overnight. The wafers were washed several times in Milli-Q water. pH-measurement of the final washing step ensured complete removal of the acid. Wafers were stored at 120 °C before further use.

Surface silanization

For silicon nanoparticle silanization, 4,5-dimethoxy-2-nitrobenzyl 3-(triethoxysilyl)propyl carbamate (5,0 g, 10,86 mmol) was transferred into a 1 l round bottom flask. It was dissolved in 350 ml ethanol (96%). After complete dissolution acetic acid was added to adjust the solution at pH 4. The solution was stirred for 4 hours. Silica nanoparticles (2,0 g) were added to 50 ml ethanol, sonicated to a homogeneous suspension and added to the silane solution. Acetic acid was added to adjust the solution to pH4. The suspension was stirred overnight. Decorated silica nanoparticles were obtained by successive centrifugation/washing steps in ethanol and THF. Final drying under vacuum at 110 °C removed traces of solvent.

For Silicon wafer silanization, 4,5-dimethoxy-2-nitrobenzyl 3-(triethoxysilyl)propyl carbamate (170 mg, 0,037 mmol) was dissolved in 17 ml anhydrous THF. After complete dissolution 17 µl of 1 mN NaOH (aq) was added. The reaction was stirred for 1 hour before the solution was filtrated through a 0,2 µm PTFE filter. The cut wafer slides were dipped into the filtrated silane solution. The reaction was left for 24 hours under stirring at room temperature under inert atmosphere. The wafers were washed several times in THF, ensuring complete removal of unreacted silanes, before a final washing step in Milli-Q water. The substrates were left for 1 hour in the oven (120 °C) before further use.

Photopolymerization on surfaces

For photo-polymerization on silicon wafer surface, benzyl-L-glutamate NCA (150,0 mg, 0,75 mmol) was dissolved in 1 ml anhydrous DMF. Wafer substrates were equipped

with a PTFE sealant tape (GORE® Joint Sealant, 100% monoaxially expanded PTFE, 3 mm width), and fused quartz microscope slide (Alda Aesar®, 1,0 mm thickness). Both slides were fixated with clamps. Through a slit of the sealant, the NCA solution was injected until the volume between wafer and quartz slide was filled completely. The substrate was exposed to the blacklight lamp Vilber Lourmat VL-215.L at a horizontal distance of 2 cm for 60 min. After light irradiation the substrate was covered in dark at room temperature for further 24 hours. After removal of the quartz slide and sealant silicon wafers were rinsed with THF in a Soxhlet apparatus for 3 days to remove ungrafted material. The wafers were stored for 1 h at 120 °C to remove the organic solvent.

For photopolymerization on silica nanoparticles, the functionalized particles (200 mg) were suspended in 2 ml anhydrous DMF. Benzyl-L-glutamate NCA (300 mg, 1,14 mmol) and 200 mg of silane functionalized silica nanoparticles were transferred into a quartz cuvette, before the silica nanoparticle suspension was added. Under nitrogen atmosphere the cuvette was placed vertically in a distance of 2 cm in front of the blacklight lamp. Under stirring the cuvette was irradiated for 60 min, before covered in dark and further stirring at room temperature for 4 days. The grafted particles were precipitated trice in ice-cold diethyl ether, followed by five washing steps in THF to remove ungrafted material and final 3 washings in diethyl ether to remove traces of THF. NMR analysis did not detect any polymeric material in the supernatant. Therefore it was anticipated that silica nanoparticles were free from any non-covalent attached polymeric material.

Thermogravimetric analysis (TGA)

Thermogravimetric analysis was carried out on a METTLER TGA/DSC system. The sample was injected on a METTLER M3 scale and heated up by a METTLER TG50 heat block. Measurements were controlled by a METTLER TOLEDO TC15 TA Controller. Obtained data were analyzed by the METTLER Toledo AG STARe software (v. 9.10). Measurement were recorded from a start temperature of 25 °C. The heat rate was at 10 °C/min. At 100 °C the heat was hold constant for 60 min to ensure full evaporation of water or solvent, before it was heat up with the same heating rate up to 800 °C.

UV-Vis

UV-Vis samples were dissolved in acetonitrile and measured in Hellma® Quartz SUPRASIL® cuvettes, light path 10 mm. Absorption spectra were measured on a

PerkinElmer Lamda 35 UV/Vis spectrophotometer ranging wavelengths from 200 – 800 nm, slit width 2 nm, scan speed 480 nm min-1, lamp change at 326 nm. Data were analyzed by PerkinElmer UV WinLab software.

Contact Angles

Contact angles of water on silicon wafers were measured on a Krüss DSA 25 contact angle goniometer. The camera was adjusted at 3 °, measurements were performed at room temperature. As solvent ultra pure Milli-Q water was used. A drop of water (2 µl) was picked by the sample from the syringe needle. Angles were measured after 30 sec of depositing the drop on the surface. Per drop 10 pictures were taken in 2 sec. Angles were measured on five different drops, results were averaged and standard deviation was calculated. Data were analyzed by the Krüss DSA4 (v. 1.1(a)) software.

Ellipsometry

Ellipsometry was carried out at an angle of 80° on a VASE M-2000U Woolam spectroscopic ellipsometry apparatus. Measurements were performed at wavelength from 250 – 900 nm. The quartz Tungsten Halogen (QTH) lamp was used as light source and linear polarized before hitting the sample. CCD array enabled collection of multiple wavelength data. Measurements were performed stepwise, starting with the Piranha solution cleaned substrate as initial layer. Further substrates were measured according to the optical model and its layer order.

X-ray Photoelectron Spectroscopy (XPS)

The XPS measurements are carried out with a Thermo Scientific K-Alpha, equipped with a monochromatic small-spot X-ray source and a 180° double focusing hemispherical analyzer with a 128-channel detector. As electron source an aluminum anode (Al Kα = 1486,6 eV) operating at 72W and a spot size of 400µm was used. Sample scans were measured at constant pass energy of 200 eV and region scans at 50 eV. A different Argon pressure was present for background (2 x 10^{-9} mbar) and for samples (3 x 10^{-7} mbar) due to the charge compensation dual beam source.

Time-of-Flight Secondary Ion Mass Spectroscopy (ToF-SIMS)

Silicon wafers were measured on a PHI nanoTOF II ToF-SIMS apparatus. As ion source, A liquid metal ion gun (LMIG) was used with 400 µm diameter, at high flow, bunched. The images were taken on an area of 100 x 100 µm, or 400 x 400 µm, depending on the

sample. The image resolution was adjusted to 512 x 512 pixel. Per sample 5-10 scans (depending on counts measured on sample) were performed. For sputtering, 1 scan per sputtering cycle was used, 5 sec per cycle, 20 cycles. The image area was 200 x 200 µm

4.3 Results and Discussion

4.3.1 Synthesis of photoamine generator silane coupling agent

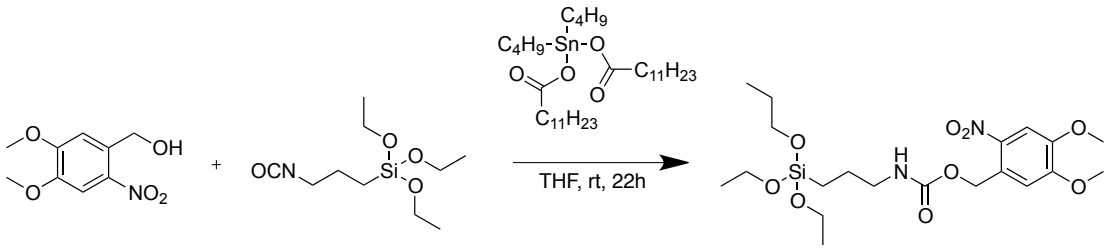

Scheme 4.1: Synthesis of 4,5-dimethoxy-2-nitrobenzyl 3-(triethoxysilyl)propyl carbamate, by reacting 3-(triethoxysilyl)propyl isocyanate with 4,5-dimethoxy-2-nitrobenzyl alcohol using a catalytic amount of dibutyltin dilaurate in THF at room temperature for 22 hours.

As shown in the previous chapters, the formation of a photocleavable carbamate involves a chromophoric alcohol and an isocyanate compound, which, after successful photopolymerization is covalently bound at the *C*-terminus of the polypeptide. Thus, 3-(triethoxysilyl)propyl isocyanate was reacted with 4,5-dimethoxy-2-nitrobenzyl alcohol in presence of dibutyltin dilaurate (Scheme 4.1). The reaction was allowed to stir for 22 h, after which thin-layer chromatography (TLC) confirmed full conversion. Final purification by column chromatography gave access to the pure product in good yield (98 %). Analysis by ^{1}H NMR confirmed the successful conversion into the carbamate without any side product or substrate traces. Especially peak 4 (Figure 4.1) is a characteristic peak for the successful conversion into a carbamate, as these protons shift from the alcohol compound at 4.93 to 5.43 ppm in the carbamate.

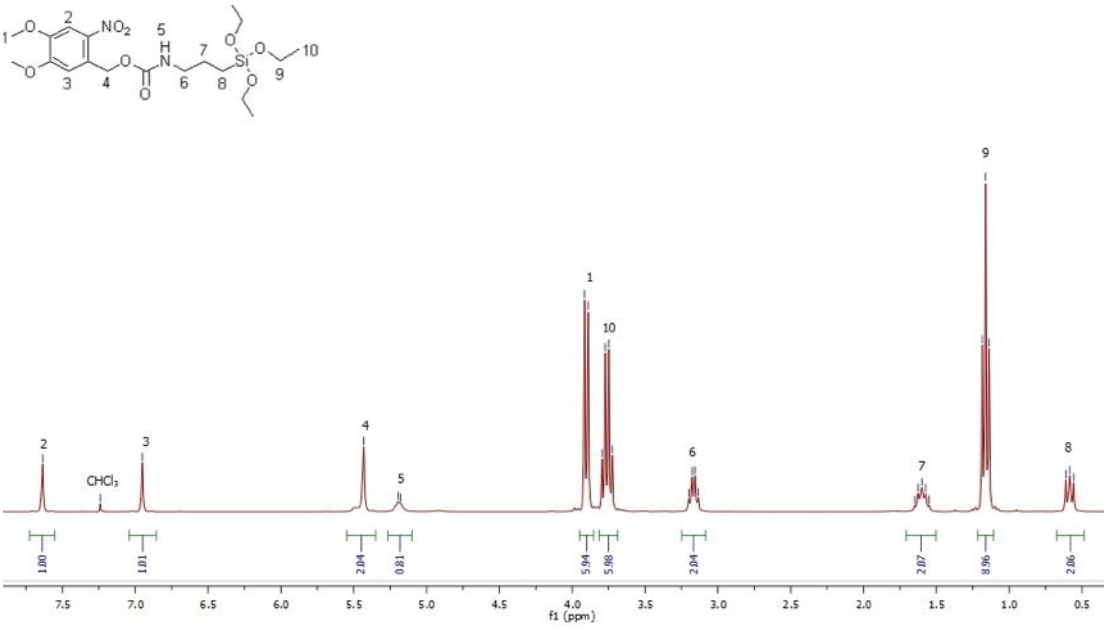

Figure 4.1: ^{1}H NMR spectrum of 4,5-dimethoxy-2-nitrobenzyl 3-(triethoxysilyl)propyl carbamate, measured in deuterated chloroform after purification by column chromatography and removal of solvents.

The use of 4,5-dimethoxy-2-nitrobenzyl alcohol as chromophoric group enables the application of the same blacklight system as described in Chapter 3. Under irradiation the carbamate compound will break down under decarboxylation into a surface-bound triethylsilylamine. Notably, the same procedure was applied by Stegmeier and coworkers [18], who demonstrated photocleavage of this surface-bound photoamine generator and the subsequent reaction of the amine with a fluorescent dye. The silane compound was incorporated either on silica nanoparticles with a size of 255 nm to obtain a spherical surface grafting, or on polished, undoped silicon wafers, to obtain a planar surface grafting.

4.3.2 Spherical surface grafting on silica nanoparticles

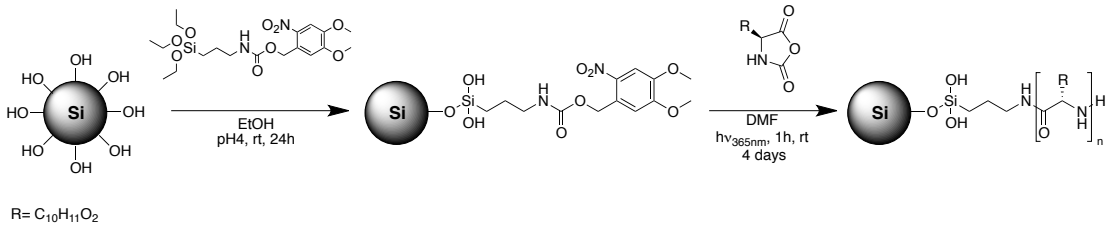

Scheme 4.2: Representation of silica nanoparticle functionalization with the silane-based photoamine generator. Hydrolyzation of the silane compound and the following condensation on the silica surface was performed at pH 4 in ethanol. Final grafting from the surface was achieved by irradiating the suspended particles at 365 nm in DMF for 1 hour. The sample was placed in the dark under stirring for additional 4 days to allow full polymerization of the NCA monomers.

The silane-based carbamate was hydrolyzed at pH 4 in ethanol for 4 hours, before suspended silica nanoparticles in ethanol with a size of 255 nm were added to the reaction mixture. After adjusting the solution to pH 4, the silane compound was allowed to condensate on the particle surface for 16 hours. Subsequently, the particles were washed several times with ethanol, and THF, ensuring complete removal of any unbound silane compounds. Due to the presence of light absorbing functional groups in the silane, UV-Vis spectroscopy is a useful tool to verify a successful attachment onto the nanoparticles. The UV-Vis spectra of the blank nanoparticles and the photoamine decorated nanoparticles were recorded from the UVC region at 250 nm up to long wavelength in the visible light at 800 nm (Figure 4.2). While undecorated silica nanoparticles do not show any significant absorption (black line) in the UVA region, surface modified particles show the specific absorption of the chromophotic functional group around 365 nm (red line). The abrupt absorption decrease at 400 nm is due to a switch between two different light sources in the spectrometer. Since the nanoparticles were modified using an excess of the silane compound, unbound silane coupling agent

could be still be present in solution leading to faults conclusions. In order to exclude that the UV absorbance is not caused by free silane coupling agent, the supernatant of the last washing step was also investigated under UV-Vis spectroscopy (blue line). No absorption at 365 nm was observed, confirming that the absorption of the decorated particle can only be ascribed to the covalently bound silanes on the surface.

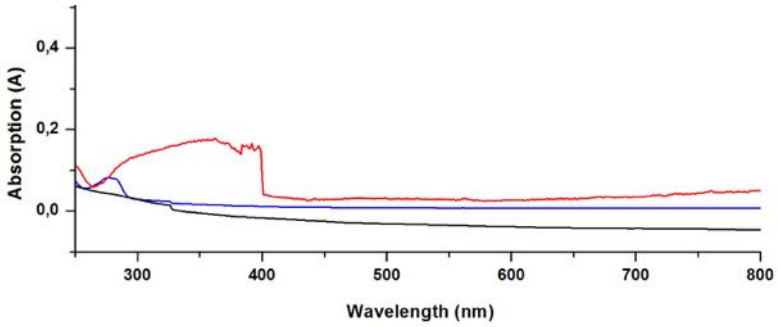

Figure 4.2: UV-Vis spectra of naked silica nanoparticles (black), silane-based photoamine generator functionalized particles (red) and supernatant of last washing step of the particles (blue).

DLS measurements in water revealed an increase of the hydrodynamic diameter after the silane based photoamine generator was reacted with the nanoparticles, denoted as **PAG** in Table 4.1. In the following the modified particles were utilized for the photo-initiated polymerization and the grafting of BLG NCA from the nanoparticle surface. NCA monomer and homogeneously suspended modified particles in DMF were transferred into a quartz cuvette. The particles were exposed to the blacklight lamp for 60 min, followed by stirring in the dark for 4 days. As a negative control one reaction mixture was kept in the dark and not exposed to the light source (-UV). In addition, another sample was prepared in which the particles were exposed to light in the presence of a polymer solution. This was done to exclude false positive results by possible physisorption of PBLG to the primary amine surface. For the work-up, the particles were washed three times with diethyl ether to remove any unreacted monomers, followed by five washing steps with THF to ensured the removal of any non-covalent attached polymer material. Final three washing steps with diethyl ether ensured complete removal of THF from the particles. The particles were dried in a vacuum oven for further analysis.

The diameter of the particles from the negative control (-UV) of 262 nm is in good agreement with the initial silane-modified particle size (269 nm). This confirms that no grafting reaction took place as expected. The diameters of the particles exposed to PBLG are only slightly higher (295 nm) than the diameter of the original particles highlighting that the washing procedure removes the majority of physisorbed PBLG. Polymer

grafting by photoinitiation (+UV) shows a significant increase of 209 nm of the particle diameter to 478 nm compared to the initiator modified nanoparticles. This increase is higher than in other literature reports. Borase reported a hydrodynamic size increase of 60 nm by initiating BLG-NCA from 150 nm APTES functionalized silica nanoparticles at 20 °C.[7]. Yang used the same functionalization of silica nanoparticles with an initial diameter of 157 nm. After surface polymerization an increase of 50 nm at a reaction temperature of 40 °C[19]. Considering that the same washing procedure was followed for all three experiments, this cannot be caused by physisorbed PBLG but rather covalently bound PBLG by surface initiation.

Table 4.1: DLS data, including hydrodynamic diameter and particle dispersity of naked (blanco), silane-based photoamine generator functionalized (PAG), photo-initiated (+UV) silica nanoparticle and its negative controls –UV and Ad.

Modification	Diameter (nm)	PDI
blank	255	0,037
PAG	269	0,107
+UV	478	0,277
-UV	262	0.098
Ad	295	0,108

The nanoparticles were dried and further investigated by FT-IR (Figure 4.3). In the presence of monomer and UV irradiation characteristic peaks of PBLG are observed (**+UV**). The peptide carbonyl group of amide I at 1650 cm^{-1} and of amide II at 1548 cm^{-1} can clearly be identified. Lower peak intensities at 1650 cm^{-1} can also be identified for the negative controls while the amide II band is absent. In case of **–UV** and **PAG**, the vibration band 1650 cm^{-1} can be ascribed to the carbamate carbonyl of the photoinitiator. Unmodified silica nanoparticles do not show any signal in the carbamate carbonyl or in the polypeptide amide I region, which is consistent with the expectation. It has to be mentioned that the obtained data are near the detection limit of the FTIR method and should be treated indicative.

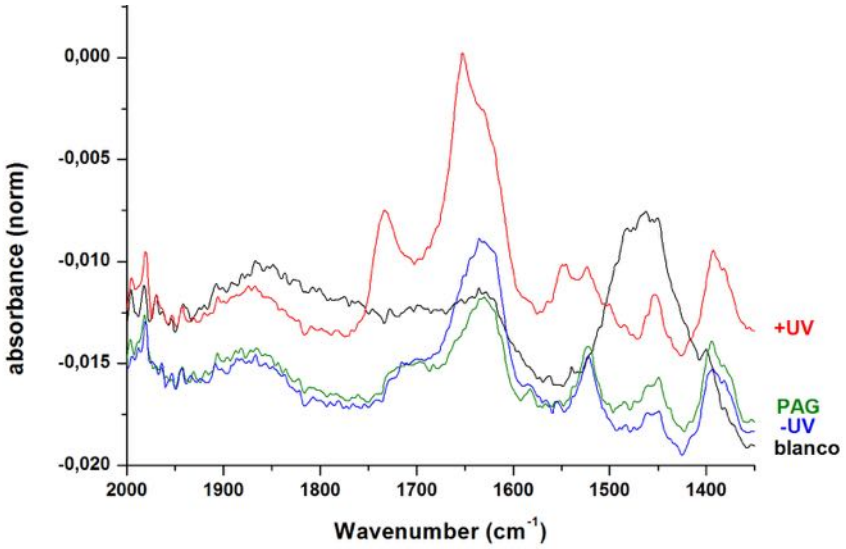

Figure 4.3: ATR-FTIR spectra of dried silica nanoparticles, naked (black), photoamine generator modified (green), photo-initiated (red), and controls without light irradiation (blue).

TGA analysis was performed to investigate a possible weight increase of the nanoparticles due to an organic layer incorporation of the polypeptide. Unmodified particles, as well as negative controls were also considered. The particles were heated up from room temperature to 800 °C, with a temporary constant temperature at 110 °C for 1 hour. This ensured a complete evaporation of water and organic solvent. From the data, a mass increase of photoamine generator assembled nanoparticles (1,5 %) compared to the unmodified nanoparticles was calculated (Figure 4.4), providing evidence of the successful coupling of the silane molecule to the surface. Particles, which underwent NCA photopolymerization, displayed an additional mass increase of 7%. It was believed, that increase of the monomer:initiator ratio would lead to an increase of polymer material on the surface of the particles. Therefore two samples with an NCA to nanoparticle weight ratio of 1:1 (dotted line) and 3:2 (straight line) were chosen. The latter was believed to result in a larger polymer weight increase on the particle surface. However, no significant increase of polymer material was observed. It can be speculated that sterical constrains limit the growths of the polymer but without additional experimental work no conclusion can be drawn. For the 3:2 ratio a typical mass reduction line is observed with a typical sigmoid shaped curve, starting at 250 °C, reaching its maximum decrease at 300 °C. With increasing temperature up to 550 °C a lower mass reduction is observed. A last interval from 550 °C to 800 °C displays the lowest mass reduction.

Major mass loss between temperatures from 250 to 550 °C was ascribed to the removal of polymer material[19],[20]. Mass loss from 550 to 800 °C can be explained by dehydroxylation of the silica material[21].

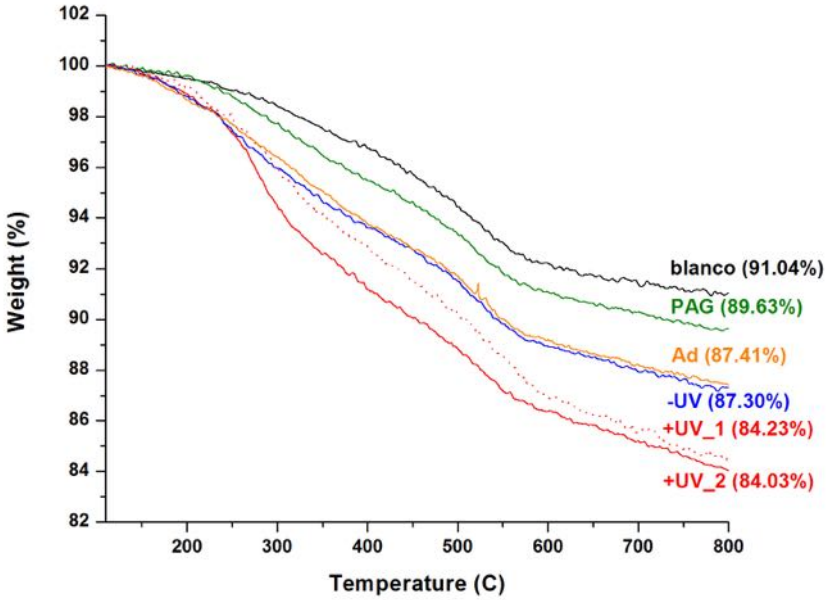

Figure 4.4: Thermo-gravimetrical analysis (TGA) results of silica nanoparticles. All samples were hold at 110 °C for one hour, before data were collected: bare Si-NP (black), photoinitiator decorated Si-NP (green), photoinitiated Si-NP (red), and negative controls (blue and orange). Photoinitiation reaction was performed with two samples, with either w% of 1:1 (dotted line) or 3:2 (straight line). All samples have been treated under same conditions.

4.3.3 Planar surface grafting on silicon wafers

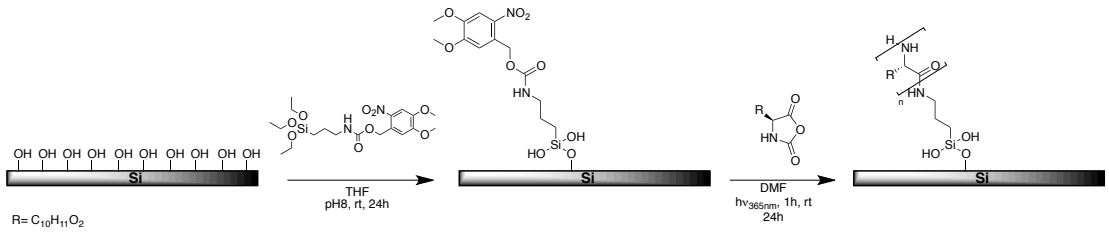

Scheme 4.3: Representation of silicon wafer surface modification with the silane-based photoamine generator. At pH 8 hydrolyzation of the silane compound is performed, before condensation on the piranha solution cleaned wafer is achieved. Additional surface grafting of PBLG in DMF is performed with 1-hour UV irradiation, followed by 24 hours conversion of the monomer into polymer material.

Before any modification on the wafer surface was performed, the wafers were cleaned by dipping the wafer pieces in Piranha solution overnight. Extensive washing with MilliQ water ensured complete removal of piranha solution. pH determination of the last washing step confirmed neutral pH, therefore piranha solution free substrates. In the following, surface modification was performed. A 1% w/v solution of the silane-based photoamine generator was prepared in THF. 5 x 10^{-5} mol eq. of sodium hydroxide was added to obtain slightly basic condition. After 1 hour of stirring, the cleaned wafer was immersed in the reaction solution (Scheme 4.3). After 24 hours, the substrate was washed extensively with MilliQ water and THF. Final storage at 120 °C ensured complete removal of water.

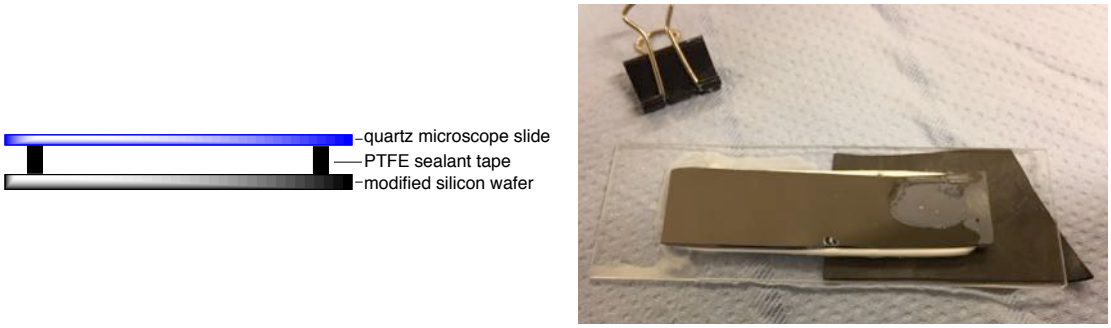

Scheme 4.4: Illustration of the preparation and construction of silicon wafers, used for photografting of PBLG. The photoamine generator equipped silicon wafer was laid on UV-light-transparent quartz microscope slide. The space between both layers consists of PTFE sealant tape, leaving a volume between the slide and wafer for BLG monomer solution.

In the following, photo-initiated surface grafting of polypeptides from silicon wafers was investigated. Various grafting approaches of polypeptides on solid surfaces are described in literature[6],[22],[23]. It has to be noted that approaches such as dipping, or spin coating of the wafers are not suitable in a photopolymerization approach. Monomer and silane based photoamine generators have to be in defined position, while exposed to the light source for 60 min. In addition, it was believed that the monomer solution

should only be a few millimeters to ensure sufficient light absorption of the silane-based photoamine generator through the solvent layer. Therefore, a system was devised in which the monomer solution was injected between a quartz microscope slide and the silane-photoamine generator modified silicon wafers (Scheme 4.4). Between both slides a PTFE sealant tape was placed as a spacer to ensure sufficient volume for the monomer solution. Clamps at the edges hold both layers together. In addition, regions on the quartz plate could be covered from the light (Scheme 4.4, black piece of paper) to obtain a region not exposed to the light.

In the first step, the silane-based photoamine generator was attached to a Piranha solution cleaned silicon wafer. In the next step, the photopolymerization was carried out by injecting the monomer solution between the wafer and the quartz plate, followed by light exposure for 60 min and further reaction time of 24 hours in the dark. Final washing in a Soxhlet apparatus, using THF as solvent, ensured complete removal of non-covalent attached polymer material. Next to the photoreaction sample, denoted as **+UV**, two negative controls were performed. These negative controls were consistent with those already mentioned in section 4.3.1, denoted as **Ad**, **-UV**, **PAG**, and **blanco**. An additional control sample was produced, i.e. the primary amine, 3-aminopropyl silane (APTES) functional wafer constituting the breakdown product of the photoreaction. This sample, denoted as **Dep,** is exclusively necessary for ellipsometry analysis, as well as for contact angle measurements. The photodeprotection of the substrate was performed according to established procedure.[18]

The set of five substrates were first analyzed by contact angle measurements. By obtaining the water contact angle on the differently treated substrates, trends in hydrophobicity can be obtained. Piranha solution cleaned silicon wafers are assumed to contain a homogenous layer of fully water wetable oxidized silica (Si-OH). The increase in the contact angle, i.e. the decrease of polarity, caused by the incorporation of the photoamine generator (**PAG**) to 65.2°, is clearly noted (Table 4.2). The following increase of polarity in **Dep** (contact angle 52,2° ± 1,4) is the result of the photo deprotection and release of the polar amine group. The contact angle and thus the polarity of both, the photoamine generator modified substrate and the deprotected substrate, are in agreement with literature in which a change from 65° ± 5 to 59° ± 2 is stated.[18],[24] Surface immobilized PBLG was believed to decrease the polarity due to the hydrophobic character of the polypeptide. Indeed, the measurement of the sample exposed to UV light displayed a significant increase of the contact angle (82,5° ±0,7), which is in agreement with expectation and previous measured contact angles on PBLG grafted substrates.[25] Moreover, all negative controls are in good agreement with

expectations. Since the **–UV** substrate should maintain the photolabile silane based photoamine generator on the surface, identical polarity is expected. Indeed, the contact angles barely differ. In case of the **Ad** negative control, the substrate was irradiated, therefore it is expected that the substrate should have identical polarity as **Dep** substrate. Contact angles of these substrates show nearly similar results, where the **Ad** negative control show a slightly higher contact angle. One could speculate that complete deprotection was not achieved.

Table 4.2: Properties of silicon wafer substrates

Substrate	Contact angle (°)	Ellipsometry	
		thickness (nm)	MSE
blanco	61,6 ± 0,5	1,54	8,569
PAG	65,2 ± 0,6	0,2	15,968
Dep	52,2 ± 1,4	0,1	1,156
+UV	82,5 ± 0,7	2,99	5,991
-UV	65,7 ± 0,6	0,87	3,755
Ad	57,8 ± 0.9	0,59	4,883

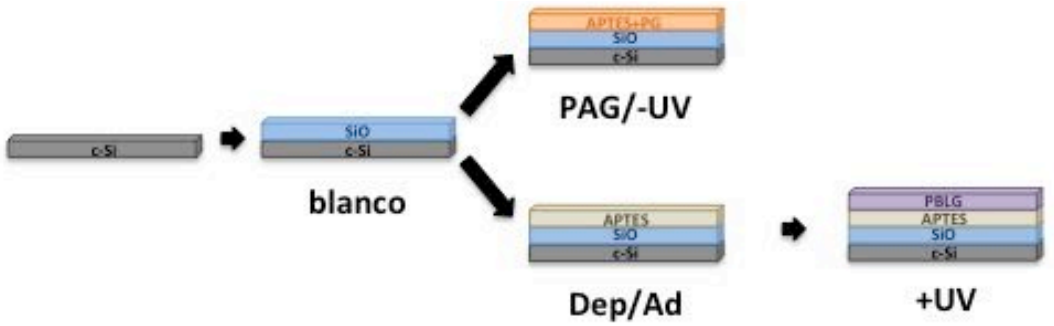

Scheme 4.5: Illustration of the optical model consideration for ellipsometry analysis.

In a next step, the thickness of generated layers was determined by ellipsometry. Spectroscopic ellipsometry is an optical measurement technique, which allows characterization of changes in polarized light upon reflection at the surface of the sample. Two angles, psi and delta, are measured and their changes due to the reflection from the sample surface are fitted mathematically. In the first step a theoretical optical model had to be considered. The model consists of different layers and the samples are ordered by the ascending number of layers; each sample is described by a new layer on top of the underlying layers (Scheme 4.5). Starting with a background layer, in this case crystalline silicon (c-Si), the model was further constructed with a first layer, the oxidized silicon (SiO), depicted as the **blanco** substrate. The blanco sample is described

by the background layer as basis and the new additional layer (SiO). In the following, according to the considered model, both **Dep** and **PAG** are based on the layers of the previous sample (**blanco**), added by the new layer APTES and APTES+PG, respectively. The additional layer of **Dep** is considered to include exclusively APTES, whereas PAG includes the complete silane-based photoamine generator with its photolabile protection group (PG). By photopolymerization the PBLG layer (**+UV**) is formed on the homogeneous layer of the primary amine based APTES layer. It was assumed that negative controls, **–UV** and **Ad**, are constructed of equal number of layers as **PAG** and **Dep**, respectively. Thickness values (Table 4.2) were calculated from the modeling and fitting of dielectric functions of both, the psi and delta angle. By fitting, the mean square error (MSE) values were calculated. The MSE is the square of differences between the measured values of psi and delta and the calculated fitted values. Values below 20 are considered acceptable and the fitted model is deemed correct. In this case MSE values of all investigated substrates were indeed below 20, signifying good fitting quality. Psi and delta values were measured over a wavelength range from 250 – 900 nm, represented by the red and blue lines in Figure 4.5. Black dashed lines depict the model fitting by using various dielectric functions, which in most cases overlap with the blue and red lines. Dotted orange and green lines help to compare between different samples: dotted lines in orange depict psi and delta values of the previous sample, dotted green lines depict psi and delta values of the **+UV** sample. The fact that the orange and green dotted lines do not overlap with the measured psi and delta values (red and blue lines) justifies the introduction of an additional layer to describe the new sample.

Piranha solution cleaned substrates showed an oxidized layer of 1.54 nm. Based on the SiO layer, the following layer, APTES was analyzed on the **Dep** substrate (Figure 4.5 b). Psi and Delta graphs (red and blue line, respectively) clearly differ from psi and delta values of the **blanco** sample (orange dotted line). Optimizing the fitting model with introduction of additional dielectric functions was not successful, which justifies the introduction of the additional layer, to describe the obtained angle graphs correctly. This is in total agreement with the successful introduction of the APTES layer. By the correct fitting a layer thickness of 0.1 nm was obtained. It is assumed that **PAG** is described by two layers, the underlying SiO layer and the silane-based photoamine generator layer (APTES+PG). Psi and Delta curves differ from the blanco sample (orange dotted line), however obtained results have obvious similarity to the **Dep** substrate (Figure 4.5 c). Small variation is observed between 700 and 800 nm. Interestingly, the fitting by dielectric functions delivers a twice as big layer thickness of 0.2 nm. An increase of the thickness is in agreement with expectations, since this layer includes the photo

protection group covalent bound to APTES. Photopolymerization on the surface of the silicon wafers (**+UV**) revealed a polymer layer with a thickness of 2.99 nm. The underlying Psi and Delta curves show a significant change in comparison with the previous sample (Figure 4.5 d, orange line). Both negative controls **–UV** and **Ad** were fitted by a two-layer model. Psi and Delta curves differ from the **blanco** sample (orange dotted line). In addition, their reflection angle values are not equal to the photo-polymerized sample **+UV** (green dotted line, Figure 4.5 e, f). This fact confirms the expectations.

Considering their theoretical molecular surface modification, **-UV** should consist of the same chemical surface structure as **PAG**. Both samples should contain the intact photoamine generator layer. However, comparing psi and delta graphs of both samples (Figure 4.5 e and c) a clear difference is apparent. Similar observations are obtained from the comparison of **Ad** with **Dep**, which should also contain the same surface modification layer, APTES (Figure 4.5 f and b). By fitting the psi and delta values with dielectric functions, layer thicknesses of both negative controls were determined. **-UV** illustrated a layer thickness of 0.87 nm, therefore an increase of 0.67 nm compared to **PAG**. **Ad** showed a layer thickness of 0.59 nm, therefore an increase of 0.49 nm compared to **Dep**. Thus, there is evidence that both negative controls include material on the surface, which however, is different from PBLG polypeptide. This can be excluded by taking contact angle measurement results into account. To ensure the absence of polymer material on the negative control substrates, additional analysis of the substrates is necessary.

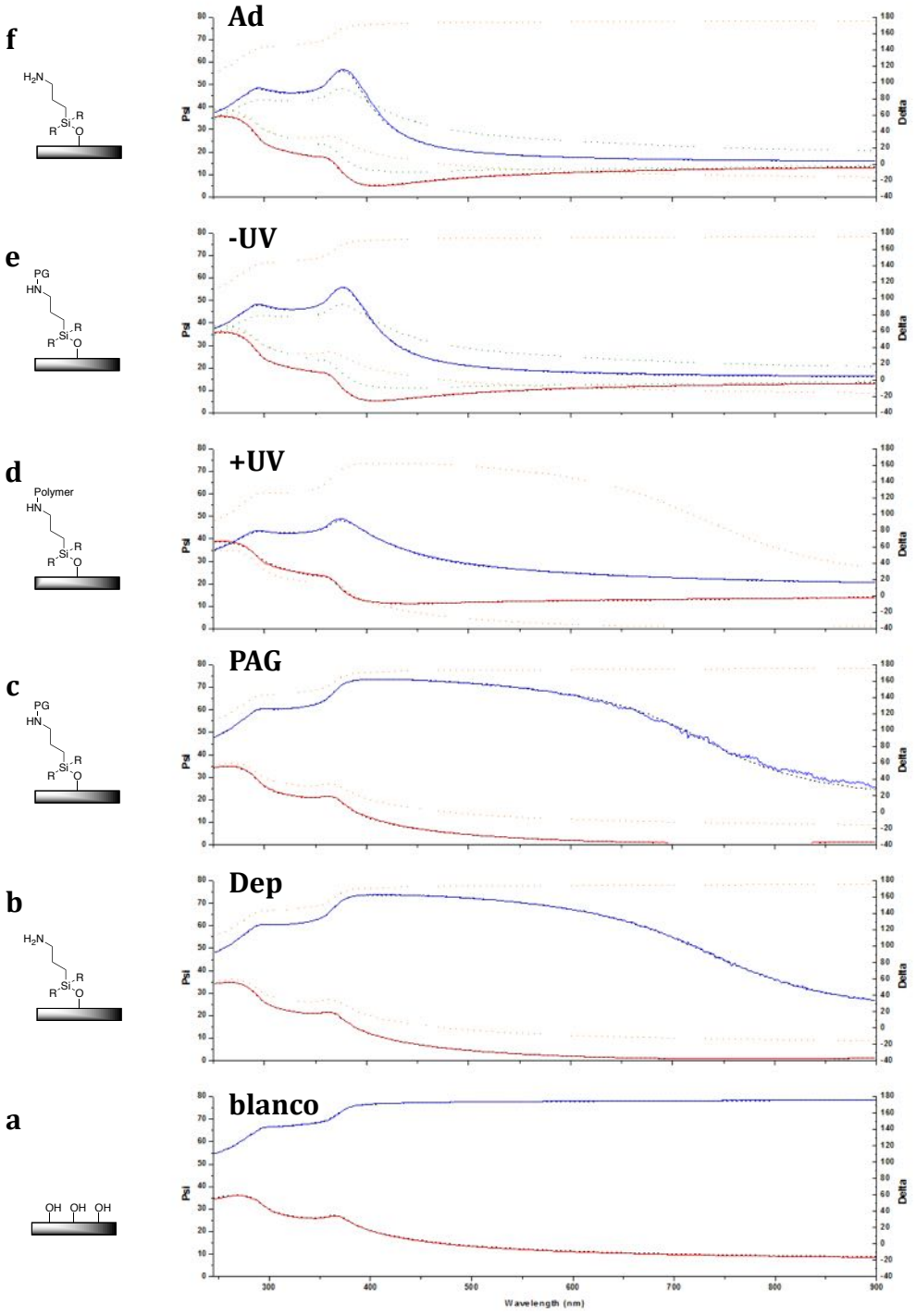

Figure 4.5: Ellipsometry results of the different wafer substrates: (a) bare, (b) deprotected, APTES modified, (c) photoamine generator modified, (d) photoinitiated PBLG grafted, (e) negative control without UV irradiation, (f) negative control with polymer solution treated silicon wafer. Psi (red) and Delta (blue) values were measured on a wavelength range from 250 – 900 nm. Orange dotted lines depict the fitted graph of psi or delta values of the previous layer (Scheme 4.5). Green dotted line depicts the fitting of **+UV** psi and delta values.

The five substrates were also analyzed by X-ray Photoelectron Spectroscopy (XPS). The analysis was based on the detection of four elements, carbon, nitrogen, oxygen, and silica. Especially the first two can reveal information of PBLG surface grafting. All spectra show the expected elemental signature signals (dark green), which can be fitted to identify chemical environment specified signals (colored lines) (Figure 4.6).

All five substrates show carbon (C 1s) signals around 10000 CPS. The highest intensity is measured for aliphatic carbons (C-C/C-H) (Figure 4.6 a). Signals on the **+UV** substrate have the highest intensity, consistent with the assumption that polymer material is grafted on the surface. The aliphatic carbon signals can mainly be assigned to CH_2 in the side chain, as well as to the benzyl protection group. Next to aliphatic carbon, also amide carbon (N-C=O) from the backbone, ester carbon (O-C=O) and single oxygen bonded carbon (C-O), both present in the side chain of the polypeptide, can be identified. On the **PAG** substrate, reduction of the aliphatic carbons, as well as the absence of amide carbon and a significant reduction of ester carbon can be observed. Although the photoamine generator has a carbamate functional group, therefore also bear an amide carbon, it is believed that the reduced number of bonds falls below the detection limit (Table 4.2). Negative controls **–UV** and **Ad** show a further reduction of the overall carbon signal intensity. **–UV** even shows low intensity of a C-O carbon, identifying traces of the unreacted photoamine generator. On the **blanco** substrate unexpected carbon signals are identified which might be the results of atmospheric CO_2 absorption.

Nitrogen (N 1s) signals reveal clearer evidence of a successful and selective photopolymerization. While detection of some nitrogen is observed on the **blanco**, amide-bound nitrogen signal is only detected on **PAG**. This signal can be assigned to the carbamate functional group of the photoamine generator. Furthermore, the presence of the photoamine generator is established by the presence of the specific NO_2 signals, which are assigned to the nitro group in the photolabile protection group. Once exposed to light in the photopolymerization, nitro signals are absent, and a significant intensity increase of amide-bound nitrogen is observed on **+UV**. This suggests that the breakdown of the photoamine generator was successful and the following polymerization of BLG NCA occurred. The absence of the photolabile protection group can be also concluded from the missing NO_2 and NO_3 signals on **Ad**. This sample was exposed to light in the presence of PBLG (absence of NCA). The low intensity of amide nitrogen in this sample also underlines the notion that amide nitrogen in the UV grafting sample is not due to physisorbed PBLG. In contrast, the second negative control, **-UV**, shows traces of NO_2 and NO_3 signals, since this control did not experienced light exposure and fully intact photoamine generator is expected.

Further elemental analysis on oxygen (O 1s) contributes only few conclusions. All substrates include silica-bound oxygen (Figure 4.6 c). On closer examination one could speculate the presence of amide-bound oxygen on **+UV** and carbon bound silica oxygen on the negative control substrates. Analysis of silica (Si 2p) does not disclose further distinction between the five substrates (Figure 4.6 d).

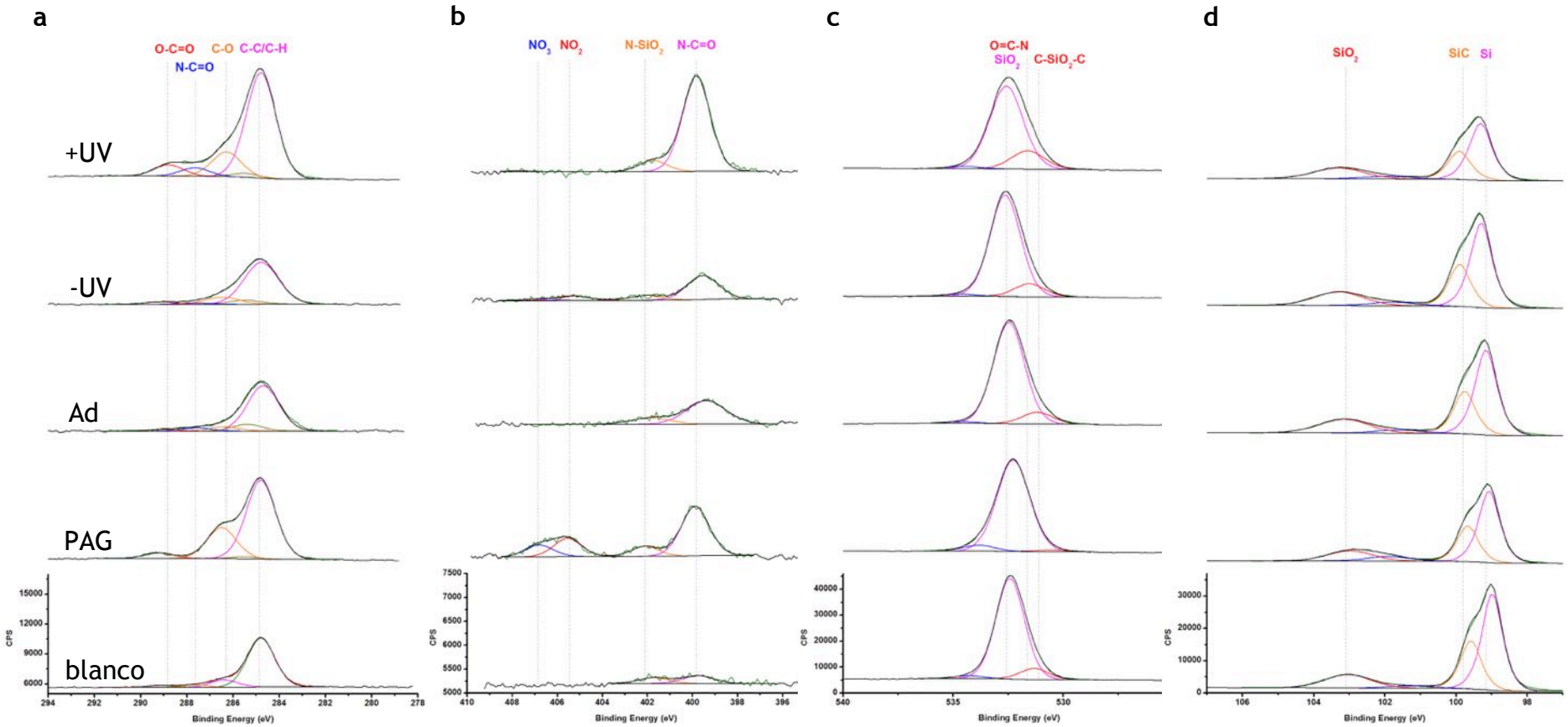

Figure 4.6: XPS elemental analysis results of silicon wafer substrates.:(a) carbon (1s), (b) nitrogen (1s), (c) oxygen (1s), and (d) silica (2p). Dark green line indicates the sum of the collected signals; colored graphs are assigned to elements, which are part of a specific functional group.

Surface analysis was further performed on the substrates by Time-of-Flight Secondary Ion Mass Spectroscopy (TOF-SIMS). This analysis technique allows detection of small ions, either positive or negative charged. In comparison to MALDI-Tof analysis, ions of TOF-SIMS are smaller, ranging from 10 to 1.000 Dalton. In the following all grafted substrates **+UV, PAG, -UV**, and **Ad** were investigated by surface TOF-SIMS and surface mapping.

In a negative mode, a variety of wafer related ions were detected and seen on all samples, including Si, SiH, SiO_2, SiO_3, and SiO_3H. Detection of these ions is the highest for the –UV and the Ad samples due to the exposure of the surface to the ionization beam, while a much lower Si ion intensity is detected for **+UV**, and **PAG** in agreement with a higher surface grafting density. However, even for these sample the data suggest an incomplete surface coverage (Figure 4.7).

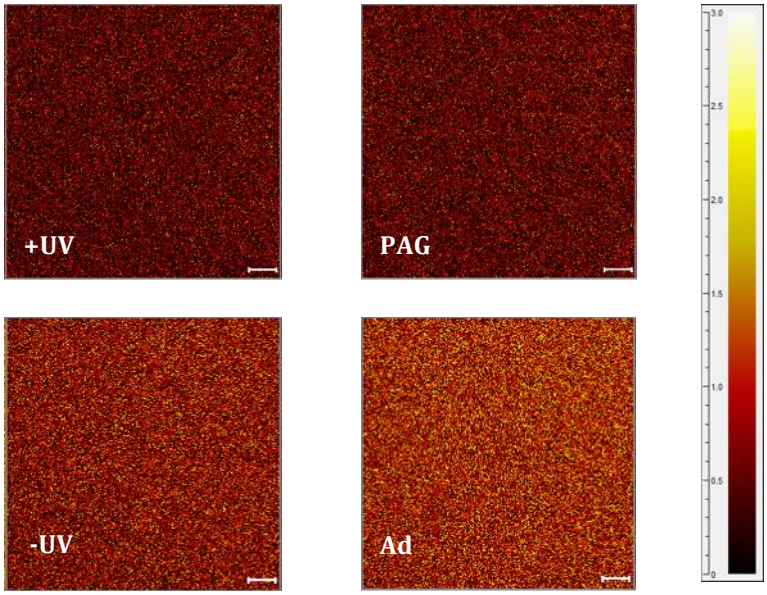

Figure 4.7: TOF-SIMS surface mapping of negative Si charged ions on **+UV**, **PAG**, **-UV**, and **Ad** substrates. The color identifies the intensity of the signal, starting from low (dark red) to high signal intensity(light yellow).

Significant distinctions between the four substrates could be observed by a signal at 91 m/z. This ion size was assigned to C_7H_7, a benzoyl ring ion. It is believed that this ion is exclusively originated from the side chain of PBLG. On **+UV** its abundance is the highest (Figure 4.8), depicted in a red color. However, detection of C_7H_7 is also observed on **PAG**, as well as on the negative controls **–UV**, and **Ad** but in much lower intensity (dark red).

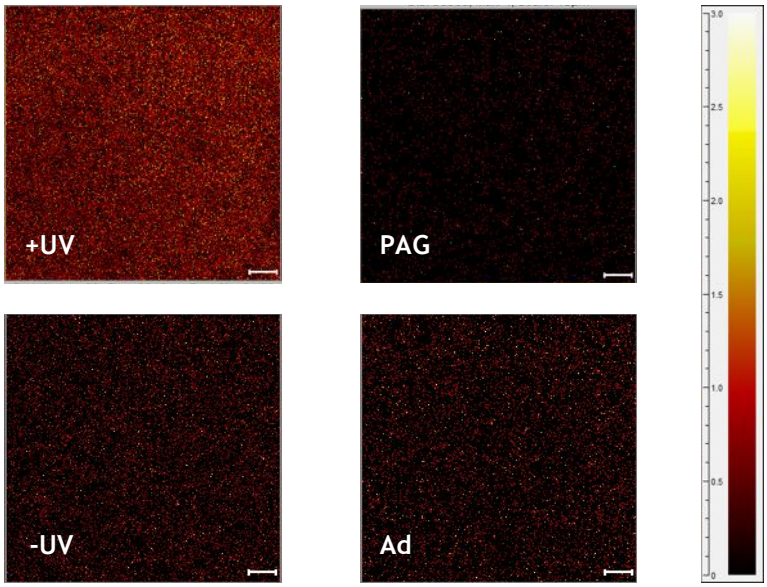

Figure 4.8: TOF-SIMS surface mapping of positive charged C_7H_7 ion on **+UV**, **PAG**, **-UV**, and **Ad** substrates. The color identifies the intensity of signal starting from low (dark red) to high signal intensity (light yellow)

After the detection of the C_7H_7 polymer specific derived ion species, depth profiling on **+UV** was performed. Sputtering under the ion beam generated the depth profiling, in which the surface layer is stepwise removed by sputtering cycles (Figure 4.9). The substrate was investigated on the presence of both, $SiCH_3$ (red) and polymer-derived C_7H_7 (green) ions. Both ion species are only present in the first few cycles, concluding only a thin layer of the grafting. In addition, it is clearly shown that the C_7H_7 containing layer, thus the polymer-grafted layer is not homogeneous and no full coverage was achieved in the grafting experiments.

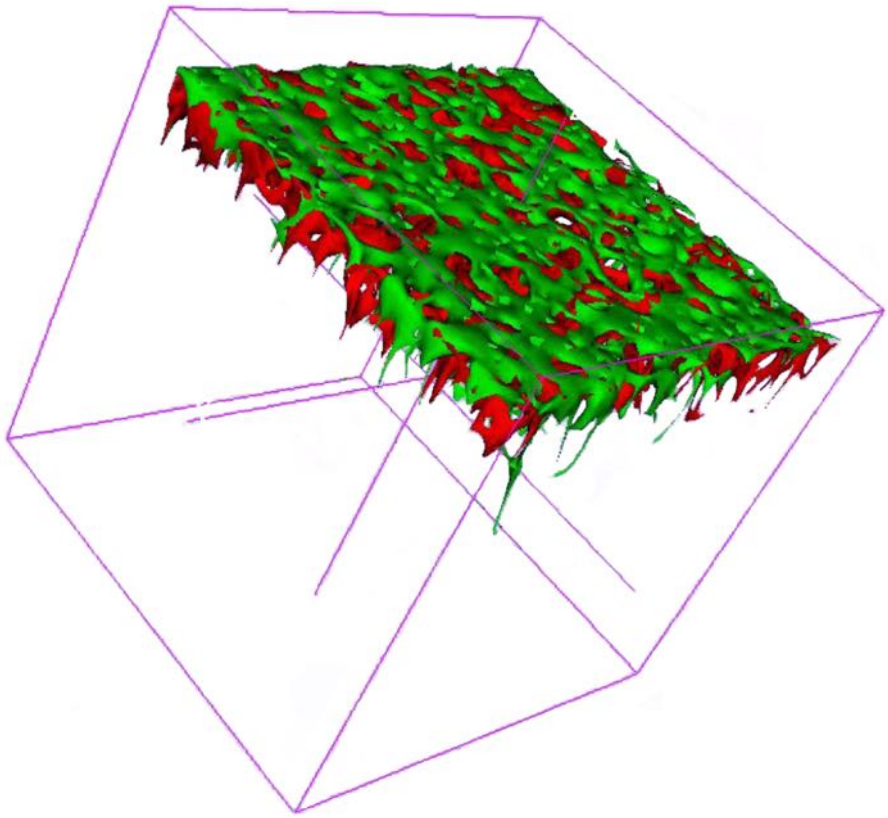

Figure 4.9: Depth sputtering profiling of **+UV** substrate of both, $SiCH_3$ (green), and C_7H_7 (red) ions.

4.4 Conclusion

In this chapter, successful photo-initiated surface grafting of PBLG polymer on solid substrates was demonstrated. Both, spherical nanoparticles and planar silicon wafers were chosen as substrates. Evidence for successful photografting of PBLG on spherical nanoparticles was obtained from TGA experiments demonstrating the presence of the organic polypeptide material on the surface. Moreover, the presence of polypeptide material on the surface was further evident from characteristic peptide amide I and amide II at 1650 and 1548 cm^{-1} in FTIR spectra. DLS analysis revealed a significant increase of the hydrodynamic diameter of the **+UV** compared to all controls supporting the conclusion of specific light-triggered NCA initiation.

Successful photo-initiated surface grafting of BLG NCA from silicon wafers was evident from a range of analytical techniques. Contact angles of **+UV** showed a significant increase of hydrophobic character of the surface, giving the first evidence of PBLG-grafted surface modification on planar substrates. Ellipsometry revealed a polymer layer thickness of 2,99 nm. Elemental analysis using XPS and TOF-SIMS revealed successful incorporation of the silane-based photoamine generator and the PBLG after photoinitiation.

4.5 References

[1] M. M. Stevens and J. H. George, *Science* **2005**, *310*, 1135 - 1138.
[2] T. Boudou, T. Crouzier, K. Ren, G. Blin and C. Picart, *Advanced Materials* **2009**, *21*, 1-27.
[3] S. S. Balamurugan, E. Sotu-Cantu, R. Cueto and P. S. Russo, *Macromolecules* **2010**, *43*, 62 - 70.
[4] M. Kar, P. S. Vijayakumar, B. L. Prasad and S. Sen Gupta, *Langmuir* **2010**, *26*, 5772-5781.
[5] M. Kar, M. Pauline, K. Sharma, G. Kumaraswamy and S. S. Gupta, *Langmuir* **2011**, *27*, 12124-12133.
[6] A. Heise, H. Menzel, H. Yim, R. H. Wieringa, A. J. Schouten, V. Erb and M. Stamm, *Langmuir* **1997**, *13*, 723 - 728.
[7] T. Borase, M. Iacono, S. I. Ali, P. D. Thornton and A. Heise, *Polymer Chemistry* **2012**, *3*, 1267.
[8] T. Borase, T. Ninjbadgar, A. Kapetanakis, S. Roche, R. O'Connor, C. Kerskens, A. Heise and D. F. Brougham, *Angewandte Chemie-International Edition* **2013**, *52*, 3164 - 3167.
[9] T. Borase and A. Heise, *Advanced Materials* **2016**, *28*, 5725 - 5731.
[10] P. Witte and H. Menzel, *Macromolecular Chemistry and Physics* **2004**, *205*, 1735 - 1743.
[11] Y. Wang and Y. C. Chang, *Advanced Materials* **2003**, *15*, 290 - 293.
[12] Y. Yagci, S. Jockusch and N. Turro, *Macromolecules* **2010**, *43*, 6245 - 6260.
[13] F. P. Melchels, J. Feijen and D. W. Grijpma, *Biomaterials* **2010**, *31*, 6121-6130.
[14] T. F. Scott, B. A. Kowalski, A. C. Sullivan, C. N. Bowman and R. R. McLeod, *Science* **2009**, *324*, 913 - 917.
[15] S. C. Clark, C. E. Hoyle, S. Jönsson, F. Morel and C. Decker, *Polymer* **1999**, *40*, 5063 - 5072.
[16] K. T. Nguyen and J. L. West, *Biomaterials* **2002**, *23*, 4308 - 4314.
[17] W. Stöber, A. Fink and E. Bohn, *Journal of Colloid and Interface Science* **1968**, *26*, 62 - 69.
[18] P. Stegmaier, J. M. Alonso and A. D. Campo, *Langmuir* **2008**, *24*, 11872-11879.
[19] J. Zheng, X. Tian, Y. Sun and W. Yang, *International journal of pharmaceutics* **2013**, *450*, 296 - 303.
[20] M. Kar, P. S. Vijayakumar, B. L. V. Prasad and S. S. Gupta, *Langmuir* **2010**, *26*, 5772 - 5781.
[21] L. T. Zhuravlev, *Colloids and Surfaces A:Physicochem. Eng. Aspects* **2000**, *173*, 1 - 38.
[22] R. H. Wieringa and A. J. Schouten, *Macromolecules* **1996**, *29*, 3032 - 3024.
[23] L. Lu, S. H. Lahasky, D. Zhang and J. C. Garno, *ACS Appl Mater Interfaces* **2016**, *8*, 4014 - 4022.
[24] N. Zhang, T. Pompe, I. Amin, R. Luxenhofer, C. Werner and R. Jordan, *Macromolecular Bioscience* **2012**, *12*, 926 - 936.
[25] Y. C. Chang and C. W. Frank, *Langmuir* **1996**, *12*, 5824 - 5829.

5. Poly(benzyl-L-glutamate)-*b*-Poly(L-arginine) – A novel block copolypeptide for drug delivery systems

5.1 Introduction

Although the research for drug delivery systems expanded during the last decade, efficient and selective drug delivery to diseased tissue still bears a huge challenge. Direct exposure of the drug to the body often results in problems such as poor solubility, rapid breakdown, unfavorable pharmacokinetics by clearance through organs such as kidney and liver. It sometimes also lacks selective diffusion into diseased tissue, therefore side effects are common. Drug delivery systems based on macromolecular material offer promising alternatives in drug administration, pharmacokinetics and biodistribution. Macromolecular material derived drug delivery systems are mainly based on liposomal or lipid-based materials, which already reached clinical trails and the market.

Approved therapeutic agents such as *Adagen* (Enzon)[1], *PEG-Intron* (Enzon)[2], or *Neulasta* (Amgen)[3] are based on the biomaterial polyethylene glycol (PEG), but also other material such as styrene-maleic acid based materials are used[4]. Both materials offer the advantage of low cytotoxicity *in vivo*.

The interest in polypeptides as alternative biocompatible materials has been highlighted in this thesis. Attractive for delivery applications is not only the fact that polypeptides are composed of amino acids but they can also be synthetized into different architectures. For example star polypeptides provide cargo space to carry and deliver genetic drugs (RNA, DNA) [5],[6]. Amphiphilic polypeptides can be self-assembled into nanoparticles (vesicles, micelles) by non-covalent interactions[7],[8]. The self-assembly of these polymers can be controlled by their molecular weight and hydrophilic/hydrophobic ratio, while the size of the nanoparticle is directly linked to the polymer chain length [9],[10]. These materials have been investigated for drug delivery to tumor cells, since this diseased tissue has increased gaps between the cells, allowing a selective penetration into tumor cells, also known as Enhanced Permeability Retention (EPR) effect[11]. Examples are the block copolymerization of γ-benzyl-L-glutamate (BLG) NCA and ε-carbobenzyloxy-L-lysine NCA, followed by the deprotection of the BLG block, revealing an amphiphilic block copolypeptide, able to encapsulate a hydrophobic drug[12]. In another example selective postmodification of a polypeptide was devised to obtain amphiphilic glycopolypeptides. These materials spontaneously self-assembled into particles with an average size of 50 nm[13]. Further integration of iminosugar

molecules in the side chains enables additional targeting ability by glycosidase inhibition[14].

Although recent breakthroughs were achieved in polypeptide-based drug delivery systems their selective targeting towards diseased tissue still remains as a significant challenge. Signal molecules for example Cell Penetrating Peptides (CPP) has been discussed to facilitate targeted delivery. These molecules are classified as cationic peptides, with a length shorter than 20 amino acids that can diffuse between the plasma membrane of most mammalian cells. Most CPPs, which are used for drug delivery and selective cellular uptake, are Antennapedia (Antp) and poly(arginine) (PArg) peptides[15]. The use of PArg-based CPP attracted much attention, starting by its ligation to transferrin proteins[17] or even quantum dots for cellular uptake[18]. In many approaches commercial PArg up to 13 kDa were used, however, optimal cellular uptake was observed with PArg length varying from 6 up to 16 residues in natural-derived peptides[19].

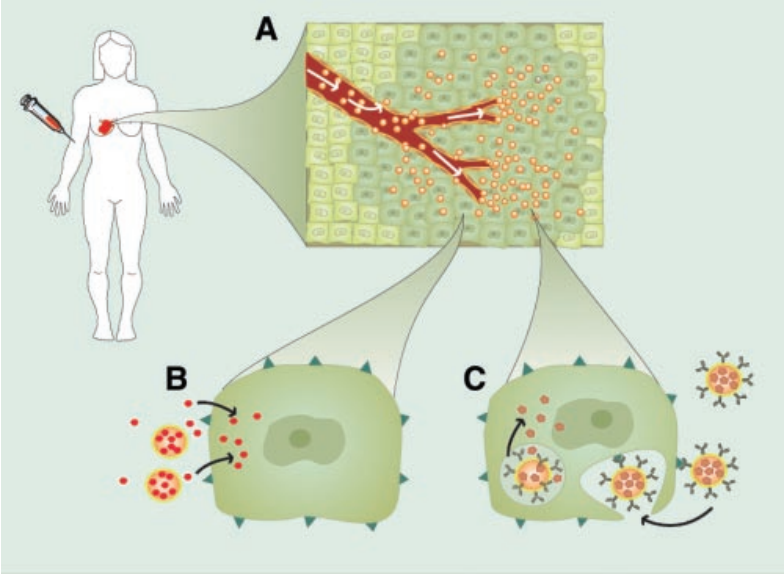

Figure 5.1: Schematic diagram depicting breast cancer, including diseased tissue (dark green) and healthy tissue (light green). Drug delivery system such as liposomal particles (orange), containing the drug (red dots) are selectively diffused into diseased tissue due to the EPR effect (A). Capsules release controlled drug doses outside the cell, followed by diffusion of the drug into diseased cells (B). CPP equipped capsules undergo endocytosis and release drug inside the cell (C)[16].

In this chapter, the synthesis of an amphiphilic block copolypeptide poly(γ-benzyl-L-glutamate-*b*-L-arginine) (PBLG-*b*-PLR) is described. Two different synthetic routes were investigated. First, the block copolypeptide was synthesized by NCA ROP, including the formation of a L-ornithine block followed by guanidinylation. Second, the desired block

copolypeptide was synthesized by the ligation of the NCA ROP derived PBLG with an SPPS synthesized PLR oligopeptide. The resulting amphiphilic diblock copolypeptide, either synthesized by NCA ROP or combined NCA/SPPS, were investigated for their self-assembly into potential micellar delivery particles.

5.2 Experimentals

Materials

N,N'-bis(tert-butoxycarbonyl)-1H-pyrazole-1-carboxamidine (DIC), trisopropylsilane (TIS), and the Kaisertest kit was purchased from Sigma-Aldrich. *N,N*-Diisopropylethylamine, Hexafluoro-2-propanol (HFIP), and Methyl tert-butyl ether (MTBE) were supplied by VWR. 2-(1H-benzotriazol-1-yl)-1,1,3,3-tetramethyluronium hexafluorophosphate (HBTU), ethyl (hydroxyimino)cyanoacetate (OxymaPure®), and H-Gly-2CT (2-chlorotrityl chloride) resin were delivered by GL Biochem Shanghai. Trifluoroacetic acid (TFA) was purchased from Biosolve B.V., 1-Methyl-2-pyrrolidinone (NMP) from ACROS, and L-Ornithine(Boc) from BACHEM.

Synthesis of L-Ornithine(Boc)-NCA

L-ornithine(Boc) (10 g, 43,1 mmol) was transferred into an already preflashed 3-neck round bottom flask, equipped with a condensator, and drop funnel. 200 ml of anhydrous ethyl acetate was added to the flask, obtaining a white suspension. After the reaction mixture was heated up to reflux, alpha-pinene (22,56 ml, 142 mmol) was added. Triphosgene (14,05 g, 47,4 mmol) was dissolved in 50 ml anhydrous ethyl acetate and added through the drop funnel drop wise to the reaction mixture. During the time of 1 hour, nearly full solubility was observed, before full addition of triphosgene was achieved. However, short after it turned back into a hazy suspension. It was stirred further under inert atmosphere under and reflux overnight. The suspension was filtrated and the supernatant was concentrated. Anhydrous heptane was added (1:1 v%) for crystallization. It was recrystallized, before the off-white crystal product was obtained in quantitative yield.

^{1}H-NMR (300 MHz, DMSO, δ, ppm): 1,37 (s, 9H, CH_3), 1,41 – 1,49 (m, 2H, CHCH_2CH$_2$CH$_2$NH), 1,58 – 1,71 (m, 2H, CHCH$_2$CH_2CH$_2$NH), 2,88 – 2,95 (m, 2H, CHCH$_2$CH$_2$CH_2NH), 4,43 (t, 1H, CH, J = 6,21 Hz), 6,85 (s, 1H, CH$_2$NHC(O)O), 9,07 (s, 1H, CHNHC(O)O). ^{13}C-NMR (100 MHz, DMSO, δ, ppm): 25,06 (1C, γ-C), 28,2 (3C, CH$_3$), 28,5 (1C, β-C), 39,1 (1C, δ-C), 56,8 (1C, α-C), 151,9 (1C, CHNHC(O)O), 155,6 (1C, CH$_2$NHC(O)O), 171,5 (1C, CHC(O)O). ATR-IR (cm^{-1}): 3382, 3265, 2978, 2930, 1798 (C=O amide), 1757 (C=O anhydride), 1692, 1517, 1442, 1364, 1279, 1165, 940, 885, 760

Homo and block copolymerizations of Poly(benzyl-l-glutamate) (PBLG) and Poly(benzyl-L-glutamate)-*b*-Poly(Boc-L-ornithine) (PBLG-*b*-PBLO)

The NCA monomer of γ-benzyl-L-glutamate (1,5 g, 5,66 mmol) was dissolved in 15 ml anhydrous DMF. Cyclohexylamine (13 µl, 0.113 mmol) was added to the medium under stirring. The reaction mixture was set under nitrogen atmosphere and stirred at room temperature for 3,5 h. ATR-FTIR confirmed full conversion. 1,0 ml was removed for homo polypeptide precipitation in 30 ml diethyl ether.

L-ornithine NCA (0,545 g, 2,109 mmol) was dissolved in 5 ml anhydrous DMF, before it was added to the reaction mixture. It was stirred under inert atmosphere at room temperature overnight. ATR-FTIR confirmed full conversion of the second NCA monomer. For N-terminus capping, acetic anhydride (1,07 ml, 11,32 mmol) was directly added to the reaction mixture. It was stirred for 1,5 hours, before the reaction was stopped by adding the reaction mixture into a 12-fold excess of ice-cold diethyl ether. After reprecipitation, the off-white solid product, Poly(benzyl-L-glutamate)-b-Poly(Boc-L-ornithine) (1,4965 g, 0,096 mmol, 91,3%) was obtained.

Homo polypeptide:

^{1}H-NMR (300 MHz, DMSO, δ, ppm): 1,81 – 2,38 (m, 2H, β-CH_2), 2,49 (m, 2H, γ-CH_2), 3,93 (s, 1H, α-C*H*), 4,92 – 5,1 (m, 2H, C(O)OCH_2), 7,13 – 7,42 (m, 5H, Ar*H*), 8,0 – 8,5 (N*H*). ATR-FTIR (cm^{-1}): 3288, 1730 (C=O ester), 1548 (amide II), 1168, 972, 748, 698.

Block copolypeptide:

^{1}H-NMR (300 MHz, DMSO, δ, ppm): 1,35 (s, 3,82H, CH_3(Boc)), 1,45 – 2,4 (m, 4,45H, β-CH_2 (BLG), β-,γ-CH_2 (Orn)), 2,50 (m, 2H, γ-CH_2 (BLG)), 2,97 (m, 0,82H, δ-CH_2 (Orn)), 3,9 – 4,3 (m, 1,35H, α-C*H* (BLG, Orn)), 4,9 – 5,27 (m, 2H, C(O)OCH_2), 7,08 – 7,47 (m, 5H, Ar*H*), 7,73 – 8,95 (m, 1,39H, N*H* (BLG, Orn)).

Synthesis of Poly(benzyl-L-glutamate)-b-Poly(L-ornithine) (PBLG-*b*-PLO)

For the deprotection of Boc-L-ornithine the coblock polypeptide Poly(benzyl-L-glutamate)-b-Poly(Boc-L-ornithine) (1 g, 0,064 mmol) was dissolved in 30 ml anhydrous DCM (35 mg/ml). After full dissolution, 30 ml of TFA (DCM:TFA 1:1) was added to the solution. It was stirred at room temperature for 20 min. The solvent was evaporated, followed by a washing step with DCM. After evaporation, the solid was frozen and freeze-dried overnight to remove traces of TFA. The off-white solid product Poly(benzyl-L-glutamate)-b-Poly(L-ornithine) (1,115 g, 0.070 mmol, 109%) was obtained.

^{1}H-NMR (300 MHz, DMSO, δ, ppm): 1,3 – 2,31 (m, 4,59H, β-CH_2 (BLG), β-,γ-CH_2 (Orn)), 2,50 (m, 2H, γ-CH_2 (BLG)), 2,79 (m, 0,83H, δ-CH_2 (Orn)), 3,92 (s, 1H, α-C*H* (BLG)), 4,30 (s,

0.55H, α-CH (Orn)), 4,89 – 5,23 (m, 2H, C(O)OCH_2), 7,11 – 7,46 (m, 5H, ArH), 7,92 (s, 1,33H, NH_2 (Orn)), 8,1 – 8,74 (m, 1,17H, NH (BLG, Orn)).

Synthesis of Poly(benzyl-L-glutamate)-*b*-Poly(Boc$_2$-L-arginine) (PBLG-*b*-PBLR)

Poly(benzyl-L-glutamate)-*b*-Poly(L-ornithine) (0,943 g, 0,059 mmol) and *N*,*N*'-bis(tert-butoxycarbonyl)-1H-pyrazole-1-carboxamidine (0,98 g, 3,156 mmol) were both separately dissolved in 19 ml of anhydrous NMP. Both solutions were mixed to each other, while DIPEA (0,551 ml, 3,156 mmol) was added to the reaction mixture. It was stirred for 24 hours at room temperature. The reaction mixture was transferred drop wise into an excess of ice-cold diethyl ether for precipitation. After reprecipitation, the off-white solid product, Poly(benzyl-L-glutamate)-*b*-Poly(Boc$_2$-L-arginine) (0,728 g, 0,039 mmol, 66%) was obtained. The degree of guanidinylation was determined by comparing the peak intensities between Boc-L-Orn-derived (1,35 ppm) and Boc-L-Arg-derived (1,37 ppm) CH_3 protons, resulted in a degree of guanidinylation of 80,6%.

^{1}H-NMR (300 MHz, DMSO, δ, ppm): 1,37 (m, 6,16H, CH_3(Boc)), 1,95 – 2,41 (m, 4,25H, β-CH_2 (BLG), β-,γ-CH_2 (Arg)), 2,49 (m, 2H, γ-CH_2 (BLG)), 3,7 – 4,3 (m, 1,32H, α-CH (BLG, Arg)), 4,78 – 5,23 (m, 2H, C(O)OCH_2), 7,09 – 7,43 (m, 5H, ArH), 7,81 – 8,9 (m, 1,04H, NH (BLG, Arg)).

Synthesis of Poly(benzyl-L-glutamate)-*b*-Poly(L-arginine) (PBLG-*b*-PLR)

Poly(benzyl-L-glutamate)-*b*-Poly(Boc$_2$-L-arginine) (0,554 g, 0,0298 mmol) was dissolved in 22 ml anhydrous DCM (25 mg/ml). After complete dissolution, 22 ml of TFA (DCM:TFA 1:1) was added to the solution and stirred for 2 hours at room temperature. The solvents were evaporated, before the product was further washed with DCM. After evaporation under vacuum, the solid was frozen and freeze-dried overnight to remove traces of TFA. The off-white solid product, Poly(benzyl-L-glutamate)-*b*-Poly(L-arginine) (0,582 g, 0,034 mmol, 116%) was obtained.

^{1}H-NMR (300 MHz, DMSO, δ, ppm): 1,5-2,3 (m, 4,9H, β-CH_2 (BLG), β-,γ-CH_2 (Arg)), 2,50 (m, 2H, γ-CH_2 (BLG)), 3,09 (m, 0,62 δ-CH_2 (Arg)), 3,92 (m, 0,89H, α-CH (BLG)), 4,25 (m, 0,49H, α-CH (Arg)), 4,8 – 5,25 (m, 2H, C(O)OCH_2), 7,08 – 7,48 (m, 5H, ArH), 7,79 (m, 0,41H, NH_2), 7,89 – 8,6 (m, 1H, NH (BLG, Arg)).

Calculation of PBLG-PBLO ratio:

The residue ratio of BLG:BLO, assigned as n;m, is based on the integration of ^{1}H-NMR peaks of CH_2-Bnz, and BocCH_3 at 1,35 , and 4,9 – 5,27 ppm, respectively. n:m ratios were

calculated using the equation $n:m = \frac{\frac{I_{Boc,theo}}{I_{CH_2,theo}}}{\frac{I_{Boc,meas}}{I_{CH_2,meas}}}$ in which the theoretical integral of BocCH_3 is depicted as $I_{Boc,\ theo}$, the theoretical integral of CH_2-Bnz as $I_{CH2,\ theo}$, and their measured integrals as $I_{Boc,\ theo}$, and $I_{CH2,\ theo}$, respectively.

Degree of guanidinylation calculations:

For degree of guanidinylation calculations the residue ratio of the two block, once it was calculated from PBLG-*b*-PBLO, are constant over the following three chemical modification steps. This consideration allows to put PBLG-*b*-PBLO and PBLG-*b*-PBLR into relation. The degree of guanidinylation, depicted as G, was calculated using the equation $G = \frac{\frac{I_{Boc,PBLR}}{I_{CH_2,PBLR}}}{2\ x\ \frac{I_{Boc,PBLO}}{I_{CH_2PBLO}}}\ x\ 100$ in which the measured integral values of CH_2-Bnz and BocCH_3 of PBLO and CH_2-Bnz and BocCH_3 of PBLR are depicted as $I_{CH2,\ PBLR}$, $I_{Boc,\ PBLO}$, $I_{CH2,\ PBLR}$, and $I_{Boc,\ PBLR}$, respectively.

Solid phase peptide synthesis of HO-Gly-Poly(L-arginine(Pbf))$_4$-Ac, and HO-Gly-Poly(L-arginine(Pbf))$_4$-Gly-Poly(L-arginine(Pbf))$_4$-Ac:

Each of the following washing steps was performed in 2 min, each coupling step 45 min, and each deprotection step 8 min.

The H-Gly-2CT (2-chlorotrityl chloride) resin (0,821 g, loading: 0,451 mmol/g) was pre-swollen by washing the resin twice with 10 ml DCM. It was washed trice with DMF, followed by washing thrice with DCM and trice DMF. For deprotection the resin was treated thrice with a piperidine solution in DMF (1/5 v/v%). After successful deprotection the resin was washed (3 x DMF, 3 x DCM, 3 x DMF). For coupling Fmoc-L-arginine(Pbf) (1,3 g, 2,0 mmol) , or Fmoc-Gly-OH (0,596 g, 2,0 mmol) (depending on coupling step), 2-(1H-benzotriazol-1-yl)-1,1,3,3-tetramethyluronium hexafluorophosphate (HBTU), and ethyl (hydroxyimino)cyanoacetate (OxymaPure®) were dissolved in 10 ml DMF. After it was added to the resin, DIPEA (0,7 ml, 4,01 mmol) was immediately added to the reaction mixture. These steps were repeated for the whole peptide sequence. Final acetylation of the *N*-terminus was achieved by adding 10 ml of the DMF solution (16 mM OxymaPure, 0,125 M DIPEA, 0,5 M acetic anhydride) to the resin. The reaction was stirred for 1 hour, before the resin was filtrated and washed under above-mentioned conditions.

Peptide cleavage from the resin was performed by adding a TFA:DCM solution (1/99 v/v%) to the dried resin (10 ml/mg) for 15 min. This step was repeated thrice, followed

by 5 washing steps with DCM. The supernatant was concentrated and dissolved in acetonitrile/water (2/1 v/v%) solution, before it was lyophilized overnight. A quantitative yield of Gly-Poly(L-arginine(Pbf))$_4$-Gly-Poly(L-arginine(Pbf))$_4$ was obtained. ^{1}H-NMR (300 MHz, $CDCl_3$, δ, ppm):1,42 (s, 6H, OC(CH_3)$_2$), 1,51 – 1,91 (m, 4H, β-, γ-CH_2), 2,02 (s, 3H, ArCH_3, *meta* to SO_2R), 2,38, and 2,41 (s, 3H, 3H, ArCH_3, *ortho* to SO_2R), 2,92 (m, 2H, CH_2C(CH_3)$_2$), 3,24 (m, 2H, δ-CH_2 (Arg)), 5,04 (s, 1H, N*H*C(O)), 8,54 (s, 1H, N*H*).

Ligation of Poly(benzyl-L-glutamate) with Gly-Poly(L-arginine(Pbf))$_4$-Gly-Poly(L-arginine(Pbf))$_4$:

Homopolymerization of PBLG (0,133 mg, 0,015 mmol) was performed as mentioned above. The oligopeptide Gly-Poly(L-arginine(Pbf))$_4$-Gly-Poly(L-arginine(Pbf))$_4$ (51,6 mg, 0,015 mmol) and OxymaPure® (14,21 mg, 0,1 mmol) were dissolved in 2,5 ml anhydrous DMF. After complete dissolution *N*,*N*'-Diisopropylcarbodiimide (DIC) (0,016 ml, 0,1 mmol) was added. The solution was added to the polymerization reaction and stirred under inert atmosphere at room temperature overnight. The reaction was stopped by adding the reaction mixture drop wise into an excess of diethyl ether for precipitation. After reprecipitation, the solid was dried under vacuum, obtaining the off-white solid product, Poly(benzyl-L-glutamate)-*b*-Poly(Pbf-L-arginine)$_8$ (148 mg, 0,012 mmol, 64%).

^{1}H-NMR (300 MHz, DMSO, δ, ppm): 1,38 (s, 1,75H, OC(CH_3)$_2$), 1,98 (s, 1,86H, ArCH_3, *meta* to SO_2R), 1,6 – 2,4 (m, β-CH_2 (BLG), β-,γ-CH_2 (Arg)), 2,41, and 2,46 (s, 0.81H, 0,65H, ArCH_3, *ortho* to SO_2R), 2,50 (s, 2H, γ-CH_2 (BLG)), 2,93 (m, 0,52H, CH_2C(CH_3)$_2$), 3,02 (m, 0,5H, δ-CH_2 (Arg)), 3,92 (s, 1H, α-C*H* (BLG)), 4,23 (s, 0,25H, α-C*H* (Arg)), 4,89 – 5,21 (m, 2H, C(O)OCH_2), 7,19 – 7,45 (m, 5H, Ar*H*), 8,30 (m, 0,87H, N*H* (BLG, Arg)).

Synthesis of Poly(benzyl-L-glutamate)-*b*-Poly(L-arginine)$_8$

Poly(benzyl-L-glutamate)-*b*-Poly(Pbf-L-arginine)$_8$ (0,122 g, 9,97µmol) was dissolved in 6 ml solution of TFA:H_2O:TIS (94:3:3). The yellowish solid slowly dissolved before it was stirred for 2 hours. The reaction was stopped by adding the reaction mixture drop wise into an excess of ice-cold MTBE/n-heptane (1/1). After reprecipitation, the solid was dried in an oven overnight, obtaining the product Poly(benzyl-L-glutamate)-*b*-Poly(L-arginine)$_8$ (106,3 mg, 9,55 µmol, 96%).

^{1}H-NMR (300 MHz, DMSO, δ, ppm): 1,3 – 2,76 (m, β-CH_2 (BLG), β-,γ-CH_2 (Arg)), 2,50 (s, 2H, γ-CH_2 (BLG)), 3,07 (m, 0,5H, δ-CH_2 (Arg)), 3,91 (s, 1H, α-C*H* (BLG)), 4,23 (s, 0,25H, α-

C*H* (Arg)), 4,8 – 5,2 (m, 2H, C(O)OCH_2), 6,9 – 7,48 (m, 5H, Ar*H*), 7,8 – 8,74 (m, 0,88H, N*H* (BLG, Arg)).

Synthesis of Poly(benzyl-L-glutamate) initiated by methyl O-(tert-butyl) L-serine, HCl

Methyl O-(tert-butyl-L-serine, HCl (5,6 mg, 0.026 mmol) was dissolved in 1 ml anhydrous DMF. Triethylamine (3,5 µl, 0,025 mmol) was added to the solution and stirred for 10 min. Benzyl-L-glutamate NCA (5,22 mg, 1,984 mmol) was transferred into an already preflashed Schlenk tube. 4 ml of anhydrous DMF was added to dissolve the monomer, before the serine solution was added. The reaction was stirred for under nitrogen atmosphere at room temperature for 5 hours. ATR-FTIR confirmed full conversion. The reaction mixture was drop wise added into excess of diethyl ether for precipitation. After reprecipitation the white polymer product, Poly(benzyl-L-glutamate) was obtained in a quantitative yield. ^{1}H-NMR (300 MHz, DMSO, δ, ppm): 1,08 (s, 0,38H, C(CH_3)$_3$), 1,6 – 2,3 (m, 2H, β-CH_2), 2,35 – 2,78 (m, 2H, γ-CH_2), 3,58 (s, 0,17H, CH_3O), 3,92 (s, 1H, α-C*H*), 5,02 (m, 2H, C(O)OCH_2), 7,18 – 7,4 (m, 5H, Ar*H*), 8,27 (m, 1H, N*H*).

Micelle formation:

The polymers were dissolved in anhydrous HFIP (1mg/ml). After complete dissolution, the same volume of MilliQ water was added (HFIP:H_2O 1:1 v%). The solution was stirred overnight. The final polymer concentration in water was 1 mg/ml.

DLS:

Dynamic light scattering (DLS) experiments were performed at 25 °C on a MALVERN ZEN3600, with a detection angle of 173°. The 3 mW He-Ne laser emitted light at a wavelength of 633 nm into a disposable 10 mm cuvette. The samples were diluted in MilliQ water and left 2 minutes contactless, to avoid detection of impurity particles.

TEM:

Transmission Electron Microscopy was performed with samples, obtained from micelle formations. 5 µl of sample was dropped on a Cu grid coated with SiO and Formvar, before it was wiped off after 10 minutes. Final staining with performed with a Gadolinium Acetate Tetrahydrate solution in water (20% v/v, 5 µL).

5.3 Results and Discussion

5.3.1 Synthetic considerations and approach

The first approach is fully based on NCA polymerization using a PBLG macroinitiator as the hydrophobic block. Arginine NCA itself is instable so that a direct polymerization of this monomer is not possible. Several publications report the polymerization of protected arginine NCA, for instance, $N^{\omega,\omega'}$-dicarbobenzyloxy-L-arginine NCA (Z_2LR) synthesized from $N^{\alpha,\omega,\omega'}$-tricarbobenzyloxy-L-arginine (Z_3LR) in presence of thionyl chloride and dioxane[20]. However, these reactions are not straightforward. Instead, a recently published procedure by Kudo was followed in which the NCA of the protected non-natural amino acid L-ornithine was polymerized and the polymer subsequently converted into PLR[21] (Scheme 5.1). The authors further demonstrated successful assembly of PEG-b-PLR [22].

The second approach relies on Solid Phase Peptide Synthesis (SPPS) to obtain the PLR block, which can then be ligated to the PBLG block (Scheme 5.1). [23].

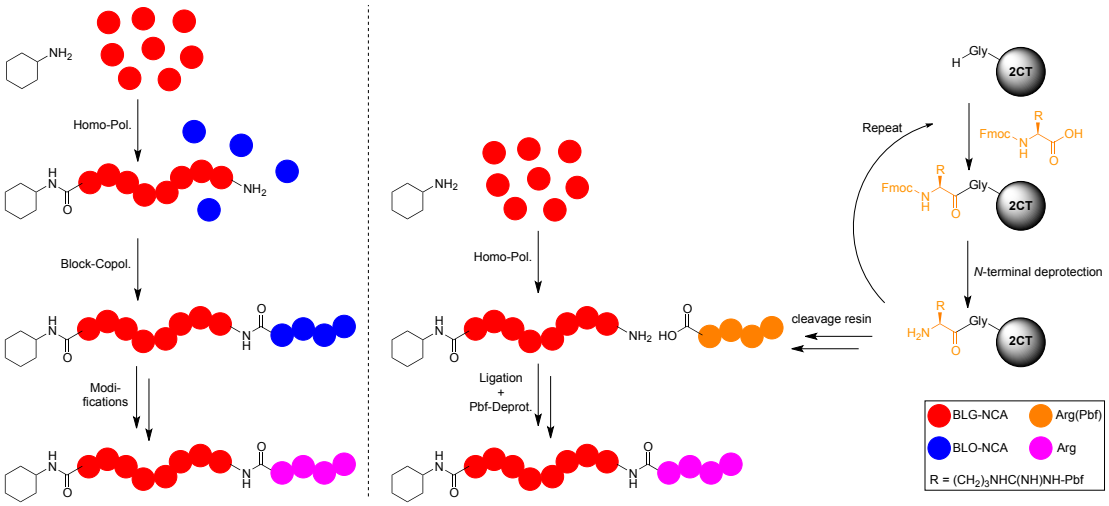

Scheme 5.1: Comparison of NCA-ROP block copolymerization (NCA-ROP, left) and ROP product PBLG ligated with the SPPS-synthesized oligopeptide product (right).

5.3.2 Synthesis of PBLG-*b*-PLR by NCA ring-opening polymerization

The synthetic approach towards the novel diblock copolymer PBLG-PLR is shown in Scheme 5.2. It is a multistep synthesis starting from a PBLG-PBLO diblock copolymer. Following several deprotection and guanidinylation steps the final product was obtained. The analysis of every individual step is crucial to demonstrate the success of the synthesis.

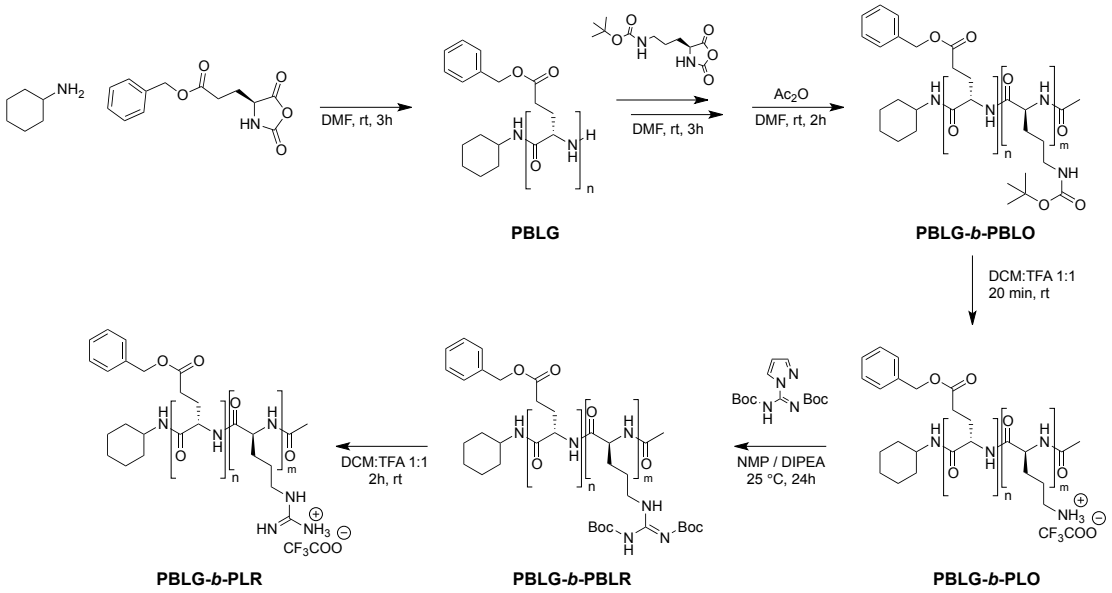

Scheme 5.2: Reaction strategy towards poly(benzyl-L-glutamate-*b*-L-arginine).

In the first step, homo polymerization of BLG NCA initiated by cyclohexylamine (ratio 50:1), was performed. Full BLG NCA conversion was confirmed by ATR-FTIR, before the second monomer, Boc-L-ornithine NCA was added to the reaction at a 1:20 ratio of PBLG:BLO NCA. After full conversion of the second monomer, the *N*-terminus was protected by acetylation. Acetic anhydride was added in excess and the reaction was stirred enabling full end-capping of the *N*-terminus. This step allowed specific side chain modification of the L-ornithine block without end-group reactions. ^{1}H-NMR spectra display peaks of both polypeptides (Figure 5.). Peak integration of CH_2-Bnz (7,08 – 7,47 ppm) and BocCH_3 (1,35 ppm) result in a BLG:BLO ratio of 2.35 corresponding to a $PBLG_{50}$-*b*-$PBLO_{21}$ diblock polypeptide. MALDI-Tof-MS analysis of a sample taken after the PBLG synthesis revealed the presence of amine-functionalized PBLG species as the mayor product (Figure 5.2 a, Figure 5.3 species A). Traces of the pyroglutamate end–group can also be identified, which is an unavoidable side product (Figure 5.3 species B)[24]. The MALDI-Tof-MS spectrum of the block copolypeptide shows two distinct distributions. Signal peaks depicted as C1 and C2 (Figure 5.2 b, Figure 5.3) can clearly be assigned to the block copolypeptide. The fact that the second distribution is at a higher molecular weight than the PBLG macroinitiator provides first evidence that both blocks are covalently attached (Figure 5.2 b). Moreover, the peaks are broader compared to the homo polypeptide peaks. This is according to expectations, since the block copolypeptide bears two independent polydispersities. The broad peaks are a sum of peaks, representing a range of block copolypeptide combination, shown in Table 5.1. The distribution at lower molecular weight represents the remaining, unreactive

pyroglutamate, which was also detected in the homo polymerization (species B). The equal intensity of both distributions is misleading and does not permit any conclusion about the real ratio of both polymer species as laser desorption of high molecular weight polymers into the gas phase is inefficient.

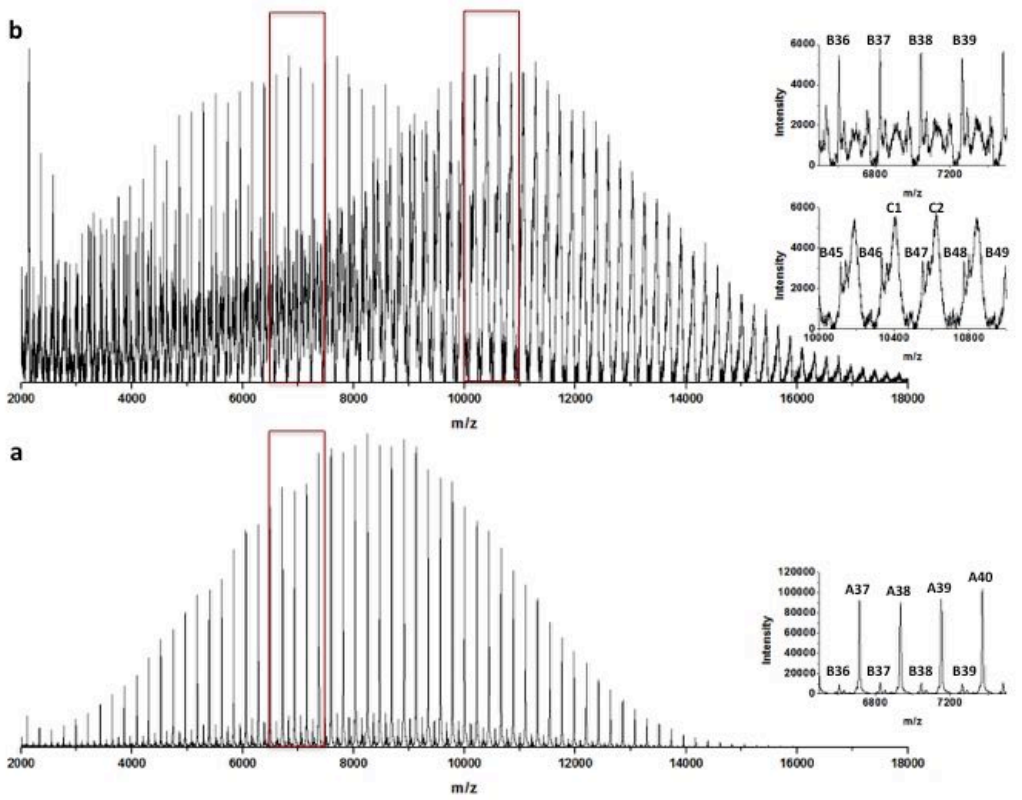

Figure 5.2: MALDI-Tof results of the PBLG macroinitiator (a) and the block copolymer PBLG-*b*-PBLO (b). Red boxes denote zoom-in regions, representing additional spectra on the right hand side. Letters depict structures shown in Figure 5.3; the numbers refer to the degree of polymerization. Letter C refers to a sum of polymer species, listed in Table 5.1. All samples were dissolved in HFIP, with addition of potassium trifluoroacetic acid (KTFA).

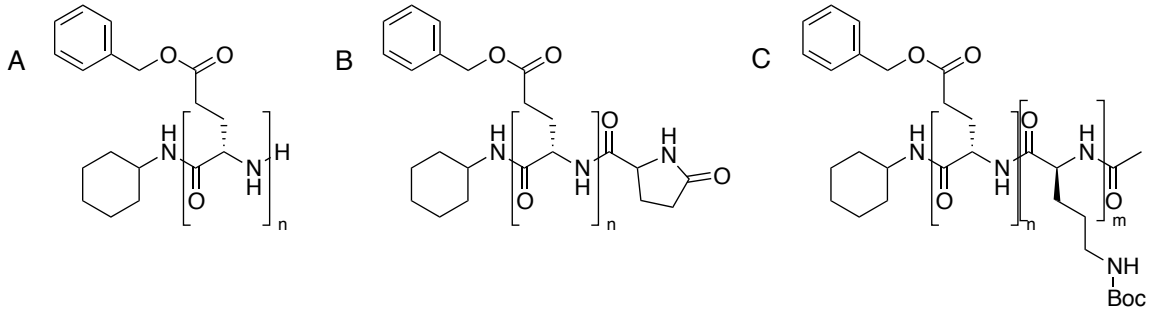

Figure 5.3: Various identified homo polypeptide (A, and B) and block copolypeptide species, assigned to MALDI-Tof-MS spectrum peaks in Figure 5.2.

Table 5.1: Calculated molecular weights of MALDI-ToF-MS detected peaks of the block copolypeptide

Signal	Interval	n	m	Calculated (initiator + n x BLG + m x BLO + acetyl + counter ion
C1	10290 - 10440			
		19	28	98 + 19 x 219,1 + 28 x 214,1 + 39.1 = **10294,8**
		20	27	98 + 20 x 219,1 + 27 x 214,1 + 39.1 = **10299,8**
		21	26	98 + 21 x 219,1 + 26 x 214,1 + 39.1 = **10304,8**
		…	…	
		44	3	98 + 44 x 219,1 + 3 x 214,1 + 39.1 = **10419,8**
		45	2	98 + 45 x 219,1 + 2 x 214,1 + 39.1 = **10424,8**
		46	1	98 + 46 x 219,1 + 1 x 214,1 + 39.1 = **10429,8**
C2	10510 - 10660			
		20	28	98 + 20 x 219,1 + 28 x 214,1 + 39.1 = **10513,9**
		21	27	98 + 21 x 219,1 + 27 x 214,1 + 39.1 = **10518,9**
		22	26	98 + 22 x 219,1 + 26 x 214,1 + 39.1 = **10523,9**
		…		
		45	3	98 + 45 x 219,1 + 3 x 214,1 + 39.1 = **10638,9**
		46	2	98 + 46 x 219,1 + 2 x 214,1 + 39.1 = **10643,9**
		47	1	98 + 47 x 219,1 + 1 x 214,1 + 39.1 = **10648,9**

The obtained poly(benzyl-L-glutamate-*b*-Boc-L-ornithine) (PBLG-PBLO) is the precursor for the final conversion to PBLG-PLR. Deprotection of the Boc-L-ornithine block was carried out by dissolving the block copolypeptide in a 1:1 (v:v%) solution of DCM and TFA. The PBLG-PLO block copolypeptide was obtained in its TFA salt form. The 'post-polymerizational' modification, i.e. the conversion of the PLO block into a PLR block was achieved by the reaction with the guanidinylation reagent *N*,*N*'-bis(tert-butoxycarbonyl)-1H-pyrazole-1-carboxamidine. Kudo and coworkers showed highest reactivity of di-Boc reagent in the guanidinylation reaction, in comparison to the mono-Boc, or in its HCl salt form as guanidinylation reagents[22]. A 2.5-fold excess of DIPEA base was added to ensure reaction under basic condition and neutralization of any traces of TFA left from the previous deprotection step. Previous acetylation prevented guanidinylation of the *N*-terminus. Final deprotection with TFA in DCM yielded the desired PBLG-PLR polymer product. Extended reaction time ensured full deprotection of both Boc protection groups in the L-arginine amino acid side chain. The final product, PBLG-PLR was obtained in its TFA salt form.

^{1}H NMR is a convenient method to monitor the success of the conversion steps focusing on the BocCH_3 group at 1.35 ppm as a reporter signal. Inspection of Figure 4 reveals the

presence of this signal in the $PBLG_{50}$-$PBLO_{21}$ sample. After successful deprotection this signal is absent in the $PBLG_{50}$-PLO_{21} polymer. In the next step the Boc protected guanidinylation reagent was added to the dissolved $PBLG_{50}$-*b*-PLO_{21} polypeptide resulting in the detection of a BocCH_3 signal. The degree of guanidinylation of 81 %. was determined by comparing integrated peak areas of Boc-L-Orn derived (1.35 ppm) and diBoc-L-arginine derived (1.37 ppm) CH_3 protons. Final deprotection of $PBLG_{50}$-*b*-$PBLR_{21}$, by removing both Boc protection groups with TFA was confirmed by the absence of the Boc-CH_3 peaks at 1,37 ppm. Traces of *t*-BuOH and *t*-Bu-TFA could be found that are deprotected products.

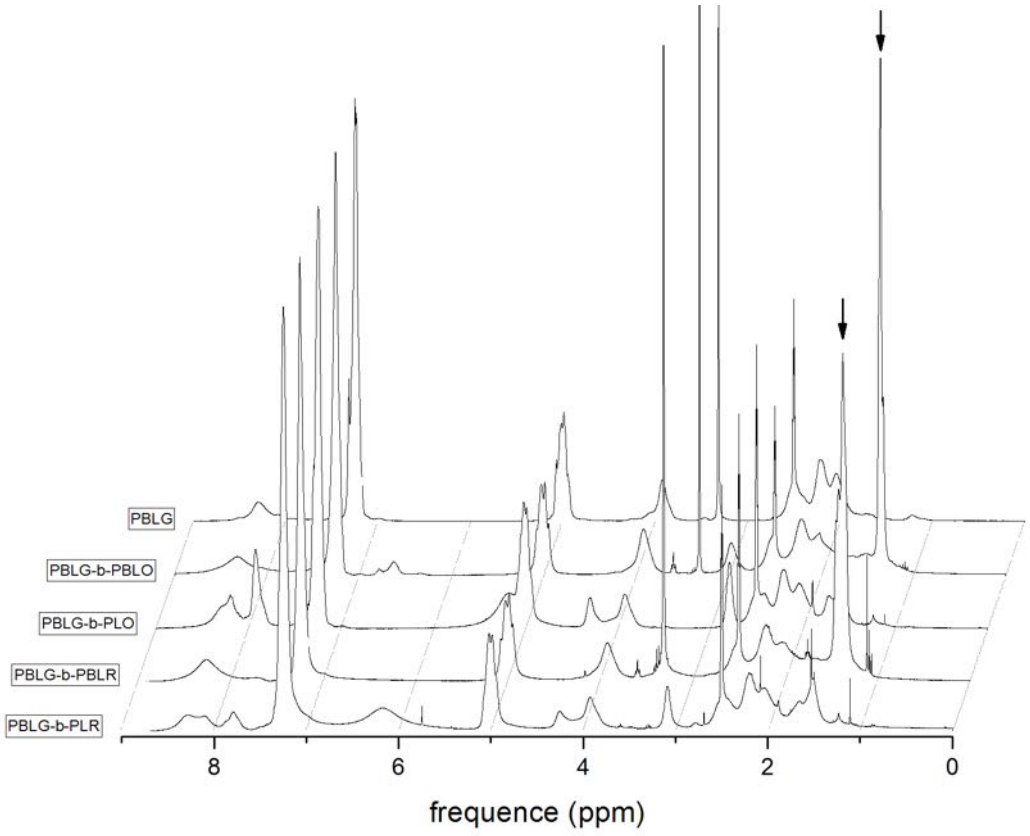

Figure 5.4: ^{1}H-NMR spectra of various polypeptide samples, including homo polypeptide (PBLG), block copolypeptide (PBLG-b-PBLO), deprotected (PBLG-b-PLO), guanidinylated (PBLG-b-PBLR), and final deprotected (PBLG-b-PLR) product. Boc and diboc peaks are highlighted with arrows. All samples were dissolved in deuterated DMSO, and measured on a 300 MHz NMR apparatus.

Every step in the synthesis of $PBLG_{50}$-*b*-PLR_{21} induces a molecular weight change, e.g. macroinitiation from the PBLG results in an increase of molecular weight. The deprotection of the Boc group in the side chain of the L-ornithine block should entail a reduction of molecular weight. The following two steps, guanidinylation and final deprotection first increase and finally decrease the molecular weight. These molecular weight shifts can clearly be seen in Size Exclusion Chromatography (SEC, Figure 5.5).

The position of the peak maximum of each polymer distribution is highlighted by a dotted line. Green and red arrows between dotted lines represent the increase und decrease of molecular weight, respectively. Indeed, SEC traces followed the expected pattern in molecular weight variations with an increase of molecular weight between homo- (PBLG) and block copolypeptide (PBLG-*b*-PBLO), followed by a molecular weight reduction due to Boc deprotection (PBLG-*b*-PLO). Due to final deprotection of the two Boc protection groups, SEC analysis shows a significant reduced average molecular weight of PBLG-*b*-PLR compared to PBLG-*b*-PBLR.

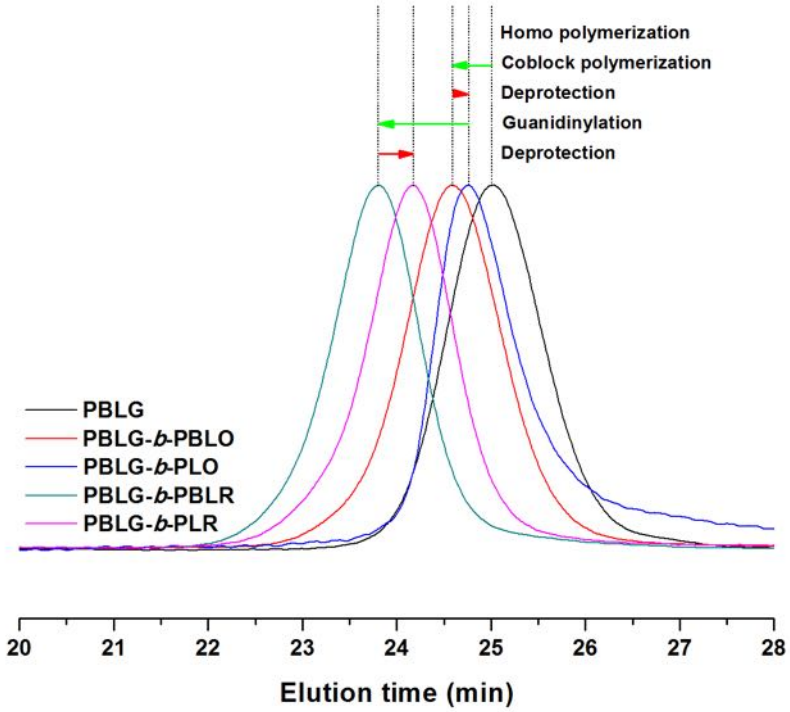

Figure 5.5: SEC chromatograms of PBLG (black) PBLG-b-PBLO (red), PBLG-b-PLO (blue), PBLG-b-PBLR (olive), and PBLG-b-PLR (magenta) polypeptides. Green and red arrows depict increase and decrease of molecular weight, respectively. All samples were dissolved in HFIP, and measured against a PMMA standards.

A summary of M_n and polydispersity values, as well as the degree of guanidinylation is presented in Table 5.2. The measured values follow the trend of the theoretical molecular weights, however, do not match because of the difference between the PMMA standards and the block copolymer. PDI values alter barely between the multiple modification steps and are below 1.25 and in most cases below 1.15.

Table 5.2: SEC results of NCA block copolymerization of BLG BLO, followed by modification.

Polymer	M_{BLG}:M_{BLO}:I	M_n^{th} (g/mol)	M_n^{GPC} (g/mol)	*Đ*	degree of guanidinylation
PBLG	50:1	11.100	9.880	1,09	
PBLG-*b*-PBLO	50:20:1	16.100	12.660	1,11	
PBLG-*b*-PLO	50:20:1	13.400	8.750	1,24	
PBLG-*b*-PBLR	50:20:1	18.200	18.980	1,14	80,6 %
PBLG-*b*-PLR	50:20:1	14.200	15.910	1,14	
PBLG	40:1	8.900	9.910	1,12	
PBLG-*b*-PBLO	40:8:1	10.600	10.340	1,19	
PBLG-*b*-PLO	40:8:1	10.700	9.760	1,23	
PBLG-*b*-PBLR	40:8:1	11.800	15.030	1,12	71,8 %
PBLG-*b*-PLR	40:8:1	11.100	14.400	1,11	

The synthesis was repeated with a different monomer:initiator ratio to obtain shorter blocks. The goal was to synthesize a block copolypeptide with an average PLR block length of 8 arginine residues as arginine-rich polypeptides were found to have an optimal number of arginine residues to undergo translocation[25]. Comparison of the integrals of the CH_2-Bnz (7.08 – 7.47 ppm) and BocCH_3 (1.35 ppm) showed a BLG:BLO residue ratio of 4.86, which is conforming to a block copolypeptide of $PBLG_{40}$-*b*-$PBLO_8$. Further modification followed the same molecular weight variation trend as for $PBLG_{50}$-*b*-PLR_{21}. Comparing ^{1}H-NMR peak intensities of Boc-L-Orn derived (1,35 ppm) and diBoc-L-arginine derived (1.37 ppm) CH_3 protons revealed an overall degree of guanidinylation of 71.8 %. The reasons for a lower degree guanidinylation are unknown. ^{1}H-NMR revealed full removal of the Boc protection group of PBLG-*b*-PBLO, resulting in the full access of the primary amine. One might speculate that an increased amount of TFA is still present in the PBLG-*b*-PLO polypeptide chain that could influence the coupling reaction under basic conditions.

5.3.3 Synthesis of $PBLG_{40}$-*b*-PLR_8 by amino acid initiation

The NCA macroinitiation approach towards PBLG-PLR was further explored with the aim to introduce amino acid initiators. This would provide a fully amino acids based polypeptide omitting the use of non-natural initiators.

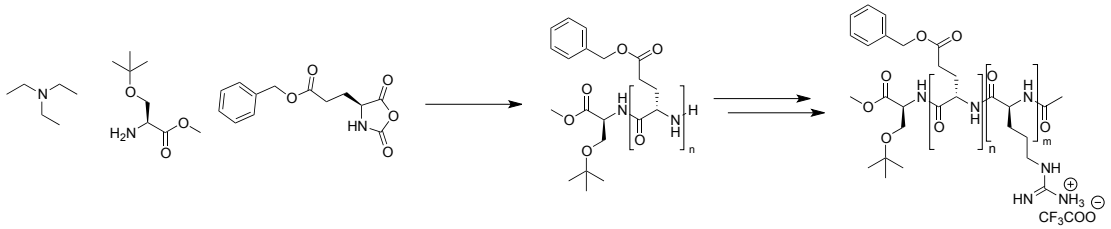

Scheme 5.3: Synthesis of O-methyl(tert-butyl) L-serine initiated PBLG-*b*-PLR block copolypeptide according to similar modification steps as introduced in Scheme 5.1. 0.9 mol eq of TEA was used for neutralization

To introduce a functional amino acid on the *C*-terminus of the polypeptide an O-methyl protected (tert-butyl) L-serine/HCl salt was chosen. The three methyl-groups of the tert.-butyl group can be used as reference signal in ^{1}H-NMR analysis of the polypeptide and easily be selectively deprotected to generate an alcohol group if desired.

Since the amino acid initiator is commercially available in its salt form, the HCl salt was quenched with triethylamine in solution before it was added to the BLG-NCA monomer solution (Scheme 5.3). A small portion of the homo polypeptide reaction mixture was taken for analysis, before block copolymerization was performed, followed by the modification steps towards the PBLG-PLR block copolypeptide as described earlier.

In the first instance it was investigated whether a pre-quenched L-serine/HCl initiator could undergo a controlled polymerization. MALDI-Tof-MS analysis (Figure 5.6) revealed the two expected PBLG species (Figure 18) both initiated by O-methyl(tert-butyl) L-serine, confirming that the polymerization was performed via the NAM. While the added triethylamine could lead to polymerization via the AMM, no evidence for this process was found. The major species (K) is characterized by the primary amine at the *N*-terminus, while species L is the corresponding pyroglutamate product. Therefore, species K has the ability to undergo further block copolymerization.

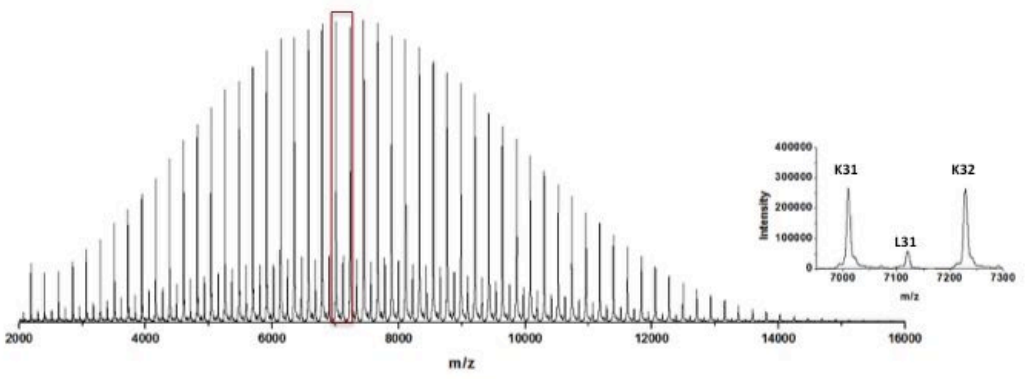

Figure 5.6: MALDI-Tof results of PBLG initiated by O-methyl(tert-butyl) L-serine. Red boxes denote zoom-in region, represented by the spectral section on the right. Letters depict structures shown in Figure 5.7; the numbers refer to the degree of polymerization. All samples were dissolved in HFIP with addition of potassium trifluoroacetic acid (KTFA).

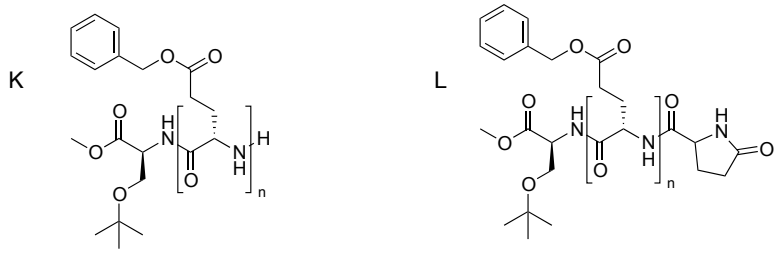

Figure 5.7: Two identified PBLG polymerization product species, assigned to MADLI-ToF-MS spectrum peaks shown in Figure 5.6. Species series include primary amine (K) and pyroglutamate (l) *N*-terminated polypeptides.

Molecular weight analysis by SEC revealed monomodal and symmetrical chromatograms with a molecular weight clearly depending on the monomer to initiator ratio (Figure 5.8). SEC data from all polymerizations are summarized in (Table 5.3). ^{1}H-NMR peak integration confirmed a good agreement of the monomer to initiator ratio of the polypeptides with the feed ratio.

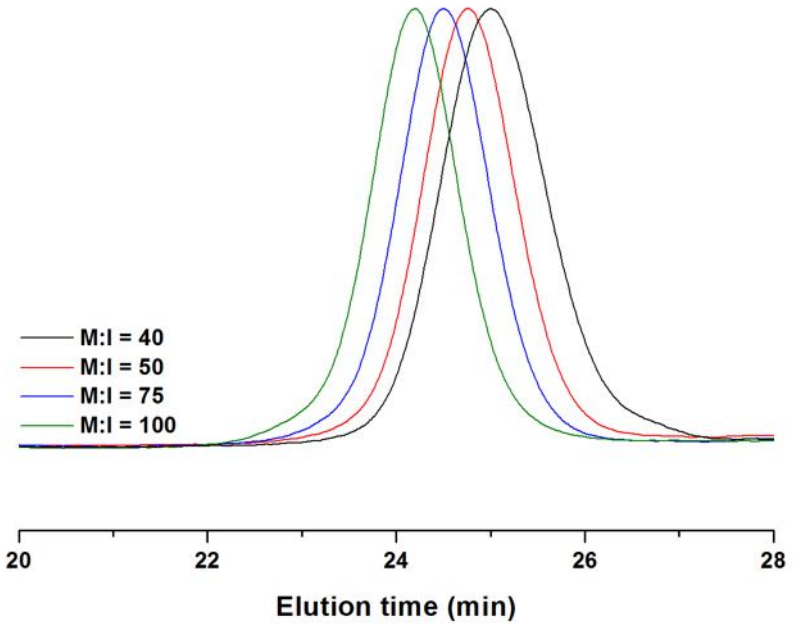

Figure 5.8: SEC chromatograms of PBLG samples initiated by O-methyl(tert-butyl) L-serine, with different monomer:initiator (M:I) ratios. All samples were dissolved in HFIP, and measured against a PMMA standard.

Table 5.3: SEC and ^{1}H-NMR results of polypeptides obtained form different monomer:initiator ratios. All polymerizations were performed in anhydrous DMF, followed by precipitation.

$M:I^{th}$	M_n^{th} (g/mol)	M_n^{GPC} (g/mol)	$Đ$	$M:I^{NMR}$
40:1	8.900	9.950	1,11	43:1
50:1	11.100	11.710	1,08	60:1
75:1	16.600	13.450	1,08	75:1
100:1	22.100	15.610	1,09	90:1

Further block copolymerization towards $PBLG_{40}$-*b*-PLR_8 was performed. Following the modification steps of Scheme 5.2 the block copolypeptide was first deprotected, followed by guanidinylation and final deprotection. The different stages of the modification were analyzed by SEC (Figure 5.5). As previously observed the expected increase and decrease of the molecular weight of the different reaction steps is apparent (Figure 5.9, Table 5.4). However, separation of peaks and quality of polymers is reduced. For example, SEC traces of deprotected polymers are nearly overlapping with traces of the polypeptide of the previous synthetic step. This phenomenon can be explained by the smaller L-ornithine block resulting in lower molecular weight reduction. Moreover, the final block copolymer display a clear high molecular weight shoulder.

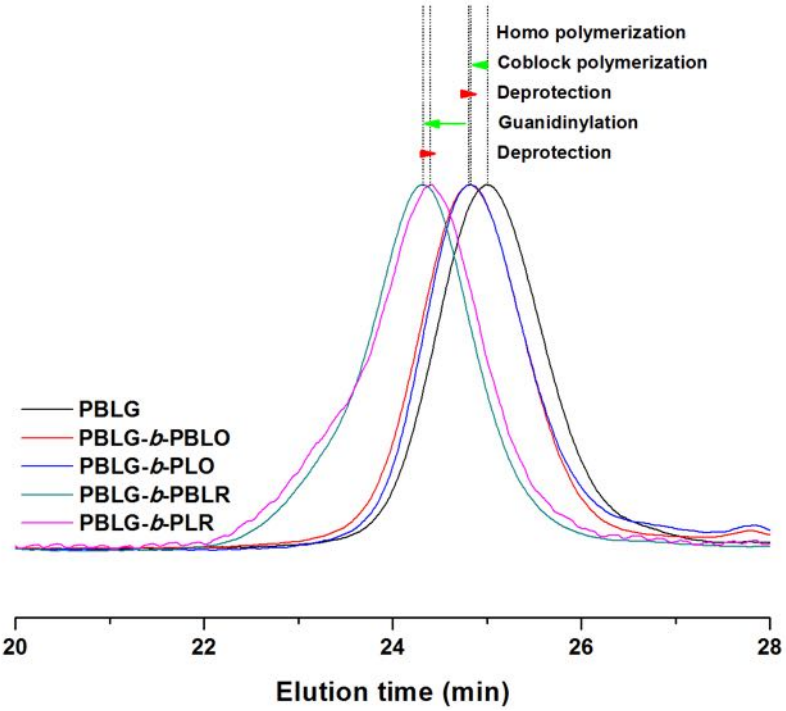

Figure 5.9: SEC chromatograms of PBLG (black) PBLG-b-PBLO (red), PBLG-b-PLO (blue), PBLG-b-PBLR (olive), and PBLG-b-PLR (magenta) polypeptides, initiated by O-methyl(tert-butyl) L-serine. Green and red arrows depict increase and decrease of molecular weight, respectively. All samples were dissolved in HFIP, and measured against a PMMA standard.

Table 5.4: SEC results of NCA block copolymerization of BLG and BLO, initiated by O-methyl(tert-butyl) L-serine, followed by modification. All reactions were initiated by cyclohexyl amine, dissolved in DMF, and followed by final precipitation

Polymer	M_{BLG}:M_{BLO}:I	M_n^{th} (g/mol)	M_n^{GPC} (g/mol)	*Đ*	degree of guanidinylation
PBLG	40:1	8.900	9.950	1,11	
PBLG-*b*-PBLO	40:8:1	10.600	10.980	1,12	
PBLG-*b*-PLO	40:8:1	10.700	10.300	1,14	
PBLG-*b*-PBLR	40:8:1	11.800	14.630	1,17	61,7%
PBLG-*b*-PLR	40:8:1	11.100	16.910	1,18	

5.3.4 Synthesis of $PBLG_{40}$-*b*-PLR_8 by combining NCA ring-opening polymerization and SPPS

Futaki et al. describe an optimal cell penetrating peptide length of eight arginine residues to undergo translocation. Synthesis of the block copolypeptide enabled the desired average block length of eight arginine residues. However, a polydispersity is inherent to polymerization processes, which results in a length distribution of the PLR block. While it is unclear whether this would have an effect on the translocation of a drug delivery system an alternative route for the synthesis of the same diblock copolymer with a precise PLR block was sought. Following a Solid Phase Peptide Synthesis (SPPS) approach the oligopeptide was synthesized on a solid support and covalently ligated to a PBLG block (Scheme 5.1, right). Final deprotection of the side chain of the oligo-L-arginine(Pbf) (Arg(Pbf)) block yields the desired PBLG-*b*-PLR block copolypeptide.

SPPS was performed using Fmoc-L-arginine(Pbf) amino acid residues. The oligopeptide, oligo-(Arg(Pbf)) was synthesized according to a Merrifield procedure, in which the residue was deprotected from the Fmoc protection, followed by ligation and several washing steps. After each successful coupling step, a Kaiser test was performed to confirm full coupling of the Fmoc-protected amino acid to the immobilized peptide chain. After the final acetylation step the oligopeptide was cleaved from the resin (Scheme 5.1, right). Notably, the final oligopeptide product differs slightly from the NCA block copolymerization. Instead of a pure arginine block two glycine residues were incorporated according to the following residue sequence (*C'-N'*):

$$HO - Gly - (Arg(Pbf))_4 - Gly - (Arg(Pbf))_4 - Ac$$

The resin itself introduces the first glycine, since the resin was pre-functionalized by glycine amino acid. By introducing the glycine residue potential *δ*-lactam formation is avoided[26]. The second glycine residue was introduced to prevent secondary structure formation of the arginine(Pbf) oligopeptide that could influence the SPPS efficiency.

After cleavage from the resin the oligo peptide was precipitated twice in MBTE/n-heptane to purify the desired product. The off-white solid was characterized by MALDI-Tof-MS analysis (Figure 5.10). The desired product with a mass of 3478,5 (including K^+) can clearly be identified. However, lower molecular weight species are also present. Mass prediction revealed products HO-Gly-(Arg(Pbf))$_4$-Gly-Ac +H_2O (1863,7, including K^+, species E), and HO-Gly-(Arg(Pbf))$_3$-Gly-H (1395,5, including K^+, species D). Both species could be fragments of the desired product. In case of species D lacking one arginine residue between two glycine residues is unlikely, since the very sensitive Kaiser test revealed full coupling in each step. This might suggest a fragmentation of the ions by the laser desorption process during the MALDI-Tof measurement. However, a breakdown of the HO-Gly-(Arg(Pbf))$_4$-Gly-H product into three fragments, HO-Gly-(Arg(Pbf))$_3$•, •Arg(Pbf)•,and •Gly-H, followed by the coupling of the first and latter to HO-Gly-(Arg(Pbf))$_3$-Gly-H is unlikely. In addition, no fragmentation events were observed in previous polypeptide MALDI-Tof-MS analysis, so that without evidence suggesting otherwise the different species are assumed to be products of an incomplete synthesis. It has to be noted that MALDI-Tof-MS as carried out here is qualitative so that no conclusions can be drawn about the ratio of the different species.

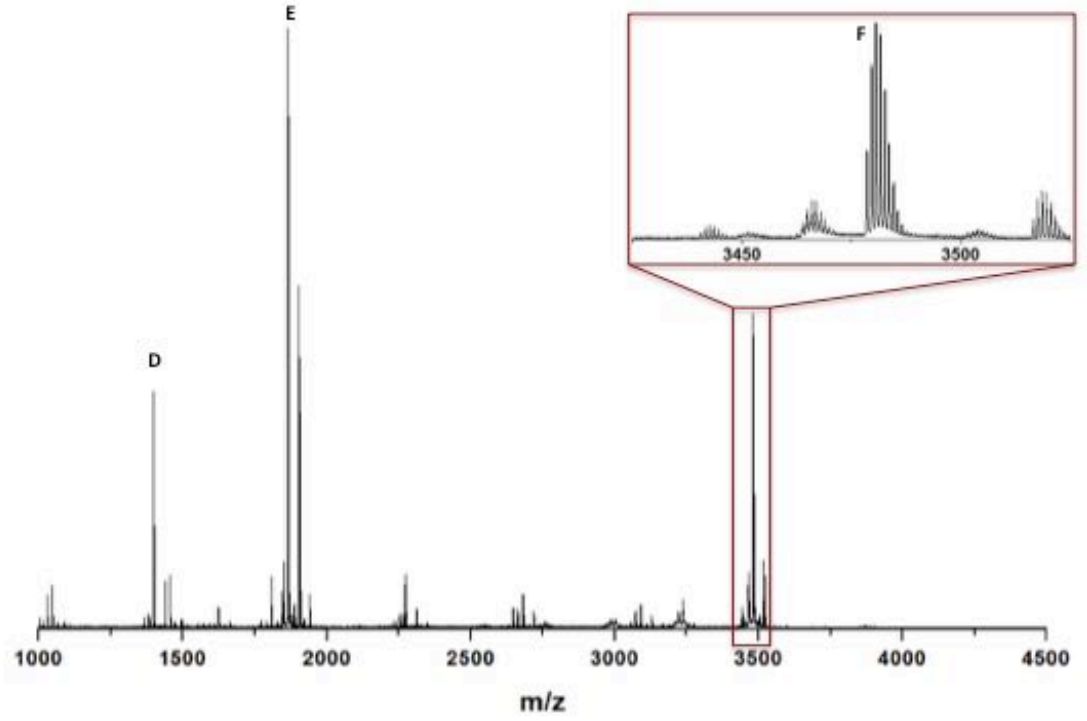

Figure 5.10: MALDI-Tof results of the SPPS synthesized oligopeptide, HO-Gly-Arg(Pbf))$_4$-Gly-Arg(Pbf))$_4$-Ac. Red boxes denote zoom-in region, illustrated in additional spectra on the right side. Letters depict structures shown in Figure 5.11. All samples were dissolved in HFIP, with addition of potassium trifluoroacetic acid (KTFA).

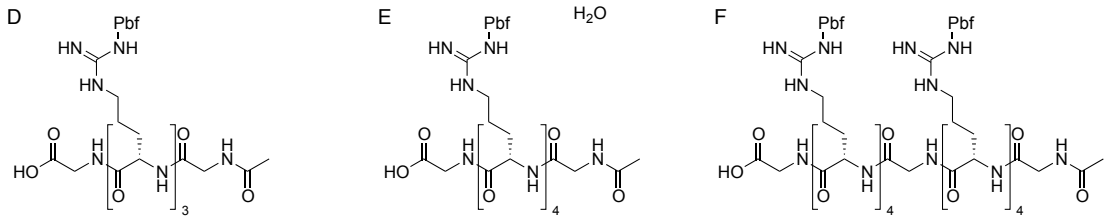

Figure 5.11: Various identified oligopeptide species (D – F), assigned to MALDI-Tof-MS spectrum peaks in Figure 5.10.

In the next step the oligopeptide was covalently ligated to a homo block PBLG$_{40}$ polypeptide. To ensure optimum conditions for the ligation, the oligopeptide was directly added to the NCA-ROP reaction mixture after full NCA conversion was reached. In this way possible pyroglutamate formation during homo polypeptide purification was avoided. After the addition of the coupling reagents OxymaPure and DIC the mixture was stirred for 16 hours. The acetylation at the *N*-terminus of the oligopeptide and the primary amine availability of the PBLG homo polypeptide ensured selective ligation of the two blocks. Comparison of ^{1}H-NMR integrals of the PBLG derived benzyl peaks (7,19 – 7,45 ppm) and the Arg(Pbf) OC(C*H*$_3$)$_2$ peaks (1,38 ppm) revealed a degree of ligation of 73 %.

Both, homo- and diblock copolypeptide were further analyzed by MALDI-Tof-MS (Figure 5.12). Analysis of the PBLG (Figure 5.12 a) shows the expected detection of the major product (species A, Figure 5.13), next to small traces of the pyroglutamate (species B). Analysis of the ligation spectrum (Figure 5.12 b) shows an average increase of the polymer distribution towards a higher molecular weight. This confirms expectations, since the ligation of the oligopeptide on the $PBLG_{40}$ block should result in a higher molecular weight. A closer look at the peak pattern reveals two ligation products, the major product species G and the minor product species H (Figure 5.13), denoted as $PBLG_{40}$-*b*-$PPLR_8$ in the following. Following the trend already observed in the MALDI analysis of the oligopeptide, the major product is the ligation product of $PBLG_{40}$ with species E. The minor product species is assigned to the desired product (species H). Interestingly, the peak at lower molecular weight can be assigned to the oligopeptide HO-Gly-Arg(Pbf)$_4$-Gly Arg(Pbf)$_4$-Ac (Figure 5.11, species F). Although a slight excess of $PBLG_{40}$ was added to the ligation mixture (0,1 mol eq), apparently most of the species F did not ligate with the homo polypeptide. One could speculate that the smaller oligopeptide (species E) is more accessible to the ligation reaction, due to higher entropy and higher probability to find the free primary amine of $PBLG_{40}$.

Due to the presence of the mayor product species E (Figure 5.11) one might speculate that the introduction of the second glycine residue could cause an interruption of a successful amino acid coupling in the processed oligopeptide. To investigate this assumption, a second SPPS was performed, including only arginine residue coupling.

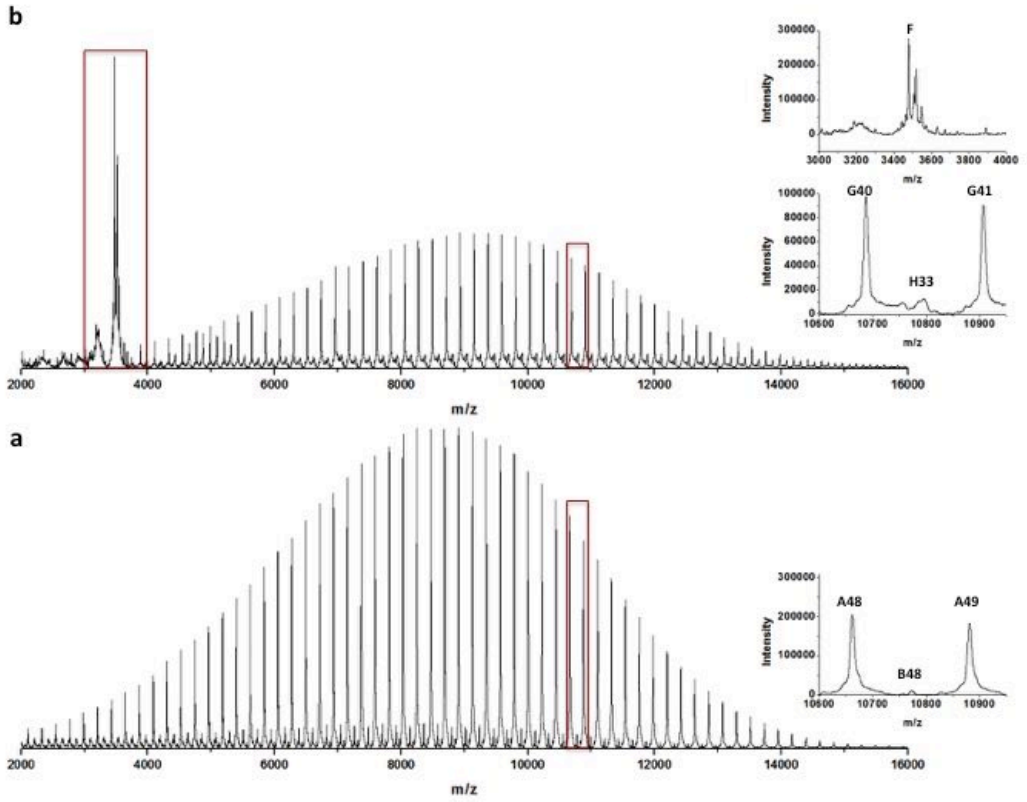

Figure 5.12: MALDI-Tof results of the homo polymerization of PBLG (a) and the ROP-SPPS ligation product (b). Red boxes denote zoom-in region, illustrated in additional spectra on the right side. Letters depict structures shown in Figure 5.13; the numbers refer to the degree of polymerization. All samples were dissolved in HFIP, with addition of potassium trifluoroacetic acid (KTFA).

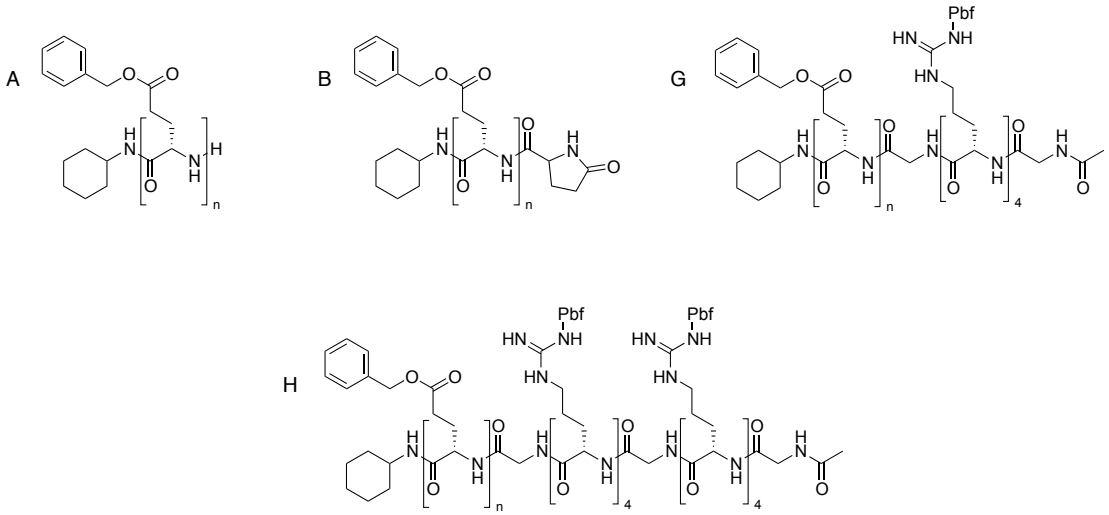

Figure 5.13: Various identified homo polypeptide (A, and B) and ligation derived coblock copolypeptide species (G and H), assigned to MALDI-Tof-MS spectrum peaks in Figure 5.12.

Therefore a second oligopeptide, HO-Gly-(Arg(Pbf)$_8$-Ac (species I, Figure 5.16) was synthesized. After each coupling step a Kaiser test revealed successful coupling of the Fmoc-protected amino acid. After eight coupling steps of HO-Arg(Pbf)-H, followed by

cleavage from the resin, the oligopeptide was purified and further analyzed by MALDI-Tof-MS (Figure 5.14). Similar results were obtained; next to the desired oligopeptide product also side products were identified as shorter chains with 3 – 7 arginine residues. Furthermore other species detected, which could not be identified.

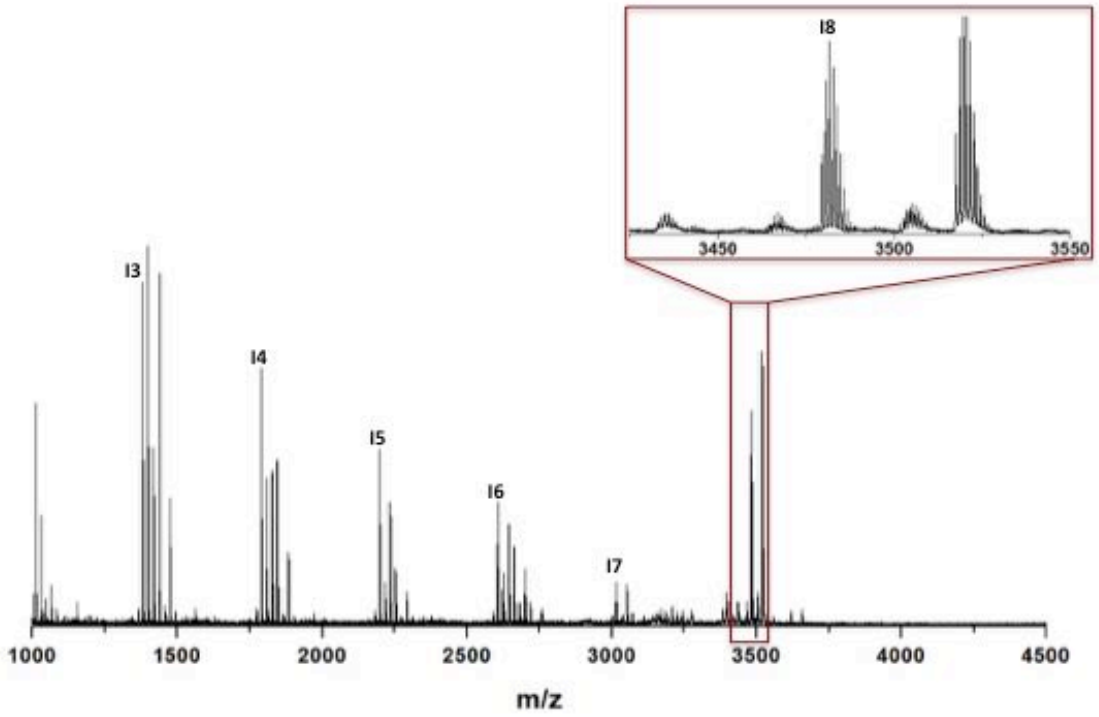

Figure 5.14: MALDI-Tof results of the SPPS synthesized oligopeptide, HO-Gly-Arg(Pbf))$_8$-Boc. Red boxes denote zoom-in region. Letters depict structures shown in Figure 5.16. The sample was dissolved in HFIP, with addition of potassium trifluoroacetic acid (KTFA).

In the next step, the oligopeptide was covalently ligated to a PBLG$_{40}$, as described before. Both, homo- and block copolypeptide were further analyzed by MALDI-Tof-MS (Figure 5.15). As observed in Figure 5.15 b selective ligation is observed with the oligopeptide, consisting of four residues (Figure 5.16, species I). Apparently, the abdication of a second glycine residue did not show the desired results. Still, the ligation products, including four instead of eight arginine residues were depicted as mayor product. The reason why especially ligation with the 4-arginine residue oligopeptide is favored remains further unknown.

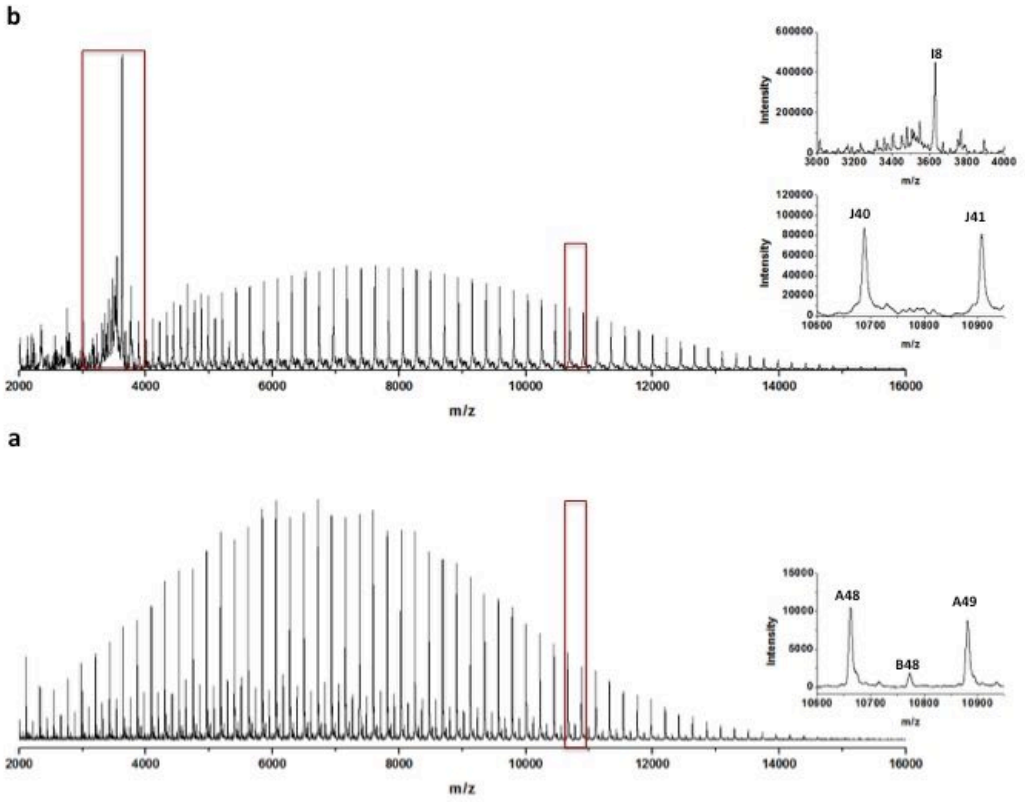

Figure 5.15: MALDI-Tof results of the homo polymerization of PBLG (a) and the ROP-SPPS ligation product (b). Red box denotes zoom-in region, illustrated in additional spectra on the right side. Letters depict structures shown in Figure 5.16; the numbers refer to the degree of polymerization. All samples were dissolved in HFIP, with addition of potassium trifluoroacetic acid (KTFA).

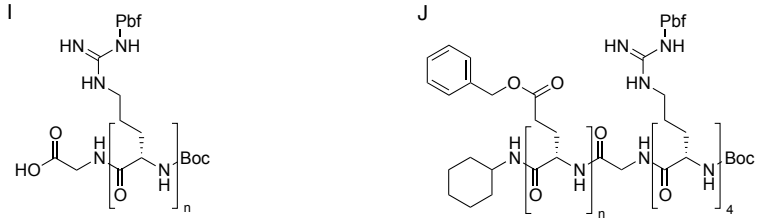

Figure 5.16: SPPS derived oligopeptide species (I) and ligation derived coblock copolypeptide species (J), assigned to MALDI-Tof-MS spectrum peaks in Figure 5.14, and Figure 5.15.

Since the first synthesis of the oligopeptide (species F) showed the presence of fewer side products, further SEC analysis was continued with this ligation product (Figure 5.17). Theoretical and measured molecular weights of $PBLG_{40}$ and $PBLG_{40}$-*b*-$PPLR_8$ are summarized in Table 5.5. Homo polypeptide traces (black line) shows narrow mono modal distribution of the polymer. Trace of $PBLG_{40}$-*b*-$PPLR_8$ (red line) indicates a molecular weight increase, however a bimodal distribution is observed, which results in an increase of the polydispersity. By comparing this trace with the oligopeptide trace (blue line), evidence arises that the bimodal distribution is the result of unreacted oligopeptide.

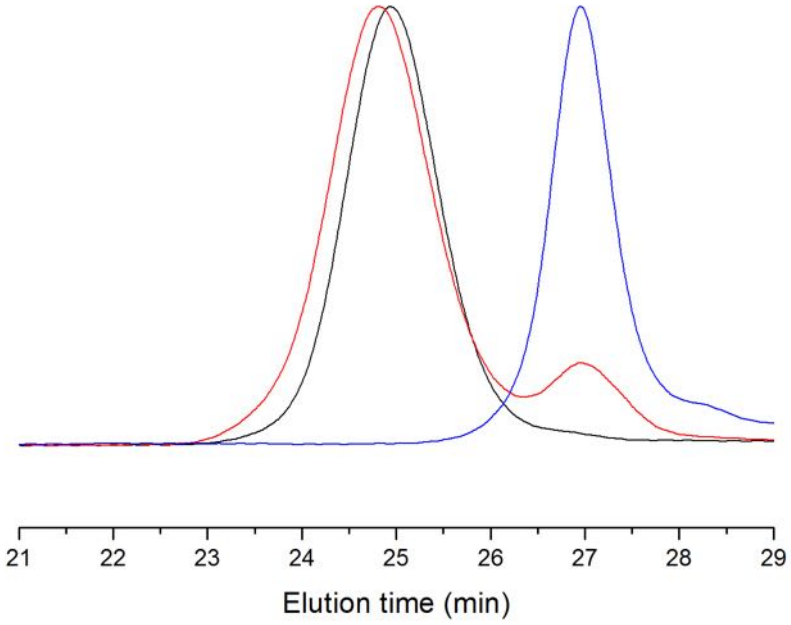

Figure 5.17: SEC chromatograms of PBLG (black) ligated block copolypeptide (red), and SPPS derived oligopeptide (blue). All samples were dissolved in HFIP, and measured against a PMMA standard.

Table 5.5: SEC results of NCA block copolymerization of BLG BLO, followed by modification.

Polymer	M_n^{th} (g/mol)	M_n^{GPC} (g/mol)	$Đ$
$PBLG_{40}$	8.900	8.750	1,22
Oligo(Arg(Pbf))$_8$-Boc	1.400	3.190	1,19
$PBLG_{40}$-*b*-$PPLR_8$	10.300	10.850	1,50

In a final step, deprotection of the $PPLR_8$ block by the removal of the Pbf protection group was performed to obtain the desired amphiphilic diblock copolypeptide. The polypeptide was dissolved in a solution of TFA:H_2O:TIS (94:3:3) to ensure selective removal of the Pbf protection group, while letting the benzyl protection group unaffected. Both protected and deprotected block copolypeptides were monitored by ^{1}H-NMR. While the spectrum of the protected block copolypeptide $PBLG_{40}$-*b*-$PPLR_8$ (Figure 5.18 a) shows the presence of the Pbf CH_3 peaks at 1.38, 2.41, and 2.46 ppm, a successful deprotection can be concluded by the absence of these peaks in the spectrum of $PBLG_{40}$-*b*-PLR_8 (Figure 5.18 b). Peaks at 0.85 and 1.24 are due to traces of n-heptane, which was used for purification of the product.

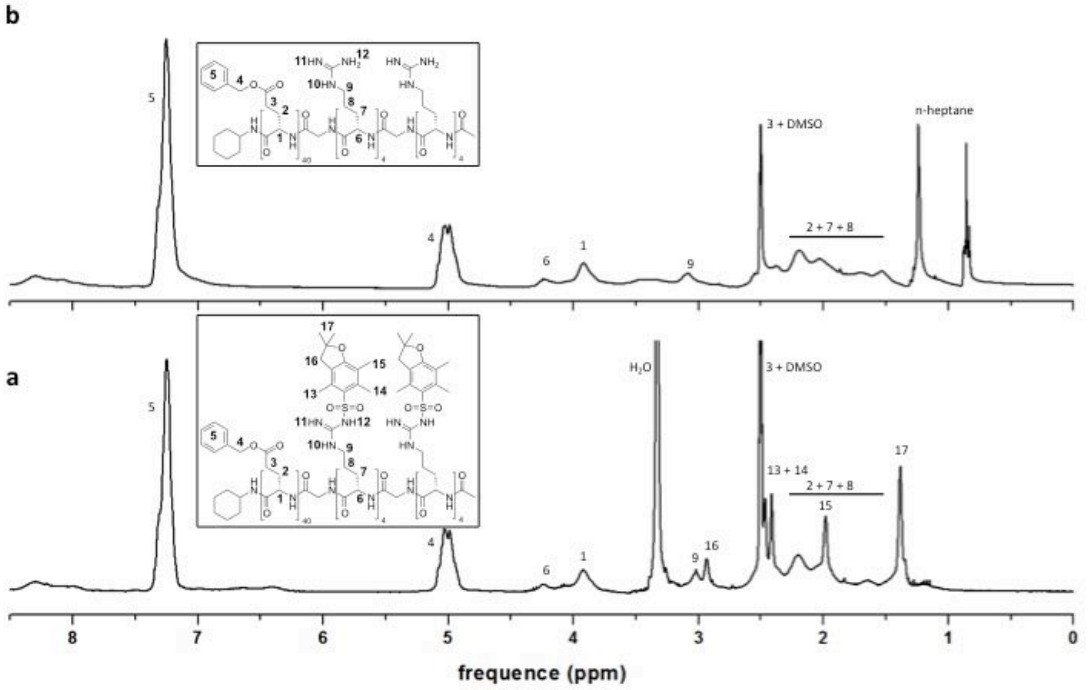

Figure 5.18: ^{1}H-NMR spectra of PBLG-b-PPLR (a) and Pbf deprotected PBLG-b-PLR b. Both samples were dissolved in deuterated DMSO, and measured on a 300 MHz NMR apparatus.

The final Pbf-deprotected block copolymer has an analogous amphiphilic and structural character as the fully NCA derived diblock copolypeptide.

5.3.5 Self-assembly of PBLG-PLR block copolypeptides

The block copolypeptide PBLG-PLR, synthesized by NCA-ROP copolymerization and the SPPS approach were self-assembled into micellar nanoparticles. The self-assembly was performed following the solvent switch method. In the first step, the block copolypeptide was dissolved in anhydrous HFIP (1mg/ml). After full dissolution, the same volume of MilliQ water was added (HFIP:H_2O 1:1, v:v%). The solution was stirred overnight, allowing the organic solvent to evaporate. The obtained hazy aqueous suspension (1 mg ml^{-1}) was diluted to 1 x 10^{-1} mg ml^{-1} before Dynamic Light Scattering Analysis (DLS) was performed. Nanoparticles synthesized by SPPS and NCA-ROP showed both narrow dispersities of $Đ \sim 0{,}1$. In addition, their Critical Micelle Concentration (CMC) is identical at 1 x 10^{-3}. However the diameters of the formed nanoparticles differ at 83 and 105 nm, respectively. Differences in the diameter of nanoparticles can often be explained by their composition. In case of these two block copolypeptides, it was already shown that the polypeptide, synthesized by SPPS has a shorter hydrophilic block. The difference in this block is believed to cause the difference in the diameter of the resulting nanoparticles.

Table 5.6: Self-assembly dynamic light scattering data of PBLG-*b*-PLR obtained by NCA ROP and SPPS synthesis approach

Polymer	**Particle diameter (nm)**	***Đ***	**CMC (mg/ml)**
PBLG-*b*-PLR (ROP)	83,6	0,103	1×10^{-3}
PBLG-*b*-PLR (SPPS)	105,6	0,089	1×10^{-3}

Transmission Electron Microscopy (TEM) images of the micelles were obtained. Self-assembled samples were dropped on a Cu grid, before they were treated with a Gadolinium Acetate stain. The sample of ROP-originated polymers shows spherical particles below a diameter of 100 nm (Figure 5.19). Smaller dots in the background are caused by the interaction between sample and the Gadolinium acetate stain. Therefore, the bigger spheres depict the sample while small spheres in the background can be neglected. Samples obtained from the ligation between PBLG homo polypeptide with SPPS-originated oligopeptide show also spherical particles with a diameter above 100 nm (Figure 5.20). The image shows a cluster of particles with their sharp shell borders clearly visible.

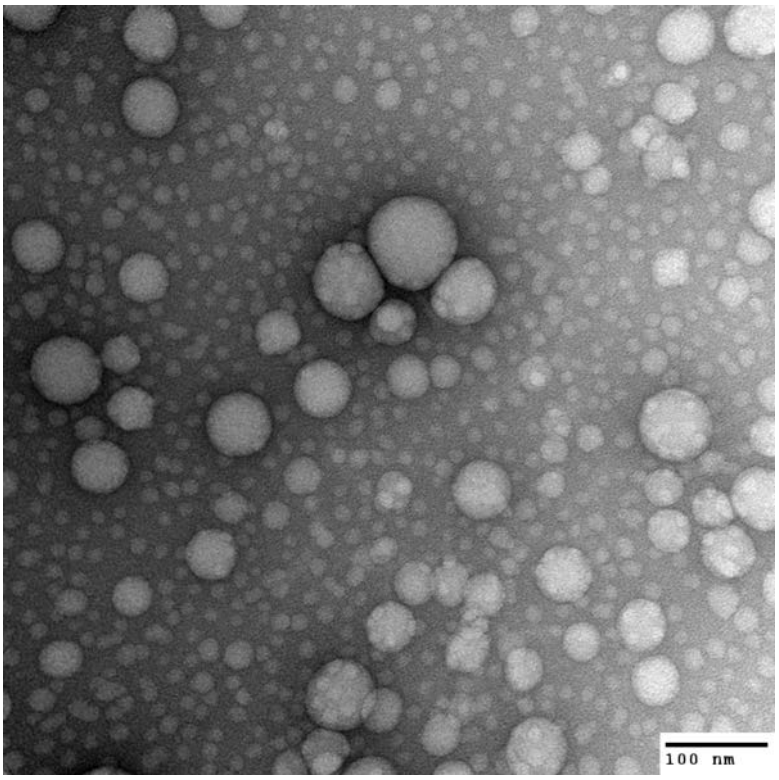

Figure 5.19: TEM picture of PBLG-*b*-PLR micelles, synthesized by NCA macroinitiation. Scale bar is 100 nm.

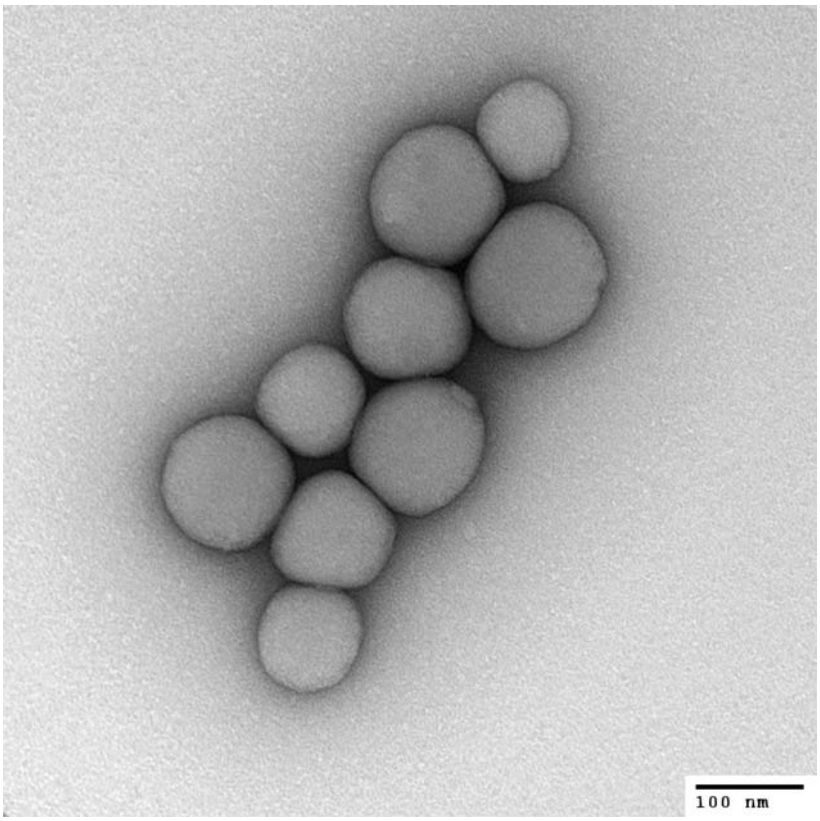

Figure 5.20: TEM picture of PBLG-b-PLR micelles, synthesized by ligation of PBLG homopolyepeptide with SPPS-synthesized PLR oligopeptide. Scale bar is 100 nm.

5.4 Conclusion

The synthesis of PBLG-*b*-PLR block copolypeptides by macroinitiation and polymer modification was successfully demonstrated using cyclohexylamine and a protected serine as initiators. To the best of our knowledge, the synthetic route, including the synthesis of the precursor PBLG-*b*-PBLO, followed by deprotection and guanidinylation, was shown for the first time. MALDI-Tof-MS and ^{1}H-NMR analysis confirm well-defined homo- and block copolypeptide structures, as well as successful selective deprotection of one of the two blocks. Guanidinylation of the PLO block by *N*,*N*'-bis(tert-butoxycarbonyl)-1H-pyrazole-1-carboxamidine revealed a degree of guanidinylation of 80%, which is in good agreement with literature reports. Combined, SEC, MALDI-Tof-MS and NMR analysis confirmed a well-controlled synthetic approach.

The second part of this chapter described the synthesis of PBLG-PLR by combining conventional NCA-ROP with SPPS approach. In the first step the oligopeptide was synthesized via Fmoc protection strategy. Analysis of the oligopeptide revealed presence of the desired product, however, side products were also identified. It is concluded that oligopeptide synthesis by SPPS can be an alternative to a block

copolymerization, however, further optimization is needed, which can possibly achieved by automated synthesizers.

Self-assembly of the block copolymers derived from polypeptides or ligated polymers show both assembly of spherical micellar particles with a diameter around 100 nm. Both synthetic approaches therefore delivered formation of spherical micelles by self-assembly approach.

The block copolymerization of PBLG-*b*-PLR, initiated by O-methyl(tert-butyl) L-serine showed a highly controlled synthesis of polypeptides with good agreement between theoretical and measured molecular weights. The O-methyl protected carboxylic acid of L-serine on the *C*-terminus of the polypeptide bears the potential to use this polypeptide for the grafting onto solid surface and the decoration of nanoparticles.

5.5 References

[1] C. Bory, R. Boulieu, G. Souillet, C. Chantin, P. Guibaud and M. S. Hershfield, *Advances in Experimental Medicine and Biology* **1991**, *309A*, 173 - 176.

[2] P. Glue, R. Rouzier-Panis, C. Raffanel, R. Sabo, S. K. Gupta, M. Salfi, S. Jacobs and R. P. Clement, *Hepatology* **2003**, *32*, 647 - 653.

[3] S. S. Siena, M. J. Piccart, F. A. Holmes, J. Glaspy, J. Hackett and J. J. Renwick, *Oncology Reports* **2003**, *10*, 715 - 724.

[4] L. W. Seymour, S. P. Olliff, C. J. Poole, P. G. De Takats, R. Orme, D. R. Ferry, H. Maeda, T. Konno and D. J. Kerr, *International Journal of Oncology* **1998**, *6*, 1217 - 1223.

[5] M. Byrne, P. D. Thornton, S. A. Cryan and A. Heise, *Polymer Chemistry* **2012**, *3*, 2825 - 2831.

[6] M. Byrne, D. Victory, A. Hibbitts, M. Lanigan, A. Heise and S. A. Cryan, *Biomaterials Sience* **2013**, *1*, 1223 - 1234.

[7] J. R. McDaniel, J. Bhattacharyya, K. B. Vargo, W. Hassouneh, D. A. Hammer and A. Chilkoti, *Angewandte Chemie* **2013**, *52*, 1683 - 1687.

[8] S. Mura, J. Nicolas and P. Couvreur, *Nature Materials* **2013**, *12*, 991 - 1003.

[9] A. Blanazs, S. P. Armes and A. J. Ryan, *Macromolecular rapid communications* **2009**, *30*, 267 - 277.

[10] A. Carlsen and S. Lecommandoux, *Current Opinion in Colloid & Interface Science* **2009**, *14*, 329 - 339.

[11] S. Barua and S. Mitragotri, *Nano Today* **2014**, *9*, 223-243.

[12] T. Stukenkemper, A. Dose, M. Caballo Gonzalez, A. J. Groenen, S. Hehir, V. Andres-Guerrero, R. Herrero Vanrell and N. R. Cameron, *Macromol Biosci* **2015**, *15*, 138-145.

[13] C. Bonduelle, J. Huang, E. Ibarboure, A. Heise and S. Lecommandoux, *Chemical communications* **2012**, *48*, 8353 - 8355.

[14] C. Bonduelle, J. Huang, T. Barragán, C. O. Mellet, C. Decroocq, E. Etamé, A. Heise, P. Compain and S. Lecommandoux, *Chemical communications* **2014**, *50*, 3350 - 3352.

[15] E. L. Snyder and S. F. Dowdy, *Pharmaceutic Research* **2003**, *21*, 389 - 393.

[16] T. M. Allen and P. R. Cullis, *Science* **2004**, *303*, 1818-1822.
[17] G. Sharma, A. Modgil, B. Layek, K. Arora, C. Sun, B. Law and J. Singh, *J Control Release* **2013**, *167*, 1-10.
[18] J. Breger, J. Delehanty, K. Susumu, G. Anderson, M. Muttenhaler, P. Dawson and I. Medintz, *SPIE Proceedings* **2016**, *9722*.
[19] N. Schmidt, A. Mishra, G. H. Lai and G. C. Wong, *FEBS Lett* **2010**, *584*, 1806-1813.
[20] T. Hayakawa, Y. Kondo, H. Yamamoto and Y. Murakami, *Bull Chem Soc Jpn* **1969**, *42*, 479-482.
[21] E. G. Bellomo, M. D. Wyrsta, L. Pakstis, D. J. Pochan and T. J. Deming, *Nat Mater* **2004**, *3*, 244-248.
[22] S. Kudo and Y. Nagasaki, *Macromol Rapid Commun* **2015**.
[23] R. B. Merrifield, *Journal of the American Chemical Society* **1963**, *85*, 2149.
[24] A. Kricheldorf, C. V. Lossov, N. Lomadze and G. Schwarz, *Polymer Chemistry* **2008**, *46*, 4012 - 4020.
[25] S. Futaki, T. Suzuki, W. Ohashi, T. Yagami, S. Tanaka, K. Ueda and Y. Sugiura, *J Biol Chem* **2001**, *276*, 5836-5840.
[26] A. Isidro-Llobet, M. Alvarez and F. Albericio, *Chem Rev* **2009**, *109*, 2455-2504.

6. Conclusion and outlook

The aim of this PhD was to develop the first photoinitiated N-carboxyanhydride ring-opening polymerization. In particular, we wanted to demonstrate that a selective grafting from solid surfaces is possible for future photolithography approaches.

In Chapter 2 we successfully presented the proof of concept, i.e. the use photoamine generators as reactive species for a photo-triggered initiation. Due to the choice of negative controls, it was proven that polymerization specific occurs in presence of photoamine generator while the sample is exposed to light, resulting in a photocleavage of the photoamine generator **2.1** into the primary amine, followed by the initiation and covalent bond into the polymer chain. The key in this proof was the end-group analysis by MALDI-Tof-MS, which revealed the covalent bond of the initiator at the *C*-terminus.

The challenge in Chapter 3 was to minimize these side reactions by less heat creation during irradiation. By introducing a new photoamine generator **3.1**, able to absorb light at a higher wavelength, it was possible to use a blacklight lamp source instead of the UV-rig H-bulb lamp. MALDI-Tof-MS analysis showed similar results as the conventional NCA ROP reaction with a significant reduction of side reactions. Molecular weight control was achieved by increasing the distance between sample and light source and by varying the irradiation time. Furthermore, the system enabled the introduction of a macromolecular photoamine generator, based on poly(dimethylsiloxane). This result demonstrated that in principle, any polymer architecture could be formed by photoinitiated NCA ROP, as in conventional NCA ROP reaction. In addition, the principle of breaking carbamate compounds into primary amines could also be used for crosslinking applications in the future. The chromophoric group could be linked with a primary amine in the side chain of an amino acid, e.g. L-lysine obtaining a carbamate. The incorporated chromophoric group and the photoamine generator should differ in their absorption spectra. Breakdown of the photoamine generator could initiate the polymerization, while a second irradiation step at a different wavelength could cause the breakdown of the carbamate bond in the side chain of the polypeptide. In presence of a suitable crosslinker, crosslinking of the polypeptide chains and network formation would be the result.

Chapter 4 showed the successful grafting of polypeptides on solid substrates by photoinitiation. These results open possibilities towards photolithography. Optical analysis as ellipsometry, contact angle measurements and FTIR revealed photo-triggered polymer grafting on both, spherical silica nanoparticle and planar silicon